CONTRACTOR REPORT

SAND81-7007
Unlimited Release
UC-63

Design and Development of a High-Concentration Photovoltaic Concentrator

R. C. Hodge
General Electric Company
Advanced Energy Programs Department
P. O. Box 8661
Philadelphia, PA 19101

Prepared by Sandia National Laboratories Albuquerque, New Mexico 87185 and Livermore, California 94550 for the United States Department of Energy under Contract DE-AC04-76DP00789

Printed April 1982

DISCLAIMER

Issued by Sandia National Laboratories, operated for the United States Department of Energy by Sandia Corporation.

Printed in the United States of America
Available from
National Technical Information Service
U.S. Department of Commerce
5285 Port Royal Road
Springfield, VA 22161

NTIS price codes
Printed copy: A06
Microfiche copy: A01

Distribution
Category UC-63

SAND81-7007
Unlimited Release
Printed April 1982

SAND--81-7007

DE82 015673

DESIGN AND DEVELOPMENT OF A HIGH-CONCENTRATION PHOTOVOLTAIC CONCENTRATOR

R. C. Hodge
General Electric Company
Advanced Energy Programs Department
P. O. Box 8661
Philadelphia, PA 19101

ABSTRACT

The design and development of a high concentration photovoltaic concentrator module is discussed. The design concept described herein incorporates a curved groove domed Fresnel lens, a high concentration etched multiple vertical junction (EMJV) solar cell and a passively cooled direct-bonded copper cell mount all packaged in a plastic module. Two seven inch diameter 1200x domed Fresnel lenses were fabricated using single point diamond turning technology. Testing at both GE and Sandia confirmed optical transmission efficiencies of over 83%. Samples of the latest available EMVJ cells were mounted and installed, with a domed Fresnel lens, into a prototype module. Subsequent testing demonstrated net lens-cell efficiencies of 10-13%. As a result of this program, salient conclusions have been formulated as to this technology. A discussion is provided in the last section of this report.

Prepared for Sandia National Laboratories under Contract #13-9434.

ACKNOWLEDGEMENT

The author wishes to gratefully acknowledge the contributions of Mr. John Egger and Dr. Larry James in the development of the domed Fresnel lens, Mr. John Henkes, Harold Grub and Charles Stillwell in the testing of the fabricated lenses, Mr. Ray Lambert and Jack Chan in the definition of an optimized domed Fresnel concentrator module, Dr. Hal Webster in the development of the high concentration cell mounts, Bob Frank in the development of the EMVJ concentrator cells and Mr. Bob Collingwood in the performance of the module testing.

Serving as the Sandia technical monitor, Dr. Eldon Boes provided many helpful suggestions during the course of this development program.

TABLE OF CONTENTS

TABLE OF CONTENTS (Cont)

LIST OF ILLUSTRATIONS

LIST OF ILLUSTRATIONS (Cont)

LIST OF TABLES

SECTION 1

INTRODUCTION AND SUMMARY

SECTION 1
INTRODUCTION AND SUMMARY

1.1 INTRODUCTION

Photovoltaic solar energy conversion systems using concentrated sunlight have the potential to provide low cost electrical power by trading large areas of relatively low cost concentrator hardware for large areas of relatively high cost solar cells. Over the past few years concentrator solar cell conversion efficiencies have risen sharply, especially for high (600x to 1000x) concentration cells (References 1, 2, 3, 4). The purpose of the program was to design and develop a high concentration concentrator module which will take advantage of the high efficiency demonstrated by the latest high concentration solar cells.

1.2 TECHNICAL SUMMARY

The overall technical objective of the program was to design and demonstrate via prototype hardware a high efficiency, high concentration photovoltaic (PV) module. In the performance of the program the following technical issues were addressed:

1. Definition of an optimum high concentration lens design.
2. Establishment of a practical concentrator module packaging design which takes into account optics-to-cell registration, component replacement, low cost manufacturing techniques and module-to-array integration.
3. Confirmation of the performance improvements possible with a high concentration domed Fresnel lens.

The primary emphasis of the technical work was to optimize the efficient coupling of the high concentration lens to the cell receiver. No major development work was undertaken in the solar cell or array tracking structures and mechanisms.

The final design incorporates curved groove domed Fresnel lenses, high efficiency solar cells along with high power solid-state device packaging schemes currently available within General Electric. These components are assembled into a plastic module consisting of

multiple lenses, a lens mounting frame, a housing shell, electrical harness with quick-mount cell receivers and a passive cooling system. Figure 1 illustrates the final conceptual module design. Nine (9) 11.5 inch square domed point focus Fresnel lenses are mounted to a molded plastic mounting frame which in turn is assembled to a lower housing shell. The housing shell has prelocated receptacles for the quick-mount cell receiver units. Precision molds would be used to manufacture the mounting frame and housing shell thus facilitating subsequent lens-to-cell receiver unit registration. This basic module would constitute a basic building block from which arrays of various output powers could be designed. Table 1 provides a module design summary.

As stated, the program's major technical development was the design and development of an efficient high concentration domed Fresnel lens. Optical Science Group (OSG) was responsible to design and fabricate the domed Fresnel lens. OSG developed two separate lens designs. A circular lens was developed for use with the selected concentrator cell and prototype module. A square lens was defined which represented an optimized, production oriented lens approach. A summary lens comparison is provided in Figure 2.

Early in the program it was agreed that the best available high concentration solar cell would be used. Microwave Associates Etched Multiple Vertical Junction (EMVJ) silicon cell was selected, see Figure 3-a. In order to reduce program risk an existing cell design, currently under development on a separate Sandia program, was selected, see Figure 3-b.

The front groove cell has a 0.26 inch diameter active area and a projected efficiency of greater than 18% at 1000x and 28^{o}C.

The problems faced in mounting and cooling solar cells in concentrated sunlight are essentially the same as those encountered with high power silicon transistors and thyristors. General Electric's experience in this area was directly applied to the design of a high concentration cell receiver. General Electric's unique contribution in this area of technology is the use of direct-bonded copper to provide a strong, low thermal and electrical resistance mount for the cell, and knowledge of high lead solder-metallization systems which will survive the required

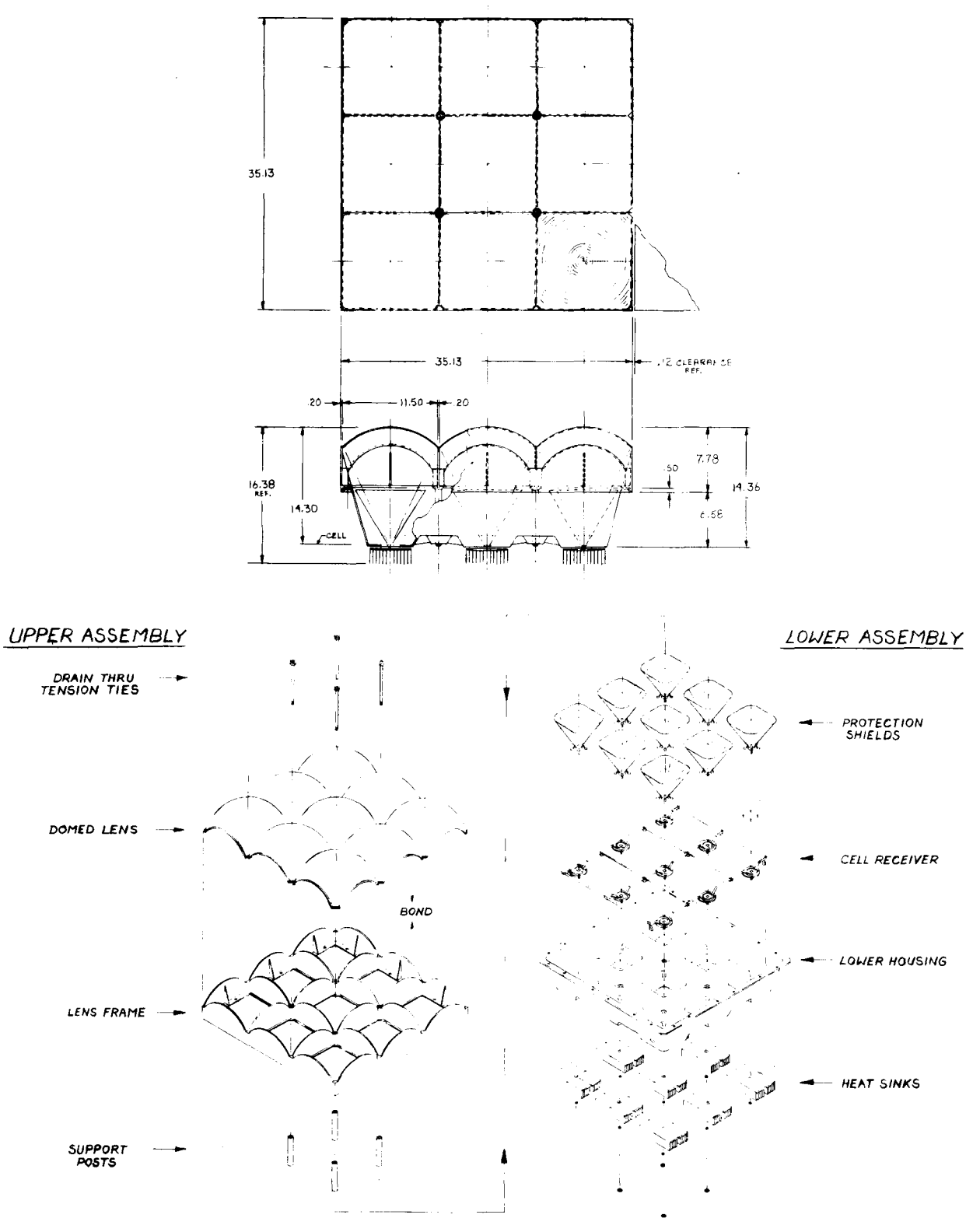

Figure 1. Production Version of the High Concentration Domed Fresnel P/V Module

Table 1. Optimized Module Design Summary

TOTAL GROSS AREA (M^2)	0.836
TOTAL ACTIVE LENS AREA (M^2)	0.768
MODULE WEIGHT (LBS)	35
RATED MAXIMUM POWER OUTPUT (WATTS)	129
AREA MODULE OUTPUT (WATTS/M^2)	166
ANNUAL MODULE OUTPUT (kWh/M^2)	442 *
MODULE EFFICIENCY (PERCENT)	16.9 **

* ALBUQUERQUE WEATHER TAPE

** 22% EFFICIENT CELL AT 28°C, 84% EFFICIENT LENS

	PROTOTYPE LENS	PRODUCTION LENS
	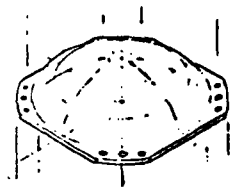	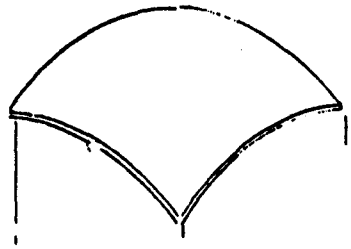
GEOMETRY	CIRCULAR 7" DIA	SQUARE 11.5"
F#	0.75	0.5
GEOMETRIC CONCENTRATION RATIO	1200	1200 - 1600
TRANSMISSION EFFICIENCY	0.84	0.84
DOME HEIGHT	2.17"	4.8"
INPUT REFRACTION FRACTION	0.70	0.65 - 0.80
0% LOSS TRACKING POINT	$\pm$ 0.23°	$\pm$ 0.19°
10% LOSS TRACKING POINT	$\pm$ 0.54°	$\pm$ 0.38°
THICKNESS/MATERIAL	0.25", ACRYLIC	0.10" ACRYLIC

Figure 2. Lens Design Summary

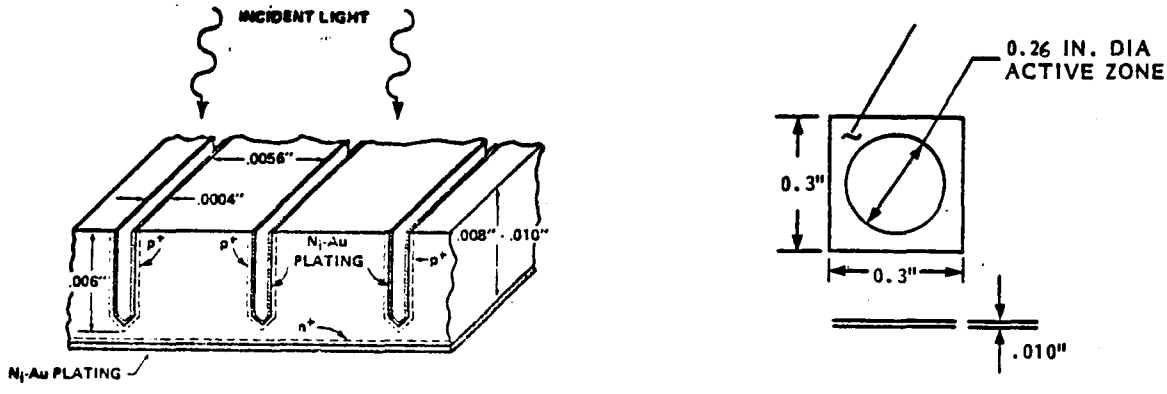

(a) Cell Crossection

(b) Existing Cell Configuration

Figure 3. Program's High Concentration Silicon Cell

temperature cycling. This technology and experience was drawn on to design, build and test a cell receiver unit which exceeded the established thermal resistance goals. Figure 4 depicts the prototype cell mount hardware.

The prototype module hardware, shown in Figure 5, consists of lens opening covers, a curved groove domed Fresnel lens, a protective steel cone, a cell mount socket (shown mounted inside module housing), a cell mount, an extruded aluminum fined heat sink and a sealed plastic housing. The complete cell receiver is shown in Figure 6.

A test result summary for the prototype hardware is provided in Table 2.

Table 2. Test Result Summary

DESIGN PARAMETERS	PROGRAM GOAL	MEASURED VALUE
1 - LENS CONCENTRATION		
PEAK	$< 3 \times I_{AVE}$	1600X *
AVERAGE	400 - 2000	609X *
2 - LENS TRANSMISSION		
0^{o} POINTING ERROR	83 %	84.0%
0.25^{o} POINTING ERROR	83%	82.6%
0.50^{o} POINTING ERROR	75%	77.3%
3 - CELL EFFICIENCY AT 1000X	> 20%	14-16%
4 - CELL MOUNT THERMAL RESIST.	$< 0.40^{o}C$/WATT	$0.25^{o}C$/WATT
5 - MODULE EFFICIENCY AT SOC	> 15%	10-13%
6 - POWER OUTPUT/CELL AREA @ 1 kW/M^2	5-6.5 W/CM^2	4-6 W/CM^2

* SENSITIVE TO FOCAL DISTANCE

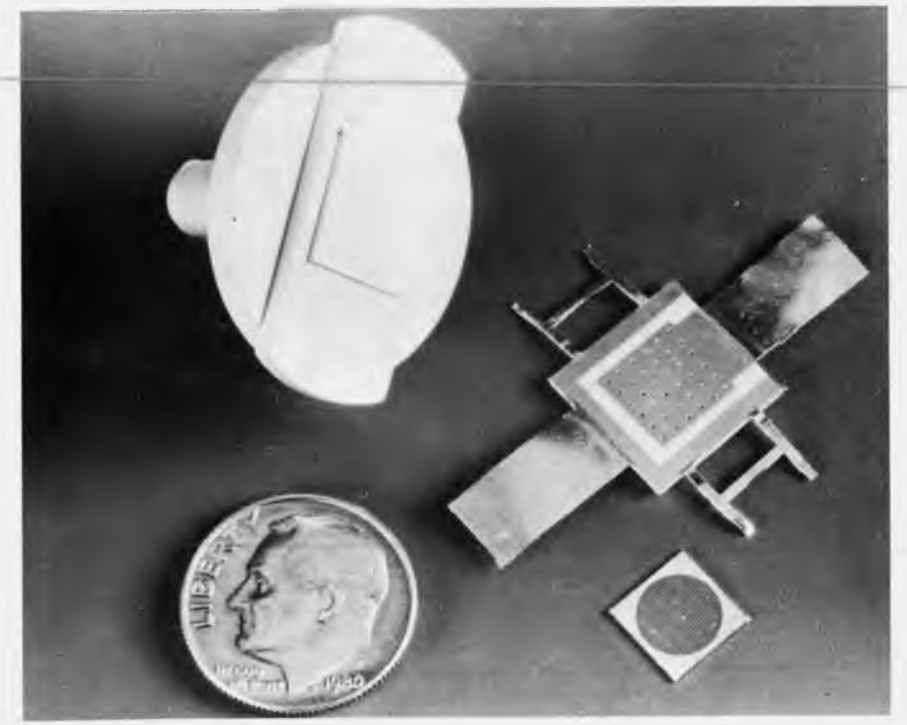

a) Cell Mount Components - Copper Heat Spreader Stud, Direct Bonded Copper BeO Substrate and the EMVJ Concentrator Cell

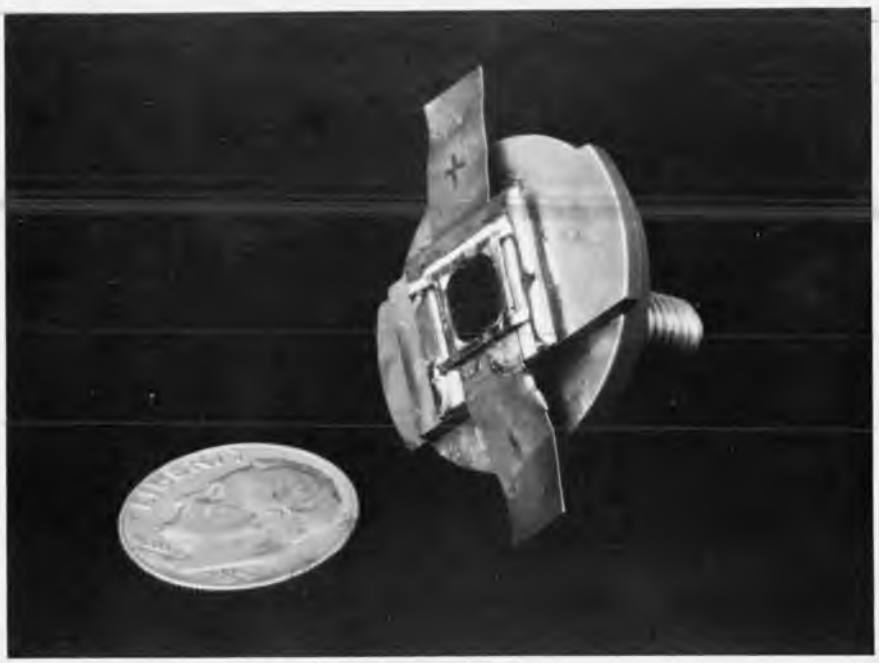

b) Assembled Cell Mount

Figure 4. High Concentration Cell Mount

Figure 5. Prototype Module Hardware

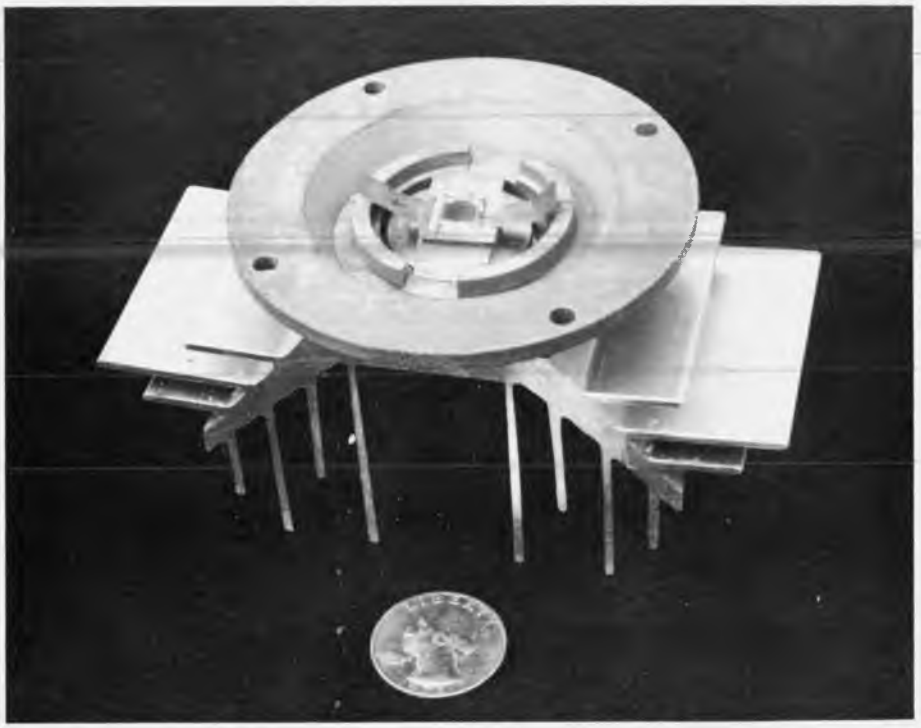

Figure 6. Complete Cell Receiver Assembly

The lenses and cell mounts exceeded their respective program goals. The module efficiency goal was not achieved primarily due to the less than 20% efficient solar cells. However, the watts/cm^2 of total cell area value was still encouraging. The balance of this report describes the module optimization effort, detailed lens analysis, cell mount development and the prototype hardware development and test.

SECTION 2

DESIGN DEVELOPMENT

SECTION 2

DESIGN DEVELOPMENT

2.1 MODULE DESIGN OPTIMIZATION

The domed Fresnel module shown in Figure 1 was developed based on minimum energy cost criterion. The energy cost was based on the total installed cost of a 400 kW array and the adjusted peak watt output from an Albuquerque location. The module, as shown in Figure 1, incorporates Microwave Associates' Etched Multiple Vertical Junction (EMVJ) silicon solar cells which have the unique feature of increasing electrical efficiency with concentration. The resultant characteristics of the optimized module are listed in Table 3. It should be noted that the optimum module configuration is based on the assumed cell and lens characteristics obtained from Microwave Associates and Optical Sciences Group at the inception of the study. Thus, these results would have to be updated when production cell and lens design characteristics become available.

Table 3. Optimum Domed Fresnel Module Characteristics

MODULE HOUSING DIMENSION		3' x 3' x 0.8'
MODULE HOUSING MATERIAL		ROVEL (MODIFIED SAN THERMOPLASTIC)
LENS SIZE		11.5" SQUARE
LENS FOCAL DISTANCE		8.5"
LENS GEOMETRIC CONCENTRATION		1200X
LENS TRANSMISSION EFFICIENCY		84%
CELL SIZE		0.49" SQUARE
COMPOSITE MODULE ERRORS (TRACKING, ALIGNMENT)		$\pm 0.38^{o}$
CELL PERFORMANCE		21.5% @ 1250X, 28°C
CELL RECEIVER DESIGN		DIRECT-BONDED COPPER W/BeO INSULATOR
MODULE WIRING LOSS		2%
FINNED ALUMINUM HEAT SINK		0.5 LB/CELL
MODULE	PEAK WATT†	166 WATT/M^2
	ADJUSTED PEAK WATT*	169 WATT/M^2
	ANNUAL ENERGY OUTPUT*	442 kWh/M^2

† AT 1 kW/M^2, 20^{o} AMBIENT AND 1 M/SEC WIND

* FOR ALBUQUERQUE LOCATION

2.1.1 APPROACH

An optimization methodology was formulated to provide a step-by-step procedure. The methodology flow diagram is shown in Figure 7. It was pre-determined that the optimum cell receiver assembly would use the direct-bonded copper approach with beryllia as the electrical insulator and that the individual module size would be approximately 3' x 3' for ease of handling by one person. There are four basic design variables that characterize an optimum module configuration: Fresnel lens, solar cell, heat sink, and electrical harness design. For a given lens size/characteristic (F#, transmission η and concentration ratio) and cell size combination, incident solar flux on the cell and subsequently the cell efficiency at 28°C were obtained. The heat sink design governs the rate of heat dissipation from the sink to the ambient and, combining with the given cell assembly configuration, the temperature gradient from cell to ambient and the cell efficiency degrading factor were obtained. The net module electrical output was calculated from individual solar cell output via the electrical harness design. Module performance was estimated annually for a particular weather location to obtain the adjusted peak watt (or average watt) output which is defined as the annual module efficiency times 1 kW/m^2 insolation. The array total installed cost was then estimated to determine the module energy cost. Combinations of varying lens solar cell, heat sink and electrical harness were analyzed parametrically until a minimum $/ave watt energy cost was achieved.

2.1.2 ASSUMPTIONS

The EMVJ solar cell and the domed lens design characteristics used in this study were summarized in Table 4. These assumptions were obtained from Microwave Associates' and Optical Sciences Group at the inception of the study. The key assumptions are that the EMVJ cell efficiency increases with increasing concentration and it is relatively insensitive to changes in cell size i.e., 0.2"-0.5" dia. It is also assumed that the lens transmission efficiency decreases by approximately 1% for every 500X increase in concentration ratio.

The basic array cost assumptions used in calculating the total installed costs are shown in Table 5. The costs of array key components which are independent of the module configuration are listed on the right side of Table 5 for a 0.569 m^2 module. The key material costs used to calculate the module FOB factory price are shown on the left of the table.

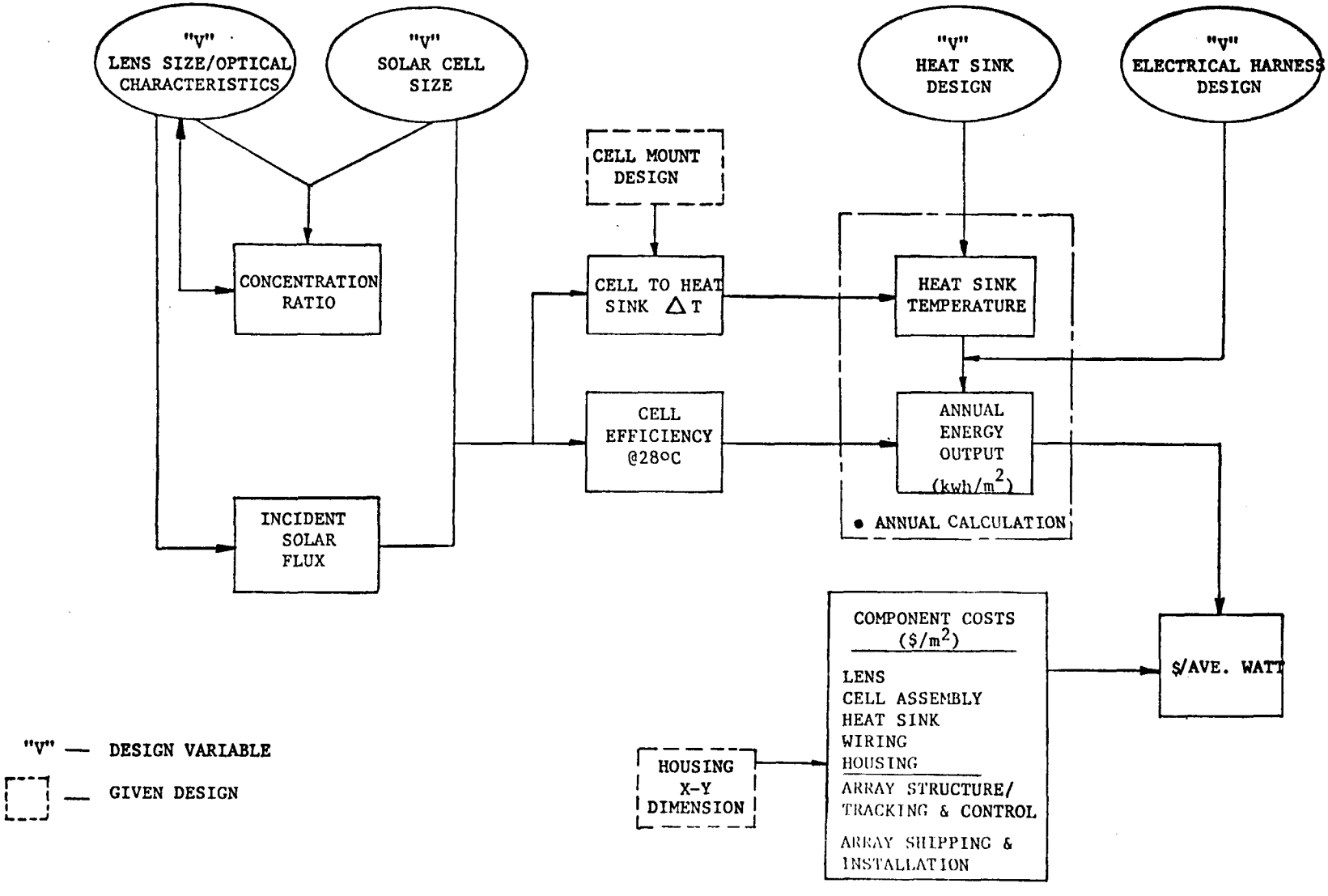

Figure 7. Optimization Methodology - Domed Fresnel Concentrator Module

Table 4. Cell and Lens Design Characterization

EMVJ CELL CHARACTERISTICS ASSUMPTIONS

Assumption #1*: Sensitivities of cell η, η and V_{oc} temp. coefficients vs. concentration ratio

CONC. RATIO	CELL η @ 28°C	η TEMP. COEFF. $\frac{1}{\eta}\frac{d\eta}{dT} \times 10^{-3}/°C$	V_{oc} (VOLTS)	V_{oc} TEMP. COEFF. $\frac{dV_{oc}}{dT} \times 10^{-3}/°C$
1	.157	-4.60	.593	-2.07
10	.179	-3.83	.676	-1.84
100	.198	-3.10	.745	-1.56
500	.207	-2.70	.783	-1.45
1000	.213	-2.60	.800	-1.40
1500**	.216	-2.53	.810	-1.37
2000**	.219	-2.50	.820	-1.35

* 0.25" sq. cell size, "A Low Series Resistance Silicon PV Cell for High Intensity Application", R. Frank, etc.
** Extrapolation from (*).

Assumption #2: Assumption #1 also applies to a 0.6 inch square solar cell

i.e. Cell Characteristics are insensitive to changes in cell area from 0.25" to 0.6" square

Assumption #3: Cell Characteristics are relatively insensitive to incident flux profile

i.e. $I_{peak} < 3^* I_{average}$

DOMED LENS CHARACTERISTICS ASSUMPTIONS

Assumption #1: Concentration ratio vs. lens transmission efficiency

CR	η	
500	86%	i.e., 1% per 500 ΔCR
1000	85%	
1500	84%	
2000	83%	

Assumption #2: Lens transmission efficiency is insensitive to changes in lens F# from 1.0 to 1.5

Table 5. Basic Array Cost Assumptions

- 1980 $
- 10^5 m^2/YEAR ANNUAL PRODUCTION

MODULE KEY MATERIALS/PROCESSES		ARRAY KEY COMPONENTS*	
COPPER	$2.00/LB	TRACKING DRIVES/CONTROL	$46.3/M^2
ACRYLIC	$ .90/LB	TORQUE TUBES, TEES, INTERFACE HARDWARE	$32.7/M^2
ABS PLASTIC	$1.00/LB	SHIPPING	$22.3/M^2
DIRECT BOND Cu/BeO SUBASSEMBLY	$ .18/CM^2	INSTALLATION	$145.0/M^2
EMVJ CELL	$1.00/CM^2		
INJECTION MOLDING PROCESS	$2.90/M^2		
CELL ASSEMBLY LABOR	$ .27/UNIT		
EXTRUDED ALUMINUM	$1.00/LB		

* CIRCULAR LENS GEOMETRY, 0.569m^2/MODULE, "PV CONCENTRATOR ARRAY PRODUCTION PROCESS STUDY", FINAL REPORT SAND 79-7055 TURNTABLE TYPE TRACKER

2.1.3 ANALYSIS

It was recognized that for every module configuration, whether or not it is the optimum, there exists an optimum heat sink design which results in the lowest array energy cost for that module. There are several parameters which characterize a finned heat exchanger: fin length and thickness, fin spacing, substrate thickness and area. In order to minimize the number of parametric trade-offs in the optimization, the heat sink design was first optimized for each of the lens sizes being considered (i.e., 6", 9", 12" and 15" diameters). The heat sink optimization procedure is as follows: (1) for a given lens size and concentration, nominal values were selected for each heat sink parameter, (2) varying one parameter (e.g., fin length) around its nominal value while keeping the remaining variables constant, the annual array energy output was calculated for each fin length value using the Albuquerque TMY weather data, (3) total array installed cost was computed for each fin length by adding a nominal array installed cost to the heat sink cost, (4) array energy costs (installed cost/average watt output) were computed and the fin length that resulted in the lowest energy cost was identified and used in the succeeding calculations, (5) steps 2 through 4 were repeated for all other heat

sink parameters, and (6) the above steps were iterated until the values for all parameters converged. All heat sink configurations are of longitudinal type with fins on one side of the base only and made from extruded aluminum. Figure 8 presents the results of heat sink optimization for a 12" diameter lens and 1000X concentration. It indicates that the optimum heat sink weighs approximately 0.5 lb. and has 1.2" long fins at 0.3" apart; the fin thickness is 25 mil; the substrate is 0.05" thick and the heat sink is 8" long by 3.5" wide. In practice the substrate thickness is at least 0.100". Calculations were then repeated to define the optimum heat sink for other lens sizes.

These optimized heat sinks were then used to determine the lowest energy cost module configurations. The optimization procedure was similar to that of the heat sink where each design parameter, Fresnel lens, solar cell and electrical harness was varied individually and evaluated for minimum array energy cost until the values for the three (3) variables converged. It was assumed that all solar cell areas included a guardband for $\pm 0.2^{o}$ composite module error due to tracking and lens-to-cell misalignment. The results of the module optimization are shown in Figure 9. At constant lens concentration and interconnect wiring loss, the smaller lens modules result in higher ($\sim$ 12%) array energy costs due mainly to the increase in cell receiver and assembly costs. The number of individual lens-cell units per module increases fourfold as the lens size decreases from 12 to 6 inches. Above 12 inches, the energy cost becomes insensitive to lens size.

For optimum electrical harness design, the copper interconnect shall be sized for less than 2% module I^2R losses. Since the copper wiring cost is a very small fraction of the total installed cost, the array energy cost is strongly dependent on module energy output. As for lens concentration, the optimum value leans towards high concentration ($\sim$ 1500X) due to the inherent characteristics of EMVJ cell efficiency and lower relative cell costs. Thus, for the optimum circular lens module, the lens size is in the range of 12 to 15 inches diameter with a geometric concentration of 1500 to 2000X. The minimum energy cost for this configuration is approximately \$2.0/ave watt.

To further reduce the array energy cost, one obvious approach is to maximize the module packing density (i.e., increase the effective aperture area per module). This can be accomplished by going with a square domed lens design. For a 3' x 3' module, an 11.5" square lens geometry will result in a 27% increase in the module effective aperture area (0.768 m^2) as

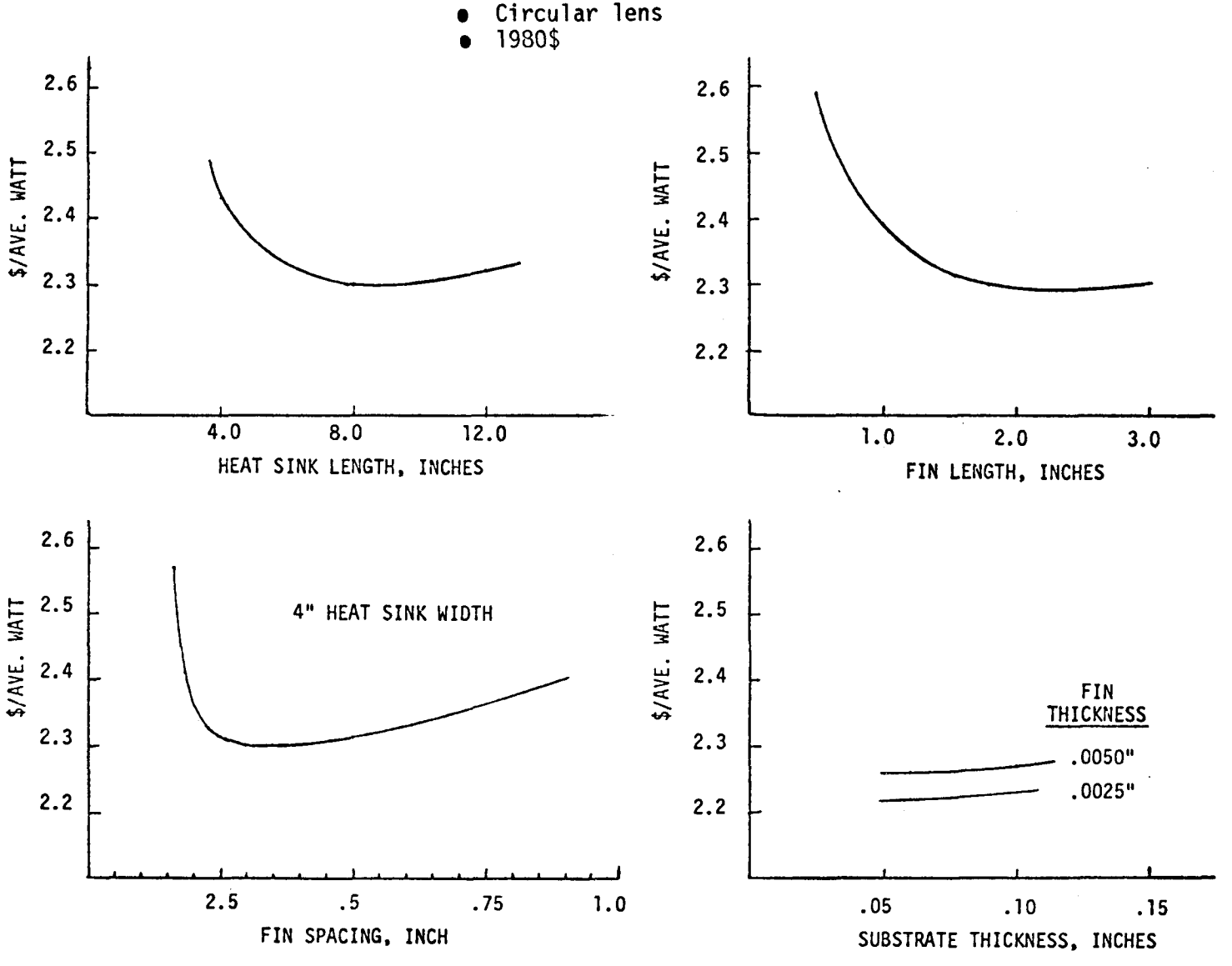

Figure 8. Heat Sink Optimization - 12" Diameter, 1000X Lens Module

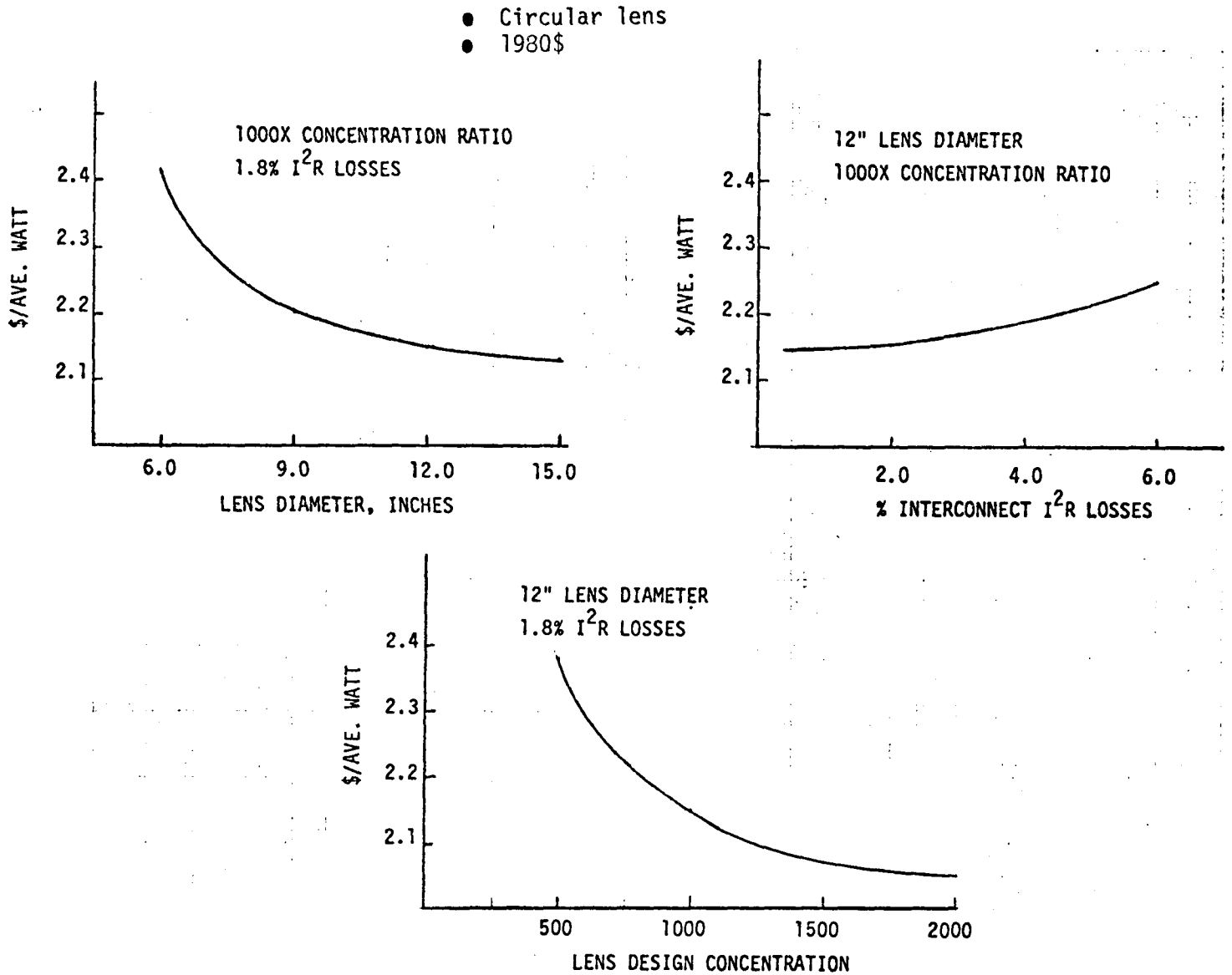

Figure 9. Domed Lens Module Optimization

compared to that of a circular lens module (0.603 m^2). Correspondingly, the $/$m^2$ cost associated with the balance of the installed array, e.g., support structure, tracking, installation is reduced by 27%. The concentrator module FOB factory price, on the other hand, is increased by about 10% due to the increase in module component costs with increasing aperture area. Thus, the net impact by going with a square lens design is a reduction of 20% in total array installed costs.

For the various module configurations considered in the study, the array total installed costs range from $275 to $335/$m^2$ aperture of square lens module. Table 6 shows the component cost ranges considered and their relative cost contributions. As expected, the cell receiver assembly is the major contributor to the module cost followed by the Fresnel lens. On the other hand, the heat sink cost is only 4% of the total array installed cost, thus, it will pay to increase the heat sink mass and achieve higher energy output without significantly increasing the energy cost. This trend is further illustrated in Figure 8 by the fact that the array energy cost becomes rather insensitive to the changes in heat sink parameter values beyond their optimum.

Table 6. Array Total Installed Cost Breakdown

- SQUARE LENS
- 1980 $

COMPONENTS	$/$M^2$	% TOTAL	VARIABLES
LENS	20	7	6"-12" SQ LENS
MODULE HOUSING	9 - 14	3 - 5	6"-12" SQ LENS
SOLAR CELL ($1/$CM^2$)	24 - 69	8 - 23	2000X-500X w/12" LENS
CELL MOUNT SUBASSEMBLY	22 - 65	7 - 22	
HEAT SINK	10 - 12	4	2000X w/12" LENS TO 1000X w/6" LENS
ELECTRICAL HARNESS	0.6 - 1.5	1	
OTHERS:			
TRACKING & CONTROL	34	11	
MODULE SUPPORT STRUCTURE	24	8	
SHIPPING & INSTALLATION	124	41	
TOTAL	275 - 335	100	

The array energy cost for the optimum square lens module design is indicated in Figure 10. With the baseline design characteristics and cost assumptions used in the study, the installed array energy cost is $1.62/ave watt. There are several areas of potential improvement that can be realized for further reduction in the energy cost. With a somewhat relaxed construction code and reduced wind loading design requirements, the array installation cost which is approximately 40% of the total installed cost may be able to be reduced. The array performance, on the other hand, can be increased by using higher efficient cell, i.e., 28 - 30%. Such a cell could be the advanced back surface grooved concentrator cell currently under development for SERI by Microwave Associates'. The net effect of these improvements potentially could result in an installed cost of $250/$m^2$ and performance of 220 W_p peak output/m^2 and annual energy output of 570 kWh/m^2. The net effect would be on installed $ per adjusted watt rating of approximately $1.00.

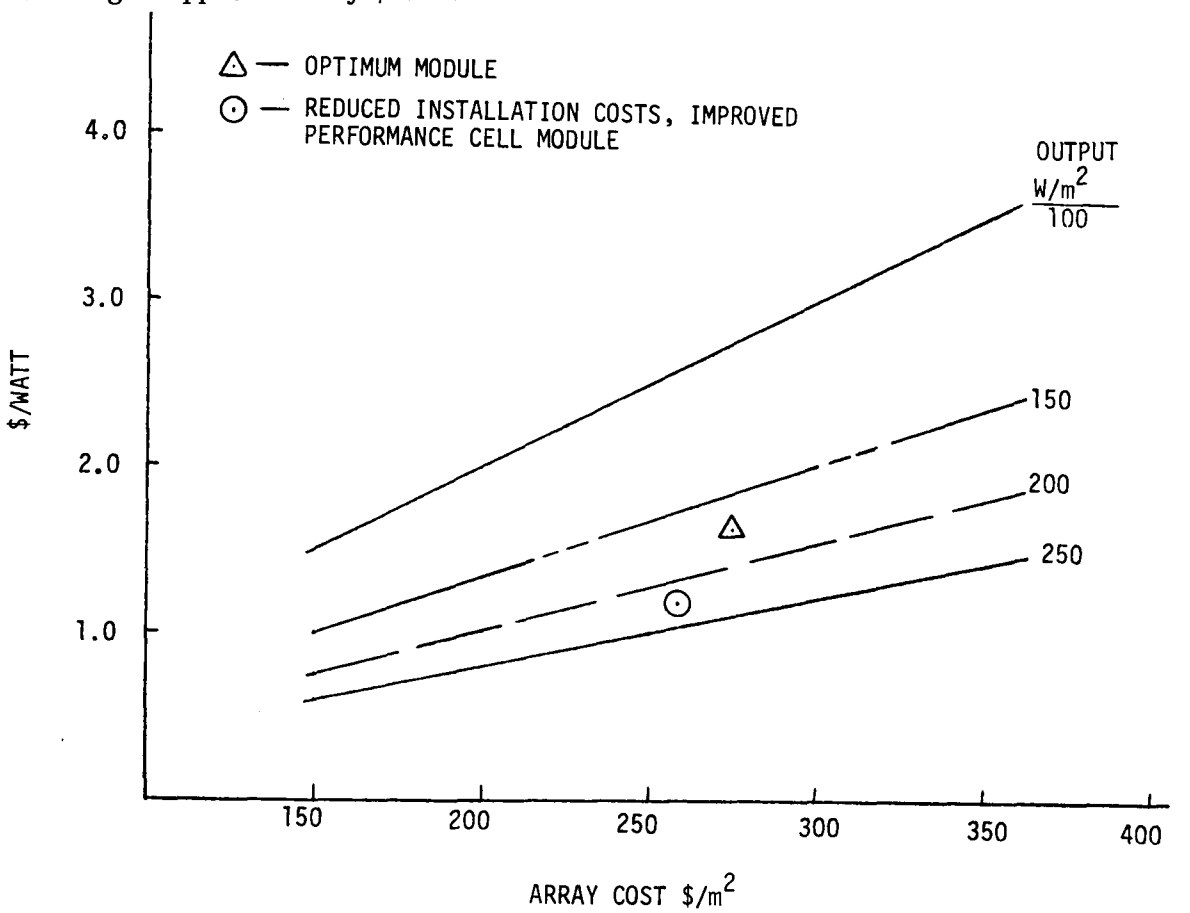

Figure 10. Array Energy Costs

2.2 LENS DESIGN

Two different lens designs were investigated. A prototype lens was designed and developed to focus onto the selected Microwave Associates' EMVJ cell. In addition, the prototype lens had to be compatible with existing direct diamond cutting equipment. These two factors resulted in the development of a seven inch diameter circular domed lens. The configuration drawing for this lens is shown in Figure 11.

To provide insight into a more production oriented lens an analysis was performed for a square domed lens. The configuration drawing for this lens is shown in Figure 12.

A design comparison summary for the prototype and square lens is provided in Table 7. The balance of this subsection describes lens background information, design criteria, description and analysis results.

2.2.1 BACKGROUND

The advantages of using deeply domed Fresnel lenses for photovoltaic concentrators has been known for several years. The benefits of such concentrators were originally discussed in a paper written by Optical Sciences Group in 1975, which included a study conducted by Ball State University, Muncie, Indiana. (Reference 5, 6.) Several cylindrically curved linear Fresnel lenses are currently being used in concentrator systems. The use of circularly symmetrical domed Fresnel lenses in photovoltaic systems has been discussed in detail in several papers written jointly by Optical Sciences Group and Varian Associates. The use of curved grooves for photovoltaic concentrators, was demonstrated as part of the Phase I effort of the PRDA-35 Program, in which OSG participated as a subcontractor to Varian Associates.

2.2.2 DESIGN CRITERIA

There are four major areas to be considered in designing solar concentrators. These areas are: transmission, or the efficiency of the concentrator; uniformity of the intensity distribution

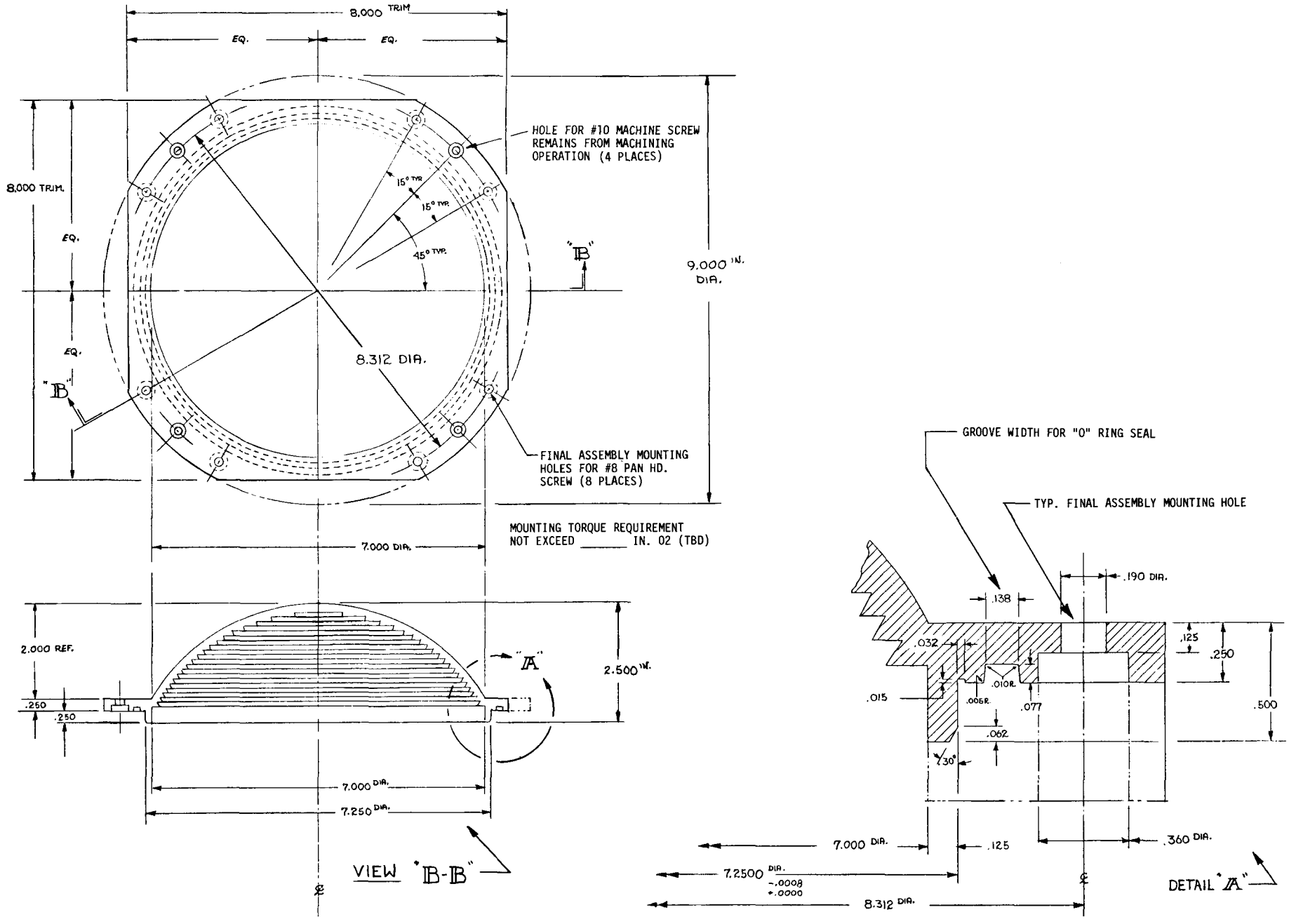

Figure 11. **Prototype Circular Domed Fresnel Lens - Final Assembly Configuration**

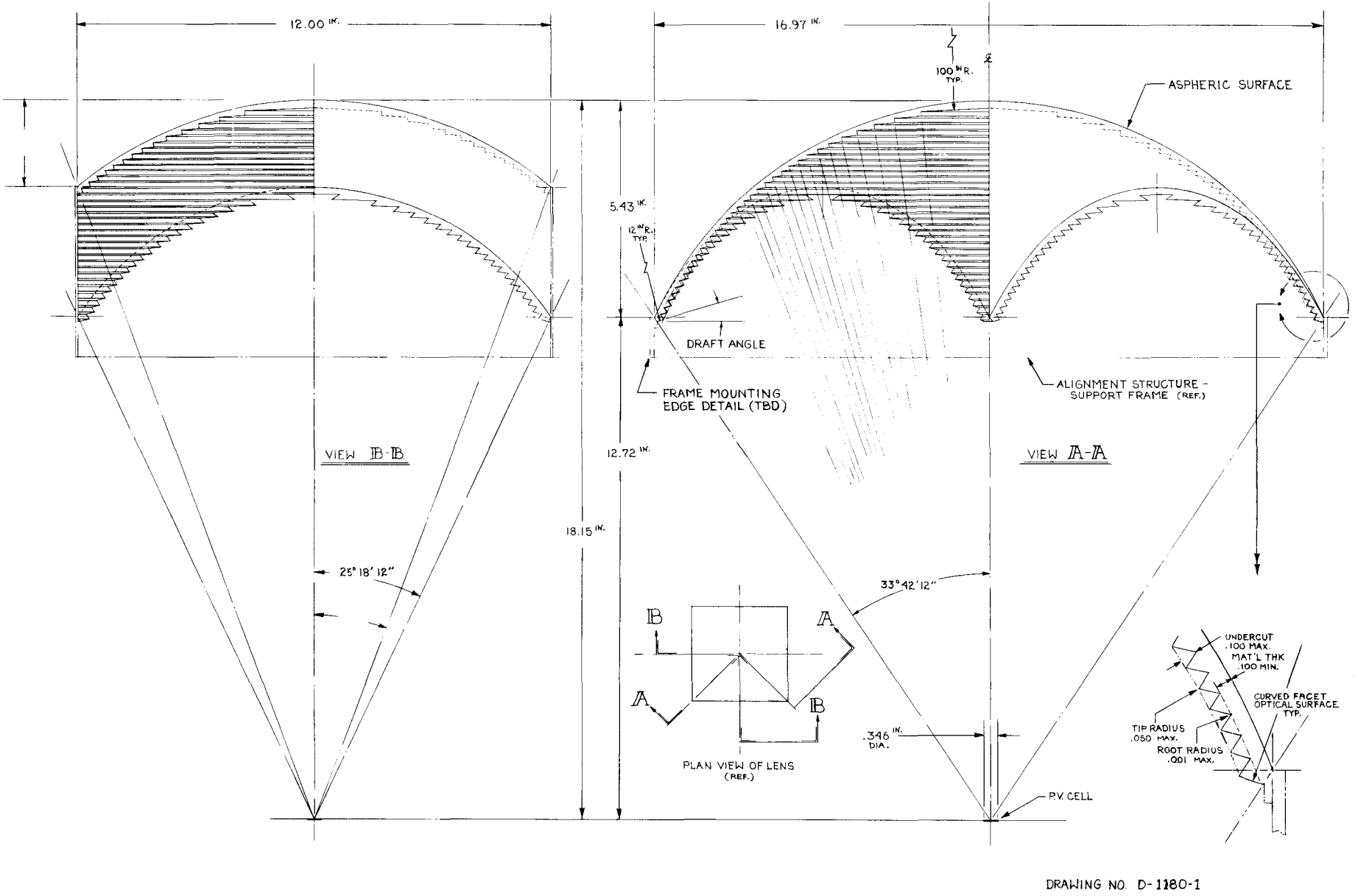

Figure 12. **Square Domed Fresnel Lens - Clear Acrylic Material**

Table 7. Lens Design Summary

PARAMETER	PROTOTYPE	PRODUCTION SQUARE LENS
GEOMETRY	CIRCULAR, 7" DIA.	SQUARE 11.5"
F/#	0.75	0.5
SPOT SIZE	0.20"	0.32 - 0.38"
THEORETICAL TRANSMISSION	0.89	0.90
GEOMETRICAL CONCENTRATION RATIO	1200	1200 - 1600
EXPECTED TRANSMISSION	0.83 - 0.85	0.83 - 0.85
INPUT REFRACTION FRACTION	0.70	0.65 - 0.80
FOCAL DISTANCE	5.25"	8.50"
DOME HEIGHT	2.17"	4.8"
PEAK TO AVERAGE	1.60	< 2.0
APEX TO CELL DISTANCE	7.42"	14"
ASSUMED GUARD BAND	12%	12%
0% LOSS TRACKING POINT	$\pm 0.23^{o}$	$\pm 0.19^{o}$
10% LOSS TRACKING POINT	$\pm 0.54^{o}$	$\pm 0.38^{o}$
THICKNESS	0.25"	0.100"
MATERIAL	ACRYLIC (V045 ROHM & HAAS)	ACRYLIC (V045 ROHM & HAAS)
FLANGE GEOMETRY	SQUARE 1.0"	SQUARE 0.10"
ATTACHMENT	MECHANICAL	BONDED
MANUFACTURING TECHNIQUE	DIRECT CUT	INJECTION MOLDED

on the photovoltaic cell; minimum spot size that can be produced; and sensitivity to angular errors introduced into the concentrating system.

1. Transmission or Lens Efficiency. In refracting systems such as domed Fresnel lenses, the transmission is maximized when the angles of refraction at each surface of the lens are kept to a minimum. Other than minimizing the incidence angles, the only additional way to reduce reflection losses is to put an anti-reflective surface or coating on the Fresnel lens. At this time, the cost of coating or imparting an anti-reflective surface on Fresnels is extremely high. In addition, anti-reflective coatings

on plastic surfaces are not durable enough to withstand the environmental conditions imposed upon solar concentrators. Thus, the only design tool for optimizing the transmission of refracting systems is to minimize the angles of refraction at both surfaces of the lens.

2. Uniformity of the Intensity Distribution Across the Solar Cell. The efficiency of photovoltaic systems is highly dependent upon the uniformity of the intensity distribution of the light striking the solar cell. The intensity distribution must be tailored to the specific cell design. In most cases, the intensity distribution required is extremely flat over the entire diameter on the cell.

3. Minimum Spot Size. For extremely high concentration photovoltaic systems, the cell is to be kept to the smallest possible diameter. The concentration ratio that is obtainable will depend directly on how well the optical concentrator can perform. In refracting concentrating systems, the desire to keep the intensity distribution extremely uniform and the necessity to keep the spot size as small as possible for extremely high concentration systems, are often not compatible. A balance between uniform intensity distribution and minimum spot size, must be obtained.

4. Angular Error Insensitivity. The less sensitive that the optical system is to angular deviations such as those resulting from the finite sun size, tracking errors, and structural tolerances, the more desirable that optical system is for photovoltaic concentration applications.

2.2.3 CURVED GROOVE DOMED FRESNEL LENS DESCRIPTION

A curved groove domed Fresnel lens is amenable to optimization in all of the areas described above for photovoltaic concentrator applications. In addition, it has the potential advantages of being lightweight, low cost, and durable under outdoor environmental conditions. Thus, for extremely high concentration photovoltaic applications, the curved groove domed Fresnel lens appears to be the best alternative as a concentrator. Flat Fresnel lenses used as solar concentrators have been used in the grooves down (grooves toward cell) configuration. The main reason for their use in this particular configuration has been to optimize the transmission of the lens. In order to keep the efficiency of the lens high, domed Fresnel lenses, with grooves facing the cell, must be produced with negative clearance angles (undercuts). Without these undercuts, losses, as shown in Figure 13, would occur as light was scattered off of the relief surfaces. This criteria (having undercut grooved surfaces) presents difficult manufacturing problems. But as can be seen in Figure 14, without these undercuts the transmission loss from such a domed Fresnel lens would be far greater than could be tolerated in a photovoltaic concentrator system. Transmission losses can also be minimized by

using single point diamond turning technology to generate curved groove facets. By producing Fresnel facets that are curved, i.e., with focusing power, each individual facet can be increased in size, thus minimizing the number of peaks and valleys where light can be lost, as shown in Figure 15. The benefits of such curved groove lenses has already been demonstrated with the lens produced by Optical Sciences Group for a Varian Photovoltaic concentration system using a galium arsenide solar cell. This system achieved a 3 to 4% increase in transmission over a comparable flat grooved concentrator.

The benefits of using curved groove domed Fresnel lenses to achieve the design criteria of uniform intensity distribution, small spot size, and insensitivity to angular errors, can best be described by analyzing the aberrational problems of refracting optical systems, and how those aberrations can be controlled by using domed Fresnel lenses with curved grooves.

When designing solar concentrators, spherical aberration must be corrected in order to minimize the spot size produced by the concentrator. Correcting for spherical aberration in Fresnel lenses is a simple matter of designing the grooves properly; but, a lens corrected for spherical aberration will have a very peaked energy distribution. Thus, the precise design for solar concentrators is slightly different from that of a conventionally spherically corrected lens. Again, the required general aspheric surface can be easily approximated with a Fresnel lens. Using a flat Fresnel lens, the design freedoms available are used up in trying to correct for spherical aberration, i.e., getting a small spot size with uniform intensity.

Coma is one of the most significant aberrations not corrected with flat Fresnel lenses. This aberration causes two major problems in designing Fresnel lenses for photovoltaic applications. First, the tracking of the system must be extremely accurate because rays striking the lens as little as 0.1^{o} from normal will cause a significant increase in spot size due to coma. Second, the sun's finite size introduces rays that strike the lens at larger angles than 0.1^{o} thus, even on axis, a significant amount of coma or blurring of the image is introduced. A domed Fresnel lens that is designed to satisfy the sine condition can minimize or eliminate the effects of coma. Angular errors up to 0.5^{o} are tolerable with little change in spot size for domed Fresnel lenses designed to minimize coma. This decrease in sensitivity to angular errors is one of the most important benefits of domed Fresnel lenses - resulting in the ability to have higher

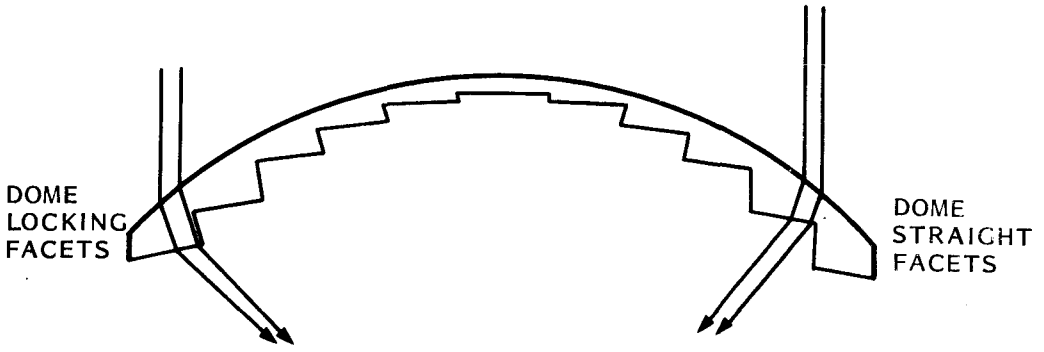

Figure 13. Locking (Undercut) Facets are Required to Avoid Light Loss (Rays Market With Stars)

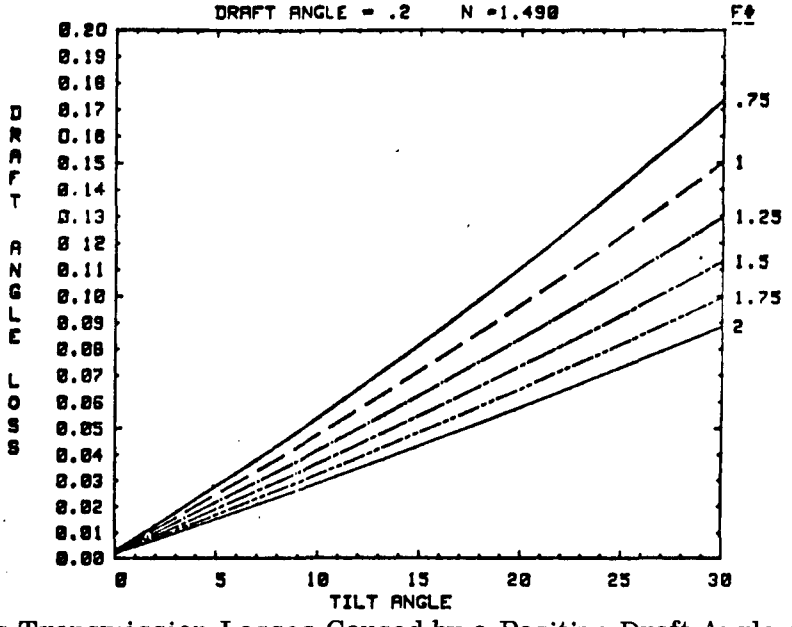

Figure 14. Lens Transmission Losses Caused by a Positive Draft Angle of 0.2 Degrees, as a Function of the Tilt Angle in Degrees at the Edge of a Domed Fresnel Lens. (A Tilt Angle of 0 Degrees Corresponds to a Flat Lens.)

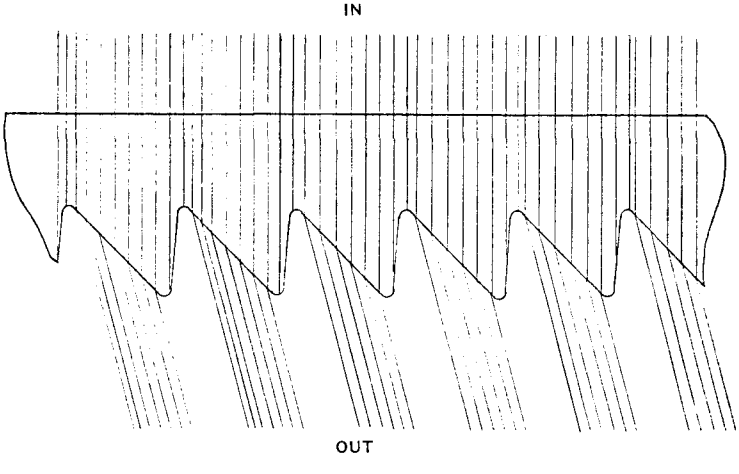

Figure 15. Efficiency Losses Due to Groove Peaks and Valleys for a Flat Grooved Lens

concentration systems as well as less accurate tracking. Thus, in comparison a flat Fresnel lens has a maximum concentration of approximately 550, whereas by doming the Fresnel lens, concentration ratios up to 1500 are obtainable. At the same time, tracking errors up to 0.5^{o} are tolerable with domed Fresnel lenses, whereas with flat Fresnel lenses at 550X tracking must be accurate to 0.1°.

Chromatic aberration (change in focal length with wave length) is also a very significant problem when designing refracting solar photovoltaic concentrators. Because of the dispersion properties of the plastic material used to produce Fresnel lenses, very little can be done to minimize the chromatic aberation of the system. Doming the Fresnel, however, does minimize the refracted angles at each surface, thus reducing the chromatic spread by a small amount. Thus, doming the Fresnel lens has the added benefit of reducing chromatic aberration which is one of the limiting factors on the maximum concentration ratio obtainable with refracting concentrating systems.

For high concentration solar applications the spot size obtainable by flat grooved Fresnel lenses is limited by the width of the grooves since each groove in a flat grooved Fresnel lens is a prism with power to deviate the beam, but no focusing or concentration power. Thus, the width of the groove limits the minimum spot size obtainable. It also restricts the freedom to place the energy from a particular groove to a precise position on the solar cell. On the other hand, if the groove spacing is made small, diffraction effects increase the spot size beyond the physical groove width. By using single point diamond turning technology, wide, curved grooves can be generated. These grooves have radii of curvature which are optimized for the particular location of the groove on the lens. Thus, by curving the grooved surfaces, not only are the limitations of minimum spot size due to finite groove widths removed, but the effects of diffraction are eliminated.

In addition to the aberrational considerations described earlier, the benefits of domed Fresnel lenses used as solar photovoltaic concentrators also include a reduction in part thickness over that used for flat Fresnel solar concentrators. This reduction in thickness will enable the costs of the concentrators to be reduced. Increased structural integrity of domed Fresnel lenses should be much improved over flat Fresnels. The ability to withstand high windloads

and changes in temperature and humidity without causing significant degradation to the system's performance, should be considerably improved for domed Fresnel lenses.

2.2.4 PROTOTYPE LENS ANALYSIS

OSG began its theoretical analysis with information from GE that the desired concentration ratio was approximately 1200 and that the cell design diameter (A.M. 1.5, Si. spectral response) was to be 0.2" in diameter. The above considerations dictated that the lens diameter be approximately 7".

One important lens performance criteria is transmission. Transmission is affected by the lens F-number as well as the degree of doming; net transmission is not significantly affected by changes in concentration ratio in the range of 400 to 2,000. F-number is defined as the focal length (measured from the base of the outer domed surface to the cell plane) divided by the diameter of the lens clear aperture.

Lens doming is characterized throughout this report by an input refraction fraction. Input refraction fraction (INFRA) is defined as the fraction of the total refraction (for a given ray) that occurs at the outer surface of the lens. An INFRA of 1.0 specifies the most steeply domed lens, all refraction is done at the outer surface. An INFRA of 0 specifies a flat lens with all of the refraction done at the inner (grooved) surface. All curves with input refraction fraction 0.7 or above have positive sloping facets which are more easily manufactured. All curves with input refraction fraction 0.6 or less have negative sloping facets which are more difficult to manufacture. Figure 16 shows dome height for various INFRAs.

Figure 17 shows the tradeoffs of transmission versus F-number at various INFRAs. High F-numbers with INFRA = 0.5 specify lenses with the highest transmission, but an important factor relating to manufacturability occurs when INFRA is greater than approximately 0.7. At INFRA less than 0.7 the groove optical surfaces must be negative sloping making eventual mass production using a collapseable core injection mold impassible. Fortunately the sacrifice in transmission at INFRA = 0.7 is only approximately 0.5%, so it was decided to keep INFRA = 0.7. F-number was chosen to be 0.75 as an appropriate compromise between transmission and module housing depth required. Higher F-numbers would give higher transmission but at the

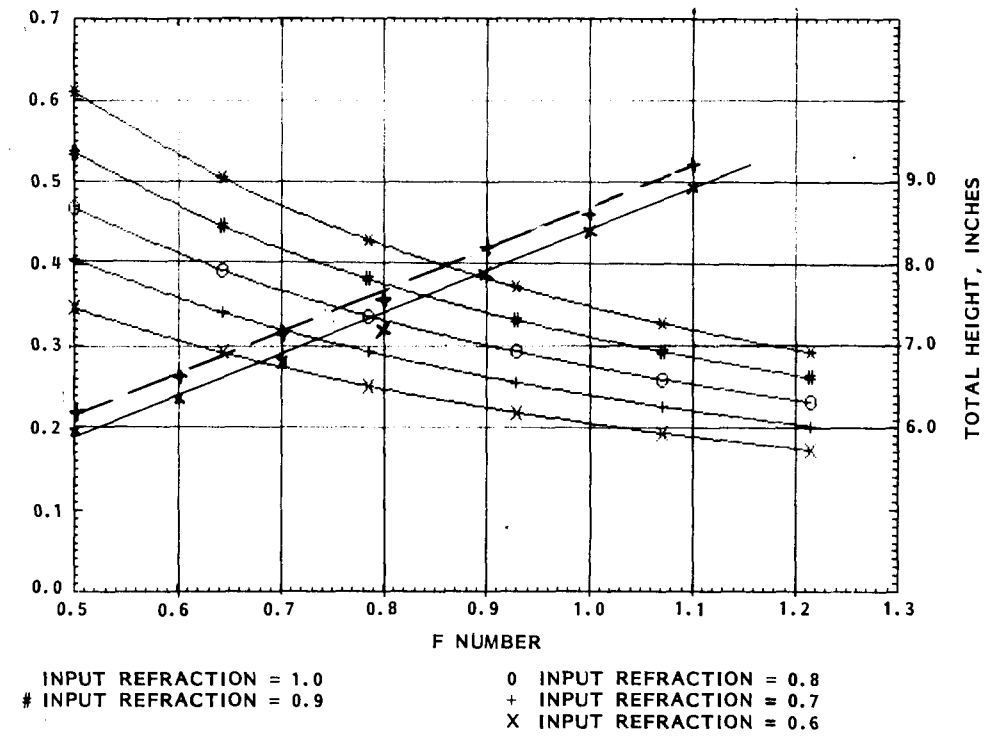

Figure 16. Height of Dome/Diameter of Lens vs F-Number and Input Refraction

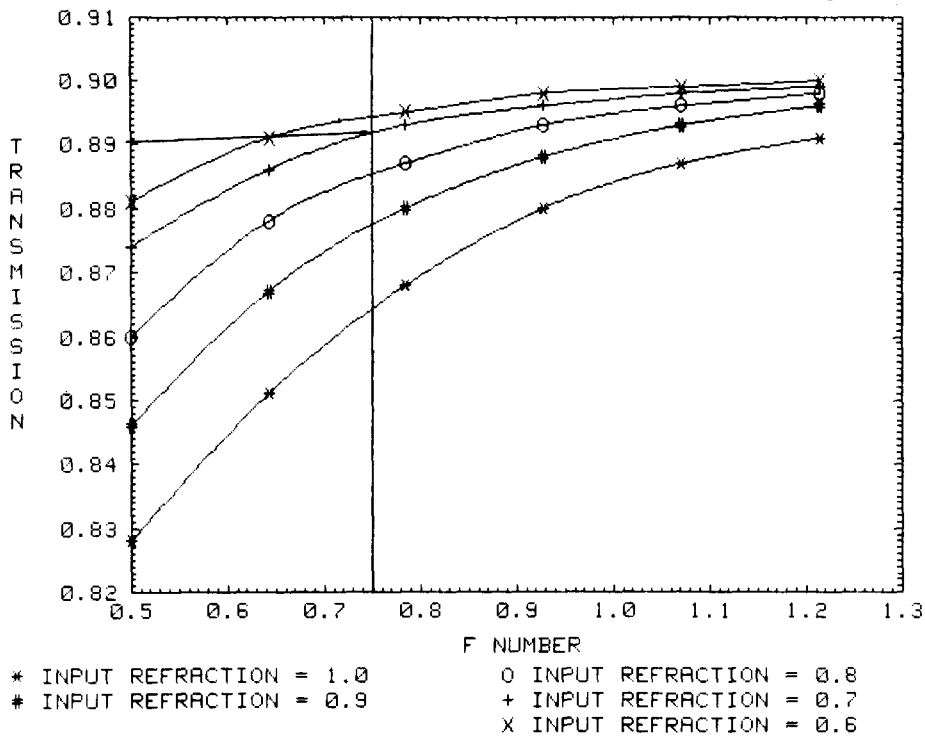

Figure 17. Lens Transmission vs F-Number and Input Refraction

expense of requiring a larger lens to cell distance. For INFRA = 0.7 the sacrifice in transmission at F-number = 0.75, compared to the highest (maximum possible transmission) F-number is approximately 0.6%.

Figure 18 shows peak to ideal flux concentration ratio versus F-number for various INFRA. Ideal concentration ratio assumes a perfectly uniform short circuit current density profile over the cell design area. Ideal concentration ratio is equal to the geometric concentration ratio, or the ratio of lens area divided by design cell area.

At INFRA = 0.7 the uniformith ratio os not at a minimum but is within the preliminary design goal of 2 for peak to ideal concentration ratio.

Figures 19 through 21 show transmission onto the cell versus tracking error for various F-numbers and INFRAs. For the range of INFRAs (0.5 tc 0.8) and F-numbers (0.5 to 0.929) considered tracking error tolerance for a 1% transmission loss is always approximately ± 0.3 degrees, therefore tracking error tolerance is not a strong function of INFRA or F-number.

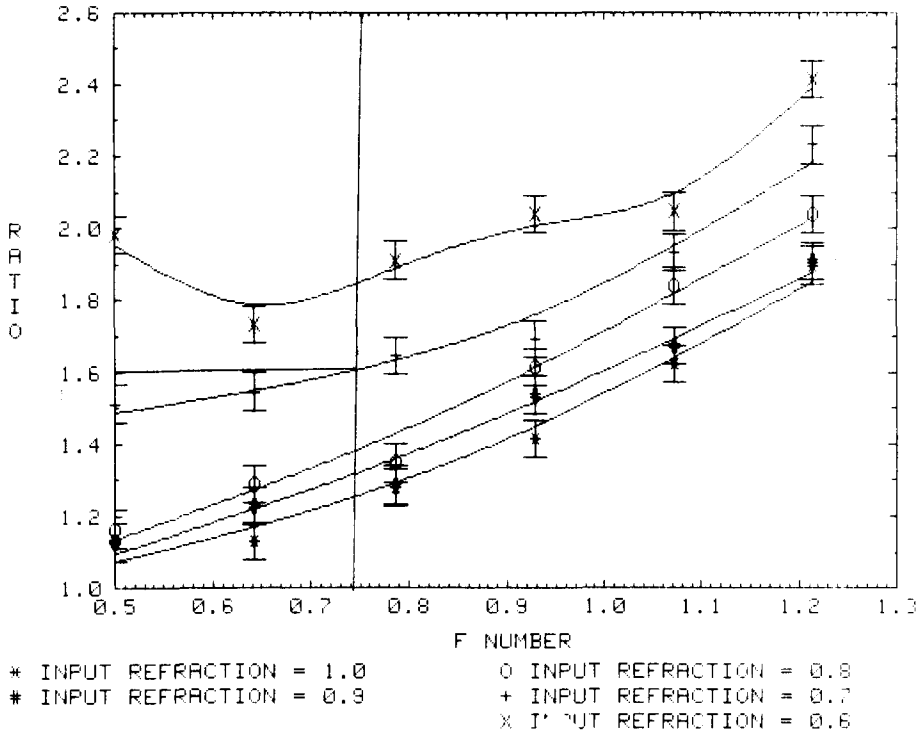

Figure 18. Ratio of Peak-to-Average Flux vs F-number and Input Refraction

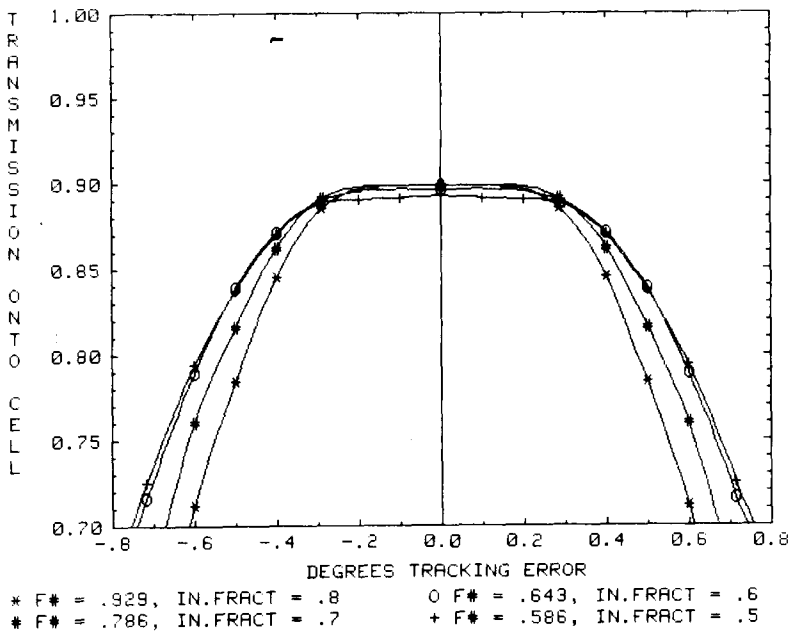

Figure 19. Transmission vs. Tracking Error and Input Refraction

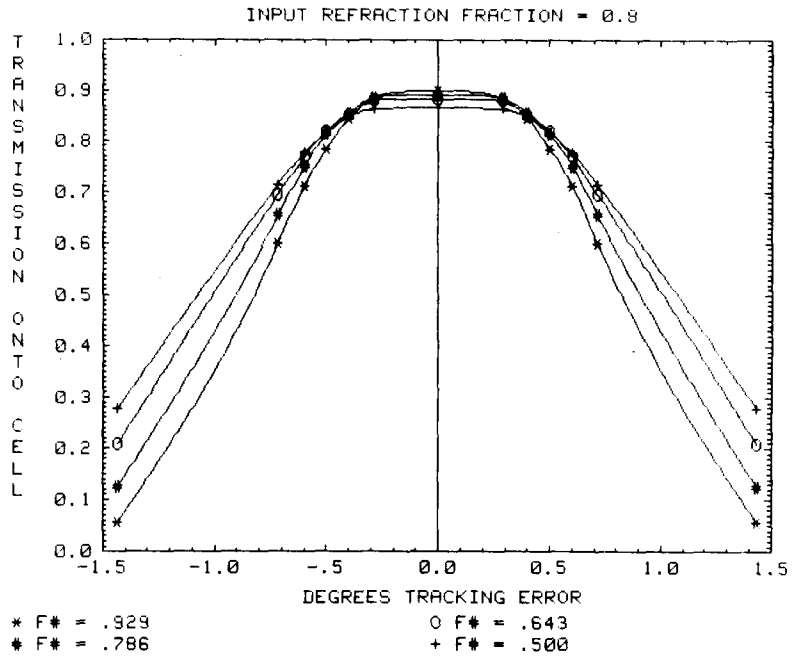

Figure 20. Transmission vs Tracking Error and F-number IN.FRACT = 0.8

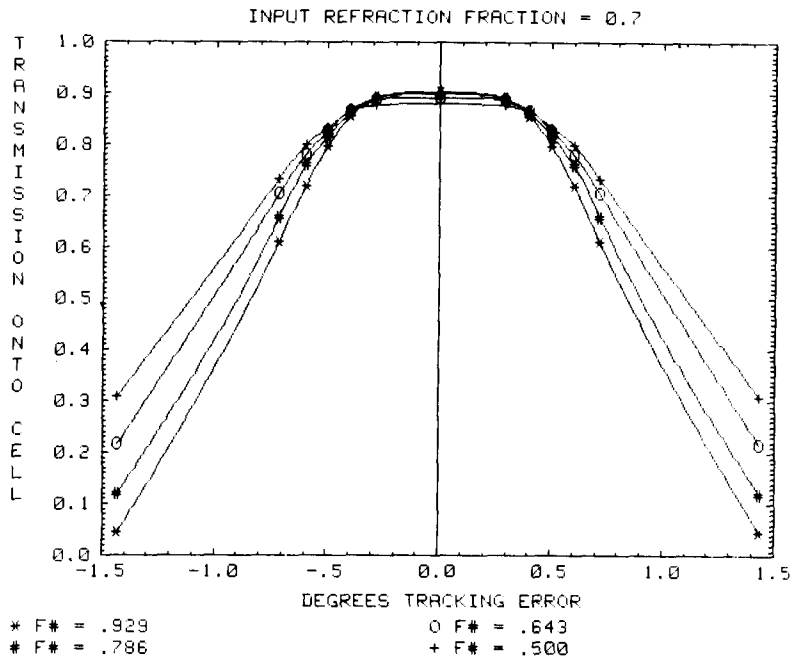

Figure 21. Transmission vs Tracking Error and F-number IN.FRACT = 0.7

This is because of the edge of the theoretical short circuit current density profiles are similar and tracking error is analogous to a shift in the Gaussian image position on the cell.

Lens thickness tolerances were analyzed for thickness variation from the design thickness and the results are plotted in Figure 22. Uniform thickness change of less than 0.025" does not significantly affect transmission. Figure 23 shows the effect of thickness change on uniformity. Error sensitivity to lens to cell spacing errors are shown in Figures 24 and 25. Over a range of spacing errors of $\pm$ 0.05" transmission is not significantly affected. Uniformity is affected, with peak to ideal concentration changing to about 3 for a spacing error of 0.04". Thus, according to the plots the module lens to cell spacing error tolerance should be + 0.010" and greater than - 0.050". However, tracking error sensitivity would be increased at a lens to cell spacing error of - 0.050", so a module lens to cell spacing error tolerance of $\pm$ 0.010" is recommended.

The above data and analysis set the optical design parameters necessary for a final lens design. The above set reasonable values for INFRA = 0.7, F-number at 0.75; lens diameter is 7" with a 0.2" diameter cell size. Expected performance exceeds the design goals.

A scale cross-section drawing of the optics layout is shown in Figure 26. The lens maximum thickness is 0.250", minimum thickness is 0.150". The height of the dome above the top surface of the mounting flange is 2.122". The inner Fresnel surface has eighteen curved facets.

Figures 27 and 28 show the result of a random ray trace of 102400 rays simulating the A.M. 1.5 solar spectrum, angular subtense and angular intensity distribution. Theoretical transmission is 89.6%. Peak to ideal concentration ratio is 2.21.

The plot at the lower right of Figure 27 shows the expected radial distribution of short circuit current density on the cell. Figure 28 is a contour plot of cell short circuit current density; the cell size represented by the outer, circular, edge of the plot is 0.025". Figure 29 shows transmission versus tracking error for the chosen design. As expected from previous analysis tracking error sensitivity is approximately $\pm$ 0.3 degrees for a 1% transmission loss.

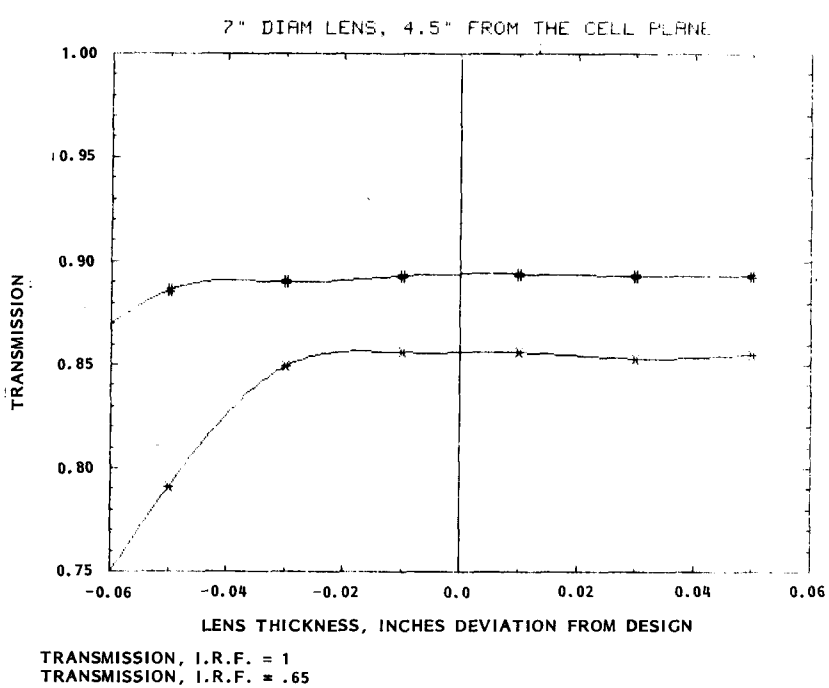

Figure 22. Transmission vs Lens Thickness Variations

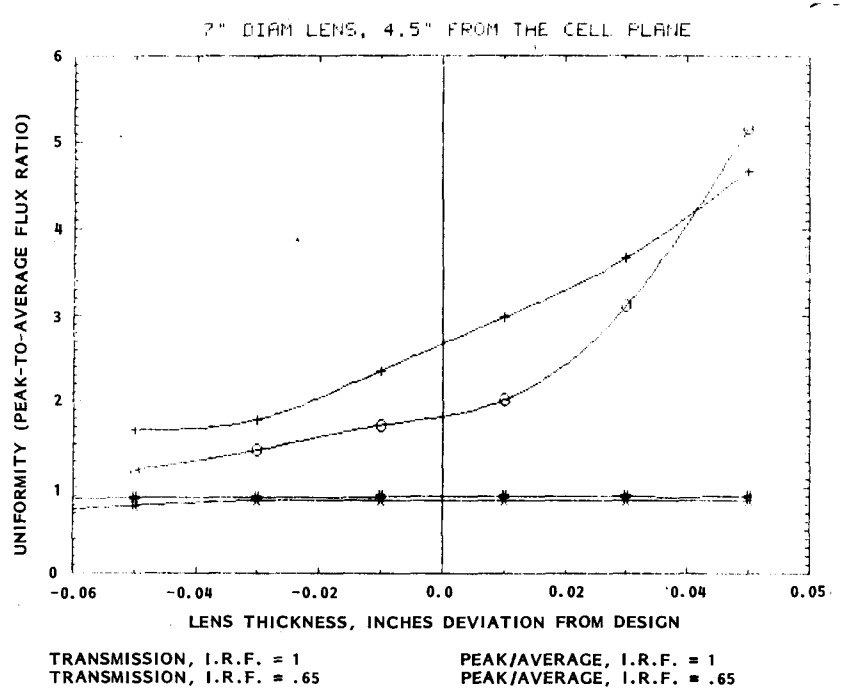

Figure 23. Focused Flux Uniformity vs Lens Thickness Variations

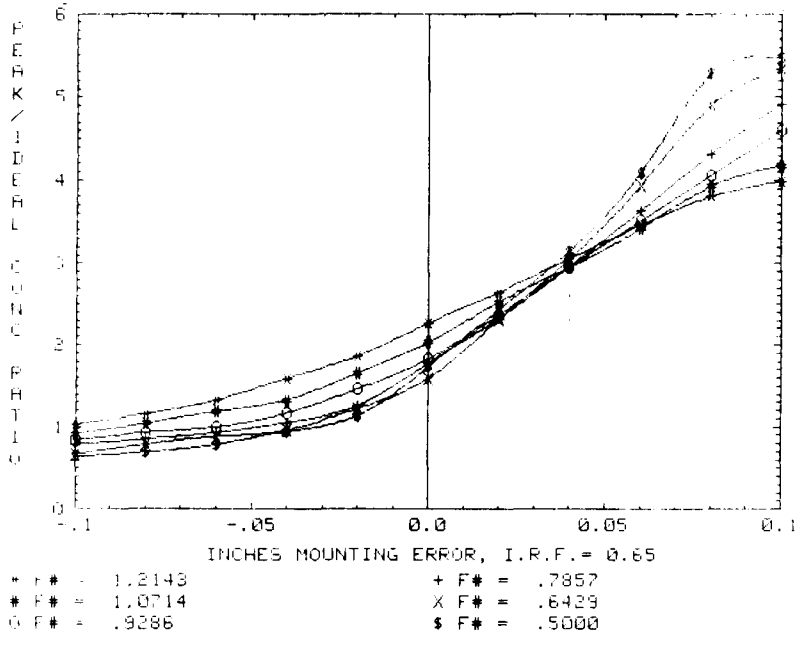

Figure 24. Flux Uniformity vs Lens-to-Cell Spacing Error

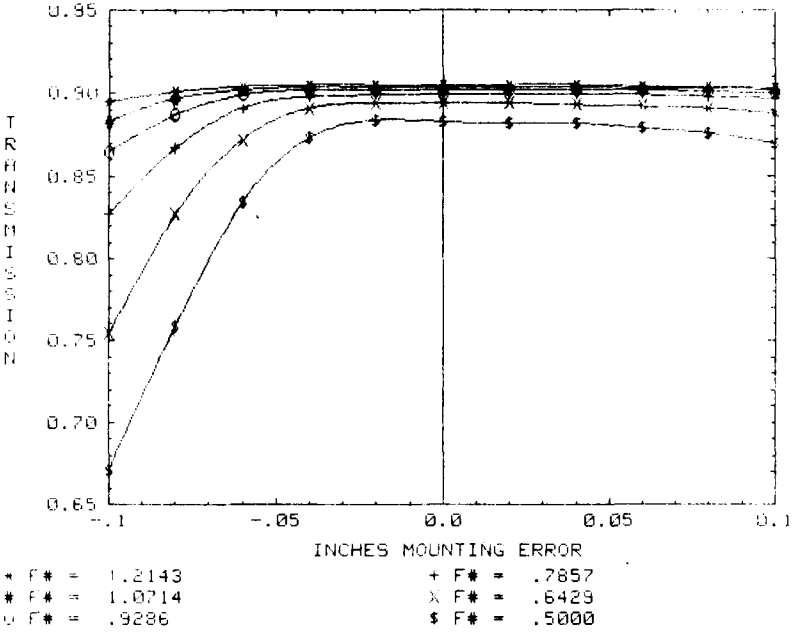

Figure 25. Transmission vs Lens-to-Cell Spacing Error

Both SENSITIVITY TO ERROR IN LENS-CELL SPACING graphs are for the Input Refraction Fraction case of 0.65. Changes in I.R.F. would produce only very minor changes in the shapes of the curves, although their magnitudes would change as indicated on the other curves for the zero mounting error case.

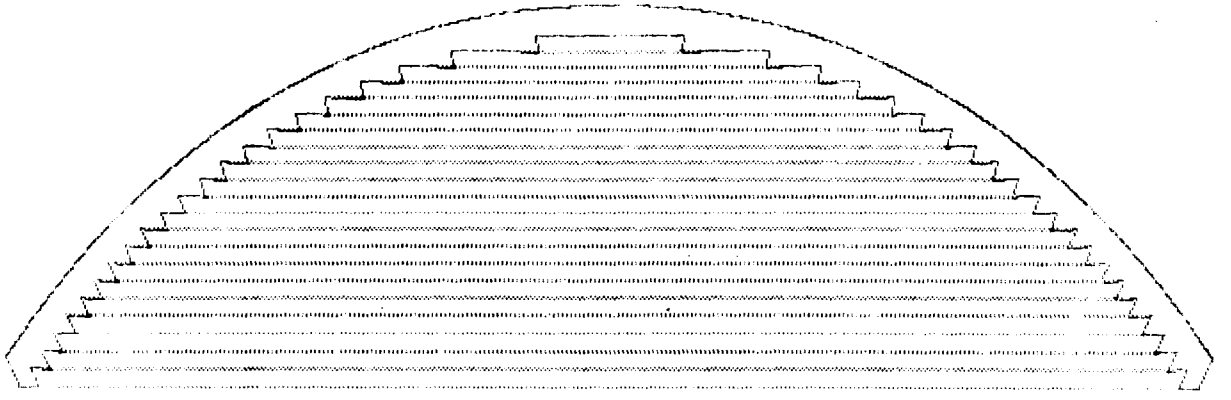

CELL

2.039 in. DOME HEIGHT
6.539 in. TOTAL HEIGHT

Figure 26. Scale Cross Section of Optics Layout

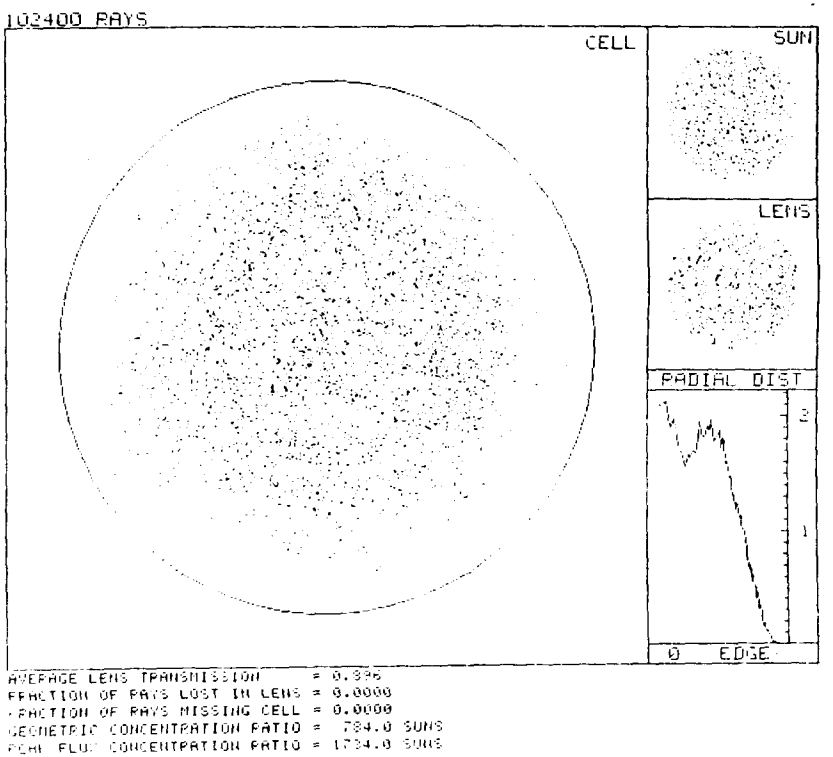

Figure 27. Lens Ray Trace Results

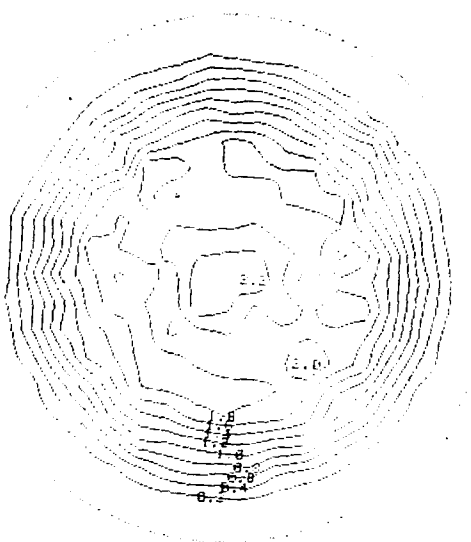

Figure 28. Contour Plot of Cell Short Circuit Current Density

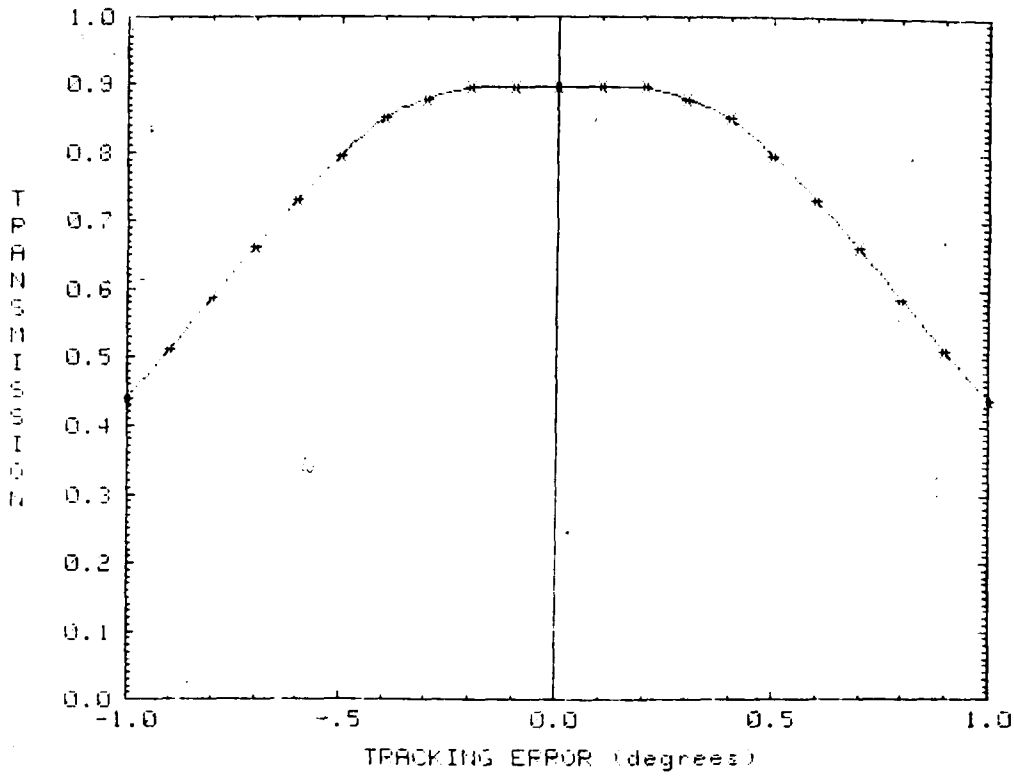

Figure 29. Tracking Error Sensitivity for Chosen Design

2.2.5 SQUARE LENS ANALYSIS

OSG studied the theoretical performance of a square aperture domed lense. Figures 30 through 33 show total transmission versus tracking error, F-number, lens-to-cell plane distance, input refraction fractions and concentration ratios. As shown, there are only minor differences in transmission and tracking error tolerance between the circular and square aperture domed lenses. The effect of the square aperture configuration on irradiance uniformity on the cell plane was not calculated.

2.3 EMVJ CONCENTRATOR CELL

Per the program groundrules no cell development was to be undertaken. Accordingly a survey was made of available high concentration solar cells. Basically, two types of cells are currently available, GaAl AS and vertical groove silicon. Early in the program it was decided to utilize Microwave's Associates' EMVJ silicon cell. The balance of this subsection describes this cell technology.

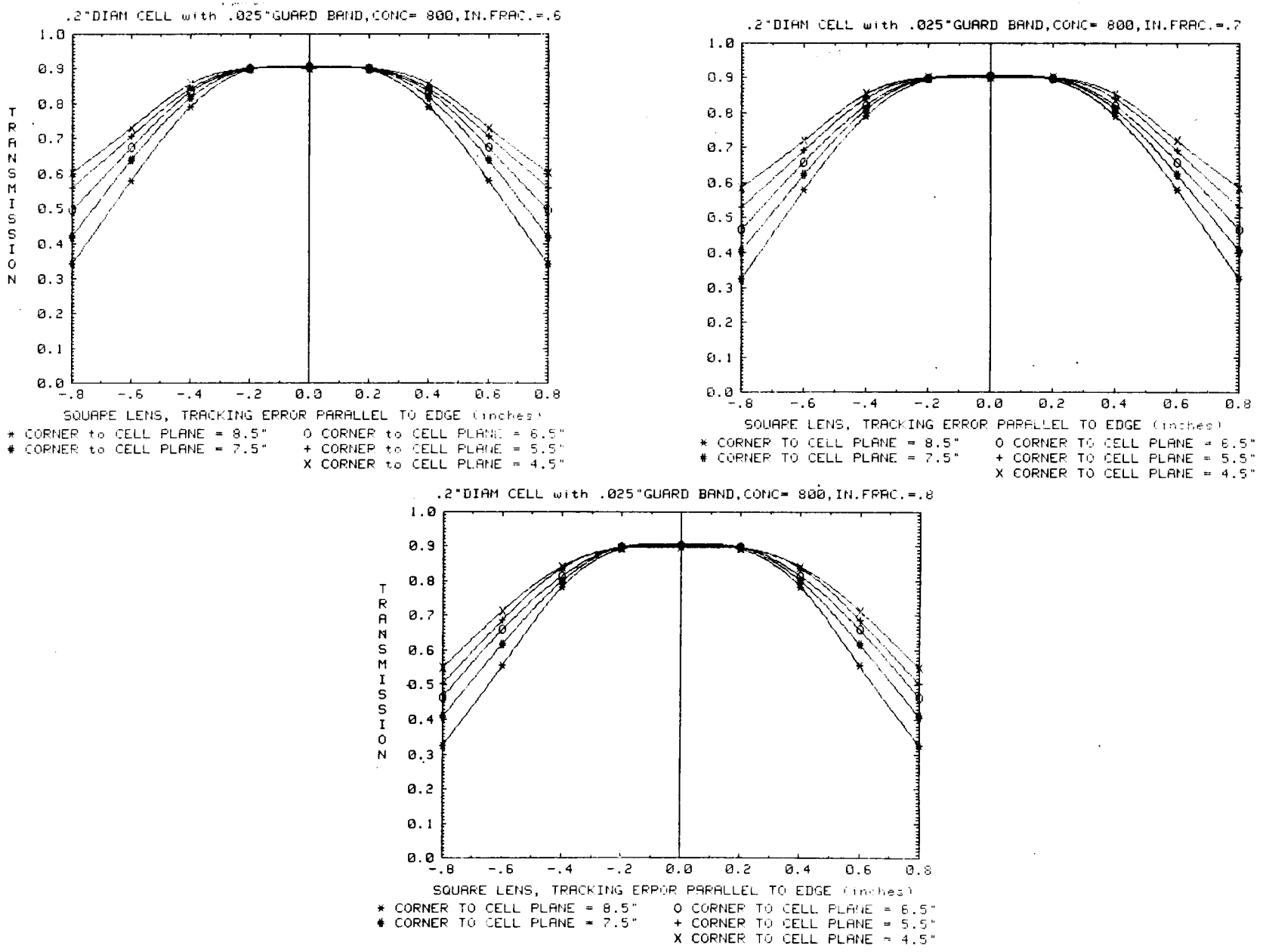

Figure 30. **Transmission vs. Tracking Error, Lens-to-Cell Spacing and Input Refraction for 800X Lens**

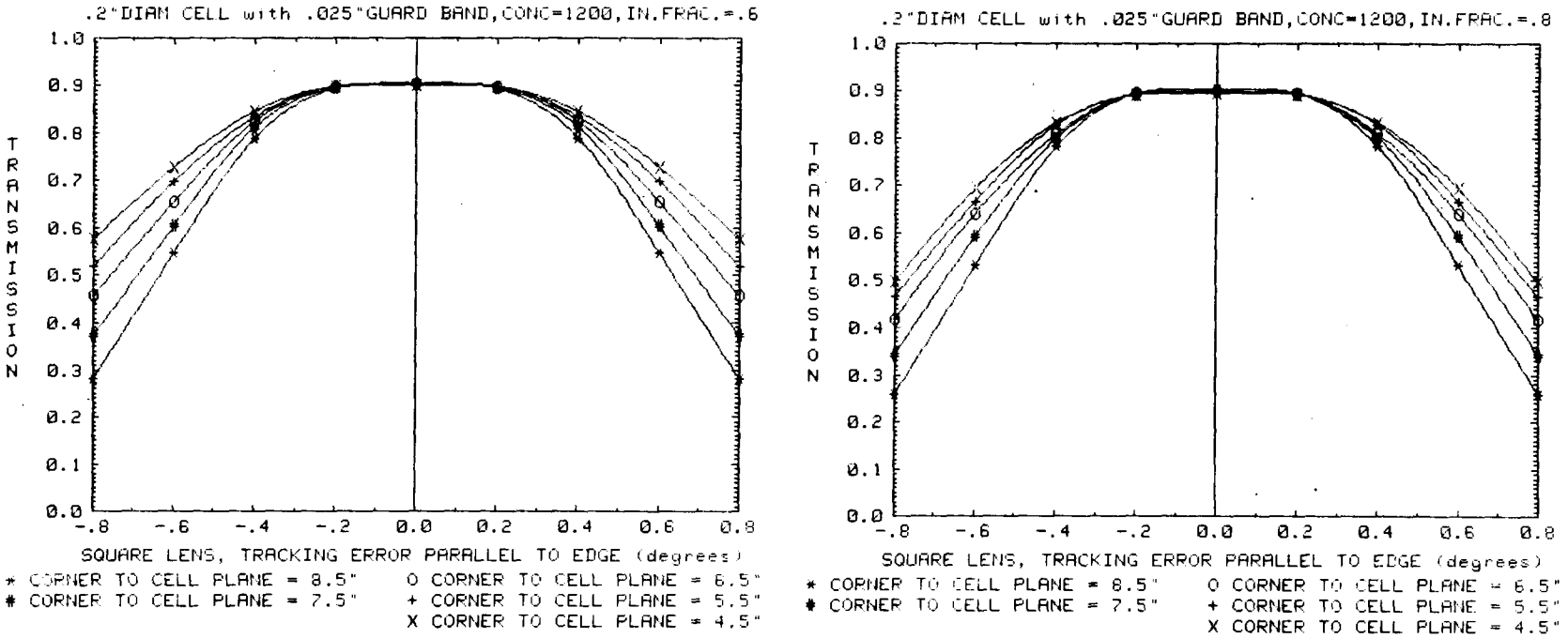

Figure 31. Transmission vs Tracking Error, Lens-to-Cell Spacing and Input Refraction for 1200X Lens

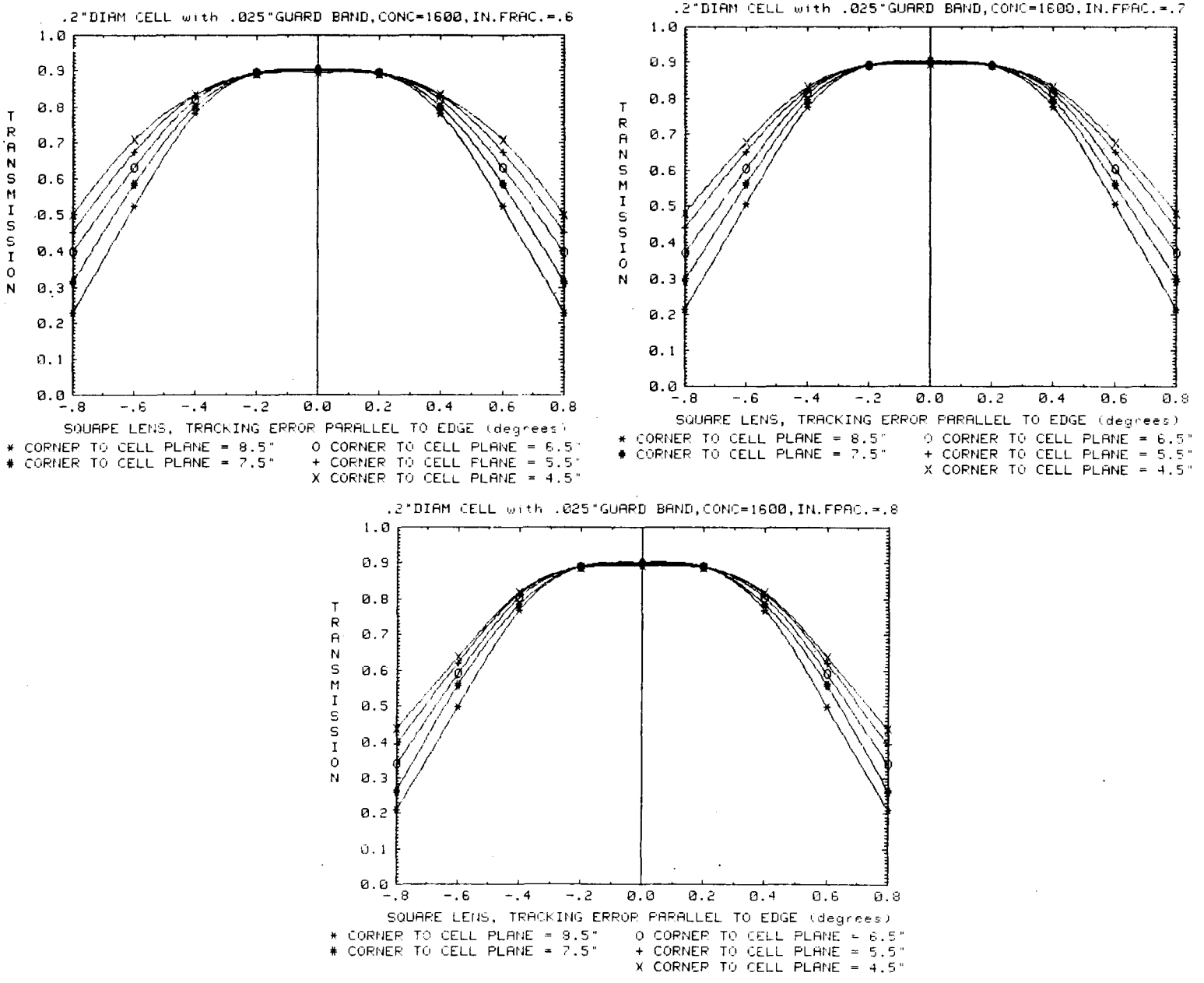

Figure 32. **Transmission vs Tracking Error, Lens-to-Cell Spacing and Input Refraction for 1600X Lens**

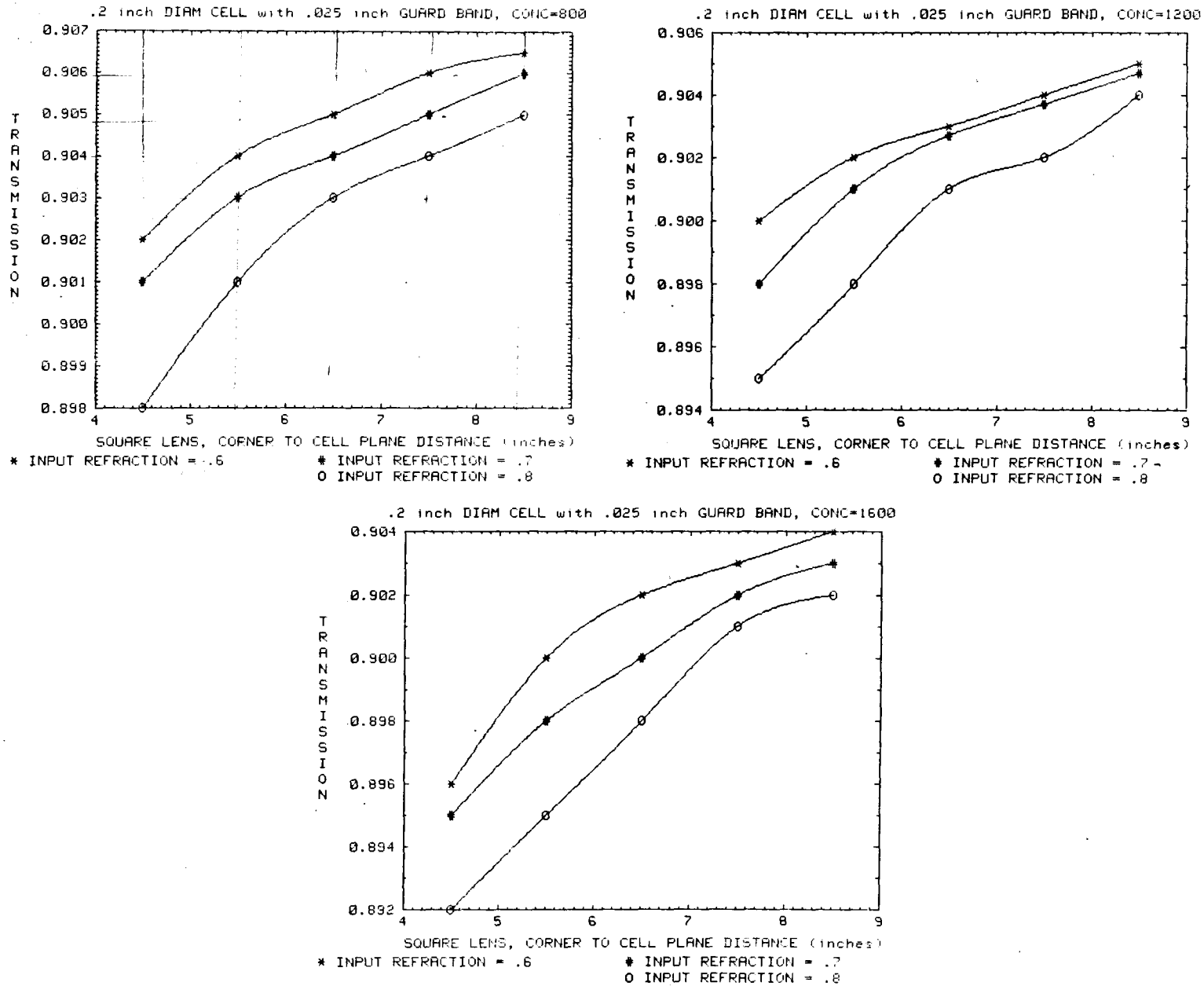

Figure 33. Transmission vs Concentration and Other Lens Parameters

2.3.1 BACKGROUND

The initial experience basis for the EMVJ cell was a three year high concentration photovoltaic collector study conducted at the Massachusetts Institute of Technology (MIT). The MIT project studied photovoltaic collectors using mirror reflectors having concentrations of 200 - 500 suns and silicon photocells having geometry of multiple junctions which provided a means of obtaining high efficiency. The MIT high-intensity photovoltaic cell work was based on the use of single crystal silicon. It was recognized at the outset that high intensity operation could provide major increases in efficiency (up to 50% increase as intensity is increased to 1000 suns), if series resistance could be sufficiently reduced and the cell adequately cooled. Thus, the conventional horizontal junction cell was not investigated because of its inherently high series resistance, which results in large internal voltage drops at high intensity operation.

The original high-intensity work focused on the vertical multi-junction edge-illuminated cell, Reference 7, which we refer to as the "sintered" cell because it was fabricated by sintering a number of silicon wafers containing p+ and n+ surface diffusions, with aluminum foil placed between the wafers, and then slicing through the resulting stack. The resulting structure had a number of p+/n junctions connected together in series, with the light incident orthogonal to the junction axes, so that light traveled essentially parallel to the junction planes. This structure had a low series resistance, since current traveled directly through (normal to) the plane of the junction and had some other attractive features, but had a number of inherent problems, such as difficulty in adequately passivating the light receiving surface, difficulty in reducing cell thickness, cooling problems, etc.

To summarize the most important results of this work, it was found that internal series resistance, the most serious problem with conventional horizontal junction devices operated at high intensity, can be reduced to negligible proportions in the orthogonal devices by appropriate configuration. Further, with these devices V_{oc} increases, as a function of intensity, at the rate of $\sim$ 0.1 V/decade to about 1000 suns, Reference 8 (with adequate cooling), the fill factor (FF) increases with increasing intensity, and J_{sc} is linearly proportional to the incident intensity. Thus, the efficiency, η, increases with increasing intensity up to the limits of the measurements made and in the absence of significant heating effects. In addition, J_{sc} is

essentially independent of temperature (0 - 100°C) at all intensities measured, while both dV_{oc}/dT and Dff/dT decrease at a significant rate with increasing intensity.

2.3.2 SELECTED CELL DEVELOPMENT

Building on the MIT study data base single crystal silicon cells were fabricated which had a new structural form. These cells took advantage of the above-noted beneficial effects of high intensity, and had a higher efficiency than any of the test devices. They were fabricated using standard microelectronic techniques; the fabrication process lends itself readily to mass production procedures and the basic structure lends itself to a large variety of configurations - providing a great deal of flexibility. The key process step involved anisotropic etching of narrow grooves into the crystal-wafer, and the structures were distinguished by the incorporation of multiple, "vertical" junctions (i.e., with the p-n junction axis orthogonal to the incoming light axis). They are conveniently referred to, therefore, as Etched Multiple Vertical Junction (EMVJ) devices, Reference 9.

Many cells are made from one silicon wafer. These preliminary cells were not optimized, since they were fabricated to demonstrate feasibility of the design and fabrication concepts, and to allow the determination of both the present and potential efficiency of this structure. These devices have a directly measured AM1 efficiency of:

Efficiency (without AR Coating)	Intensity
13 %	1 sun
18 %	100 suns
19 %	300 suns

Figure 34 is a one sun I-V curve for an experimental device about 0.3 cm X 0.4 cm, consisting of 18 "unit cells" connected in series, with a V_{oc} of ~ 9.6 volts, (at one sun and 25°C). Figure 35 shows, η, V_{oc}, and FF as a function of intensity for a device with only one "unit cell" connected electrically. The decrease in η beyond 300 suns was due to heating, as verified by pulsed measurements, and was due to the relatively simple cooling scheme that had been used in these test units, consisting simply of water flowing directly over the base of the cell. For these cells, dV_{oc}/dT decreased from - 2.1 mV/°C at one sun to - 1.6 mV/°C at 300 suns.

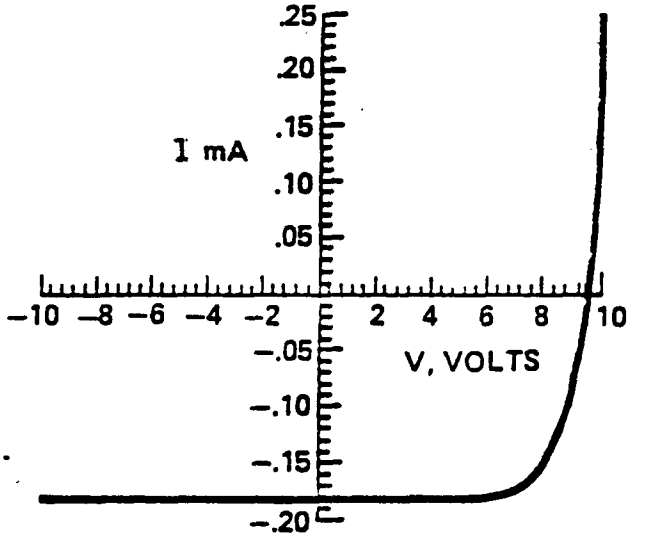

Figure 34. Curve of an 18 Junction EMVJ Cell, ~ 0.3 X 0.4 CM, at one Sun and 25°C

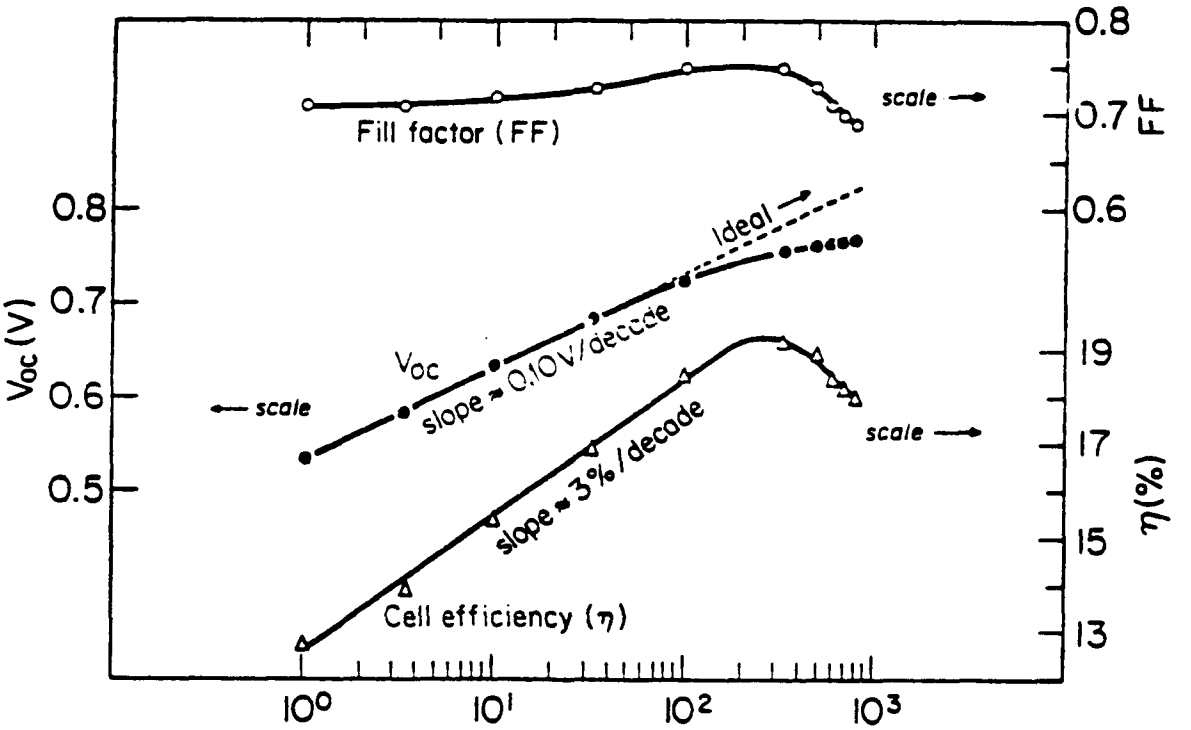

Figure 35. Experimental Test Results from 1 to 800 Suns for the EMVJ Structure of Figure 5, with only one Unit Cell Electrically Connected to the External Contacts.

Under a contract with Sandia Laboratories, M/A is now investigating simplified versions of the EMVJ cell, designed for operation in the range of 500 to 1200 suns. These structures have all the junctions connected in parallel through the use of a plated contact metalization, which eliminates a number of photolithography steps, and the cells are intended to be soldered directly to a heat sink. Under this program M/A has implemented a new structure shown in Figure 36 and a new metallization scheme. The effect of using various silicon base resistivities is also being investigated in order to optimize the carrier lifetime versus base resistivity tradeoff. In addition, M/A is using AR coatings and improved processing techniques in order to assure consistently longer carrier lifetimes with minimum series resistance.

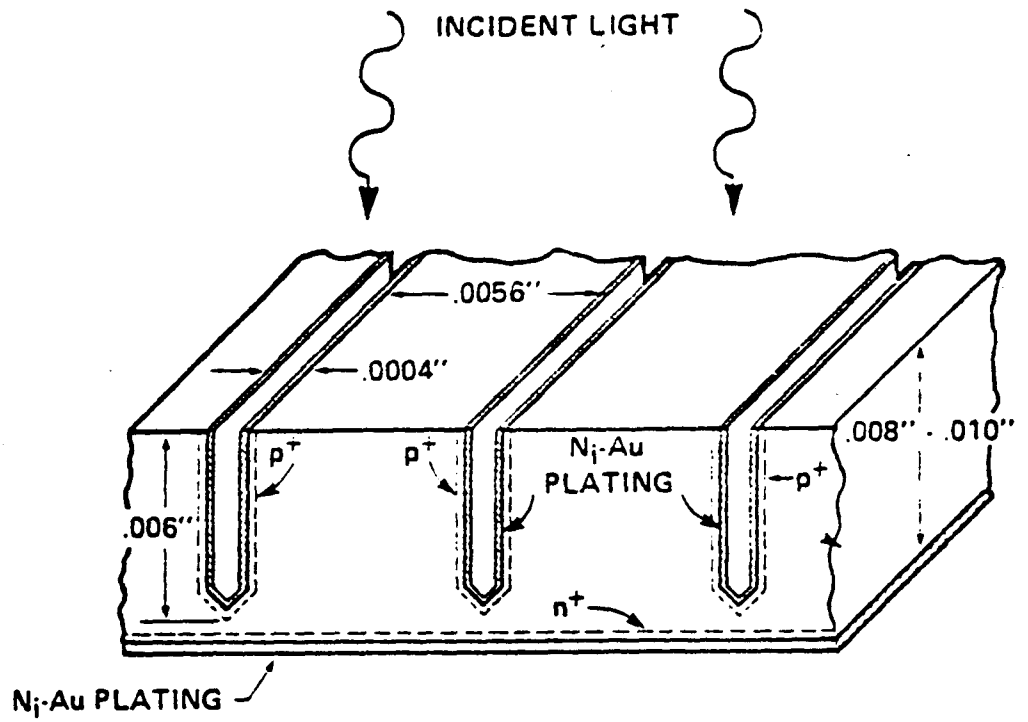

Figure 36. Schematic of Cell Structure Being Fabricated for Sandia. (End on View is a Cross-Section; AR Coating and Interconnect Buss on Top Surface not Shown.)

Under this program M/A has developed fabrication procedures for reproducible control of groove dimensions, and for achieving uniform plating, good adhesion, and low contact resistance with plated Ni-Au metallization on the groove walls. Further development is being directed towards optimization of processing parameters, cell geometry, and AR coatings. At

the present time, improved processing procedures have resulted in substantially increased values for V_{oc} and FF, due to an increase in minority carrier lifetime in the base region. Figure 36 shows results for V_{oc}, FF, and η from 1 to 600 suns (at 28°C) for devices using the older processing, for small test units with an active area 93 mils in diameter (0.044 cm^2) on a 108 X 108 mil chip. Typical results for devices using the newer processing are shown in parentheses for 1 sun only. These devices are 0.25" square with a total area of ~ 0.4 cm^2. On a total area basis, excluding only the buss stripes at either end of the cell, J_{sc} = 31 mA/cm^2 for a $\lambda/4$ oxide, and 33.5 mA/cm^2 for a non-optimized nitride AR coating at AM1. With V_{oc} = 0.58 volts and FF = 0.79, the 1 sun efficiency is ~ 15% (at 27°C). For these devices with improved carrier lifetime, V_{oc} increased with intensity at the rate of ~ 0.08 volts/decade.

The results in Figure 37 clearly show the effect on the fill factor of a reduction in series resistance - FF now increases rather than decreases with increasing intensity. The increase in V_{oc} with ln (I) now contributes to the increase of efficiency without being limited by a

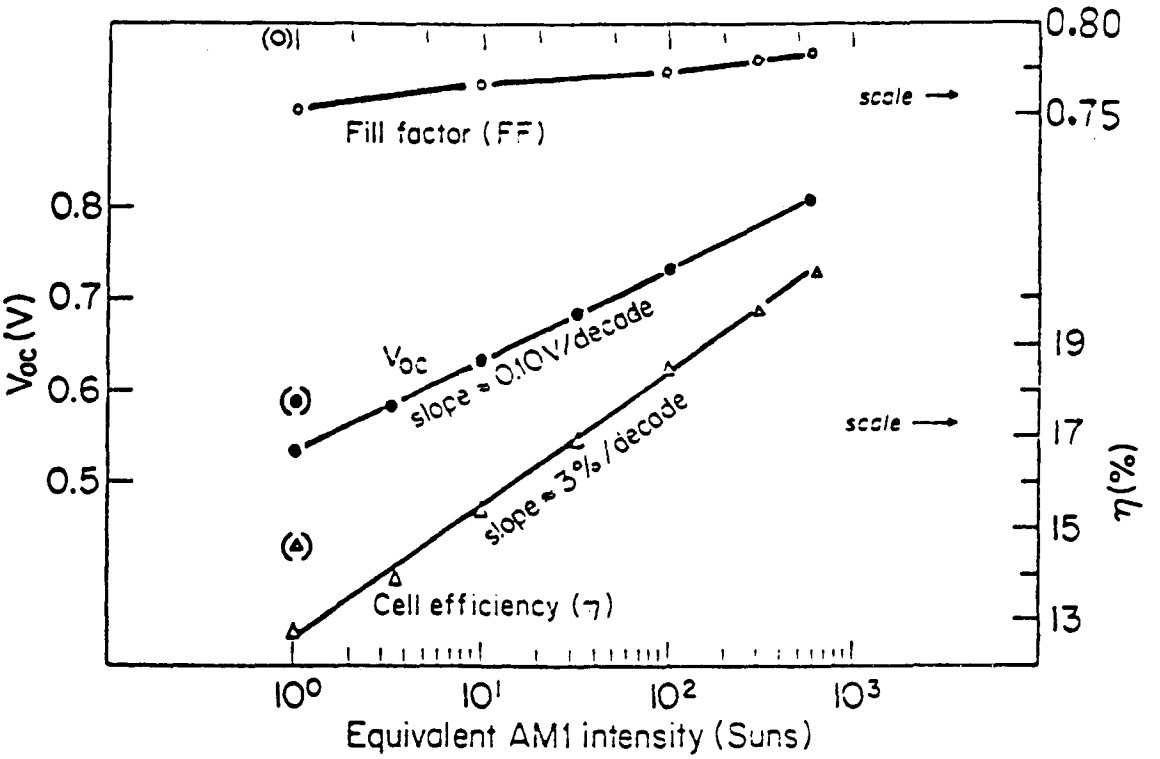

Figure 37. Experimental Results for V_{oc}, FF, and η as a Function of Intensity. Values in Parentheses are for Newer Cells Using Improved Processing.

decrease in FF. In parallel to this program, M/A has been investigating improved AR coatings and still lower temperature processing; efficiencies in excess of 22% at 100 suns or higher are expected to be realized with this cell design.

2.4 CELL MOUNT

2.4.1 INTRODUCTION

In the cell mount subsystem there are two problems to be dealt with in systems using concentrators and these are: (1) the need for effective cooling to avoid the decline of cell conversion efficiency that comes with higher cell temperatures, and (2) the minimizing of series cell resistance to keep the I^2R losses low even with the high currents that flow with concentrated sunlight. There are many solutions to these problems and it was the aim of this program to find the lowest cost, highest efficiency system that will provide reliable performance over a long life.

The cell cooling system can use natural convection, forced convection, or water cooling. Sufficient calculations were made to indicate that the system can be run in any of these ways. The ultimate method chosen will be influenced by the end application.

2.4.2 SELECTED CELL MOUNT DESIGN

An isometric view of the concentrator cell mounted on the copper-to-beryllia-to-copper sandwich with connection to the feedthroughs is shown in Figure 38. Connections to both the p- and n-contact are made to copper which is direct bonded to the top of the beryllia wafer. Another piece of copper is direct bonded to the bottom of the beryllia to make a balanced seal and this, in turn, is soldered to the copper base by #151 solder.

In temperature cycling with materials having significantly different expansion co-efficients, the weakest link is frequently not the solder, but the metallization on the ceramic joined to the solder. Normally, this metallization consists of a copper film plated on a thin moly film applied by the moly-manganese process, or thick precious metal films. The problem with these metallizations is that their interfacial thermal resistance is relatively high, and the bond

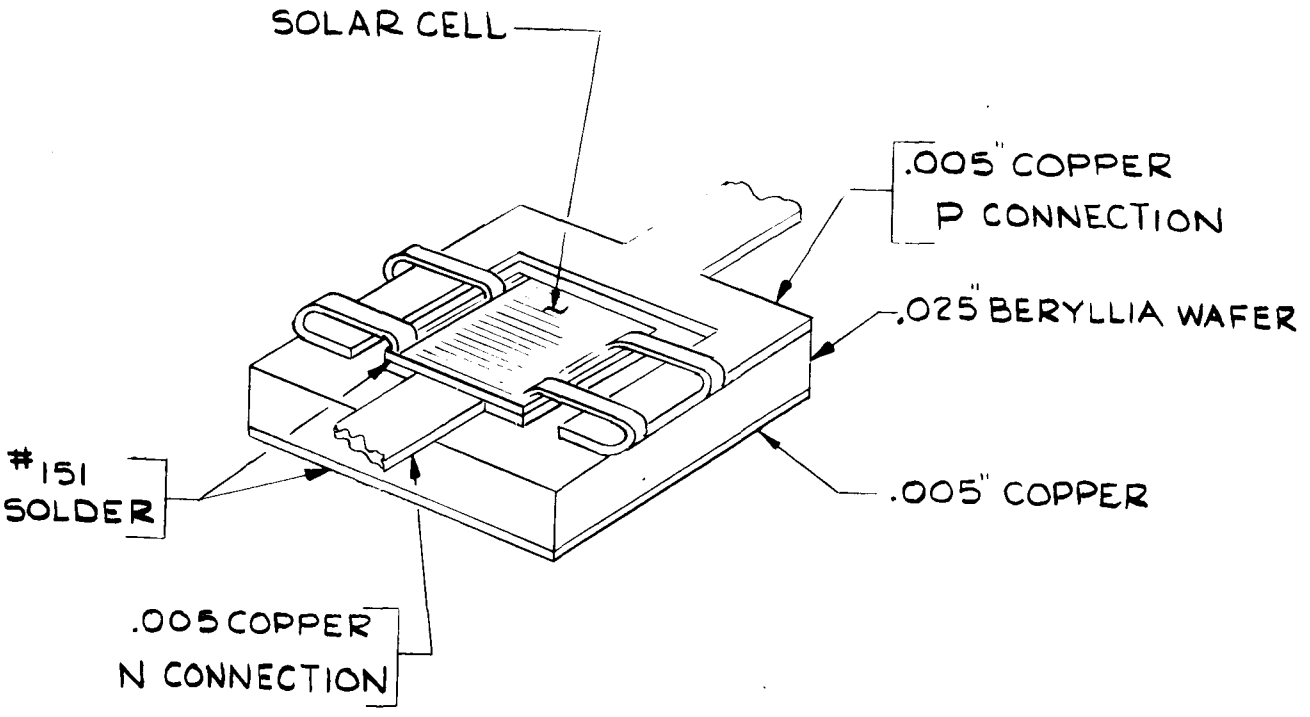

Figure 38. Isometric View of Cell Mount Design

integrity is questionable when severely temperature cycled. Another problem is the limited current carrying capacity of such films, resulting in significant IR drops, which would be particularly undesirable in the present application. Normal thick film metallization is about 1-mil thick and has a sheet resistance of the order of 1.5 milliohms per square or as high as 4.4 milliohms per square using strongly bonded copper frit films. These disadvantages are overcome by the use of "Direct-Bonded Copper," developed at GE and presently commercially available from GE in power modules and discrete power devices. In this design the beryllia insulator is clad with a 5-mil copper foil without an intermediary "glue" layer. This is accomplished with the CuO eutectic at 1065°C, using a single pass through a commercial tunnel oven in a factory grade nitrogen atmosphere. This approach results in a sheet resistance of 0.2 milliohms per cell, or an IR drop which is less by 0.009 V, and an I^2R dissipation reduced by 0.037 watts with respect to the equivalent thick film metallization. In addition, the direct-bonded copper has a bond strength in excess of 20,000 psi, and permits the attachment of contacts with negligible IR drops. Thermal cycling of such bonds has indicated exceptionally high

bond integrity. Combinations of 1/8-inch thick Cu plates, 1-inch diameter direct-bonded Cu clad 25-mil thick BeO substrates, and 0.7 x 0.4 inch semiconductor chips, soldered together in the laboratory with Indalloy 151 solder, are representative of assemblies which have successfully withstood severe thermal cycling. Mount hardware developed during the program is shown in Figure 3. Test results may be found in Section 4.3.

SECTION 3

PROTOTYPE MODULE DESIGN DEVELOPMENT

SECTION 3
PROTOTYPE MODULE DESIGN DEVELOPMENT

3.1 MODULE DESCRIPTION

The prototype module shown in Figure 4 consists of four basic components: domed Fresnel lens, lens mounting frame, lower housing, cell receiver unit. The cell receiver unit consisted of four elements: protective cone, cell mount, cell receiver mounting socket and a heat sink. It was the intent of this program to define a module design approach that is compatible with high volume production. Specifically, it is planned to injection mold the domed Fresnel lens, housing parts and cell receiver mounting socket. By molding these parts out of compatible materials alignment and attachment features can be "built-in." The intent of the prototype was to demonstrate, as much as possible, the feasibility of this approach.

To this end representative production materials were used for the lens, housing and receiver socket. Due to funding and schedule constraints the actual prototype hardware had to be fabricated using techniques more appropriate for one of a kind development hardware. The lenses were direct diamond cut out of blanks of cast acrylic. The housing was thermo-formed and machined out of sheets of capstock ROVEL and medium impact ABS. The receiver sockets were machined out of blanks of Texolite (filled phenolic).

3.1.1 PROTOTYPE LENS

Two circular seven inch diameter domed lenses were direct diamond cut by OSG. The specifications for these prototype lenses are provided in Table 7. For the prototype design, accurately drilled mounting holes in the lens mounting frame along with a lens flange were used to accurately register in X and Y the lenses in the prototype housing.

3.1.2 PROTOTYPE HOUSING

The prototype housing consisted of a top lens mounting frame and a lower housing half. Both halves were simultaneously machined and doweled to ensure accurate lens-to-cell mount registration. The housing serves to maintain the lens-to-cell spacing, resist deflections due to the various loads and maintain a reasonably clean dust-free environment for the lens facets and cell mounts.

3.1.3 CELL RECEIVER

The cell receiver shown in Figure 4 consisted of the EMVJ concentrator cell direct bonded to a copper-BeO-copper substrate which was soldered to a threaded copper heat spreader stud. A thermal resistance calculation for the mount is provided in Figure 39.

The copper heat spreader stud was configured to accurately "plug-in" to the machined Texolite socket. The socket in-turn was designed to "plug-in" to the accurately drilled locating holes in the bottom of the lower housing half. A modified 0.3 pound Wakefield #3560-2 extruded aluminum heat sink is attached to the copper heat spreader via the threaded stud. A nickel plated steel dome is used to prevent off-axis focused sunlight from damaging the housing. Figure 40 shows a cross sectional view of these components.

3.1.4 ALIGNMENT TOLERANCES

Three main sources of pointing error were evaluated:

1. Module Assembly
2. Array Tracking Structure Mount, i.e., deflections, alignments
3. Tracking Electronics and Sensors

The following array error budget was developed:

	Equivalent Angular Error
Module Assembly	0.27^{o}
Tracking Structure	0.20^{o}
Tracking Electronics	0.18^{o}
Total RMS Error	0.38^{o}

This budget correlates with less than a 5% array performance decrease.

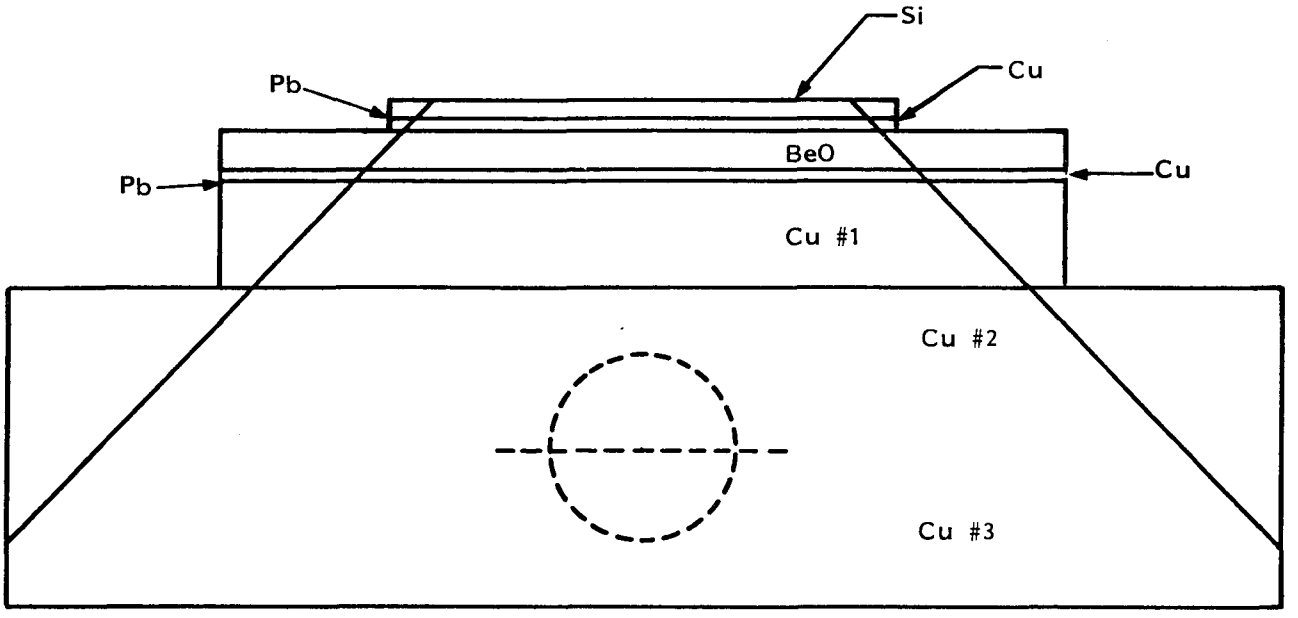

MATERIAL	K	THICKNESS	AREA $_{(IN)}{}^2$	R °C/WATT
Si	3.8	.010"	.049	.054
Pb	.883	.001"	.053	.021
Cu	10.	.005"	.057	.0088
BeO	5.85	.025"	.071	.0602
Cu	10.	.005"	.087	.0057
Pb	.883	.001"	.091	.0124
Cu #1	10.	.062"	.126	.0492
CU #2	10.	.094"	.246	.0382
CU #3	10.	.094"	.442	.0213

$$R = \frac{1}{K}\,\frac{t}{A}$$

TOTALS

.250°C/WATT

.271°C/WATT

Figure 39. Thermal Resistance Calculation

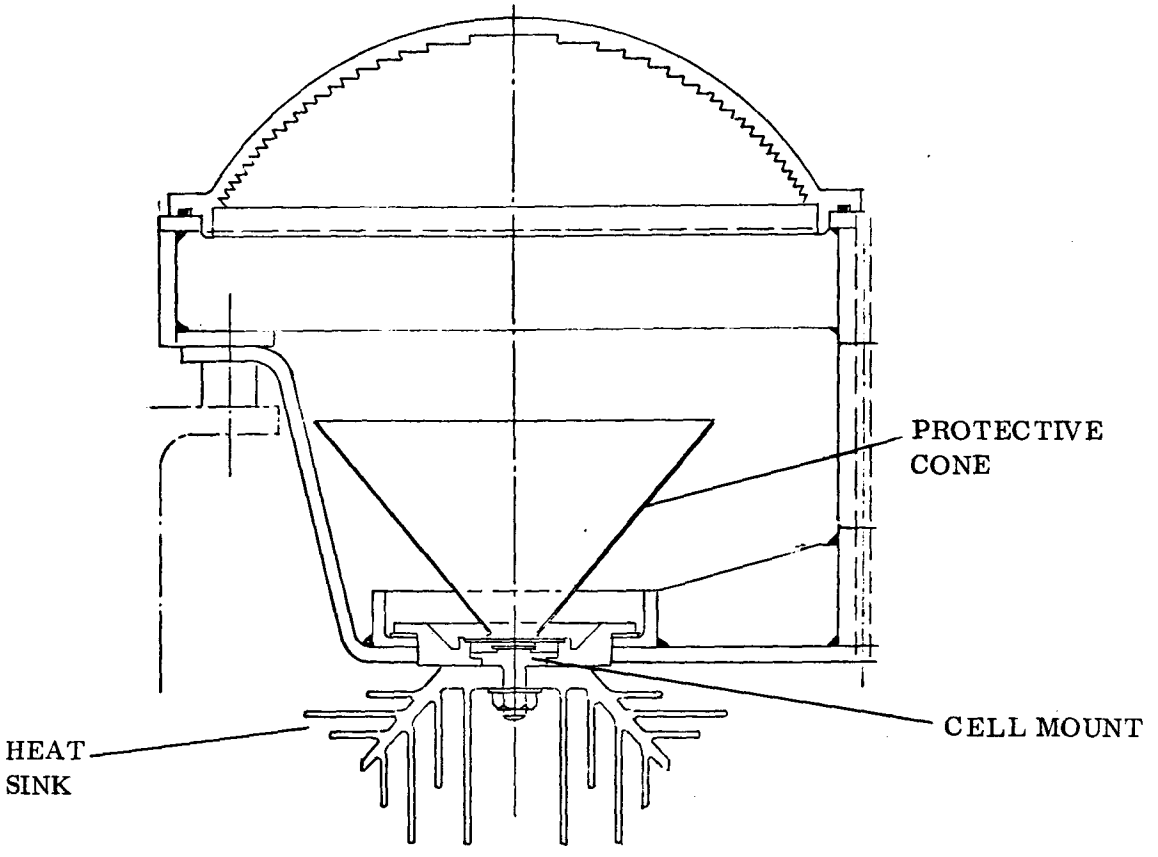

Figure 40. Cross Section View of Prototype Lens - Cell - Receiver Assembly

Based on the results of the detailed lens analysis and discussions with several manufacturing engineers the following module alignment budget was developed:

MODULE ALIGNMENT BUDGET 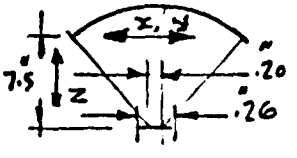	x, y''	z''
LENS/MOUNT FRAME	0.015	0.020
RECEIVER SOCKET/HOUSING	0.025	0.020
CELL RECEIVER/HOUSING	0.015	0.015
CELL/CELL MOUNT	0.010	0.010
TOTAL MODULE RMS ERROR (EQUIVALENT TO 0.28°)	± 0.035''	± 0.035''

3.1.5 THERMAL ANALYSIS

Thermal analyses were conducted in order to select a suitable heat sink, and evaluate candidate protective cone and housing materials. As a result of these analyses a 0.3 pound modified Wakefield aluminum heat sink was selected. Nickel plated steel was chosen as the protective cone material and a 75°C heat distortion temperature requirement was established for the lens and housing materials. The following summarizes each of these analysis.

Heat Sink Selection

The following lens and cell design characteristics were assumed for the prototype module:

Lens - Diameter = 7"
Geometric concentration ratio = 1250
Transmission efficiency = 85%

Cell - Active area = 0.25" diameter
Flux spot size = 0.2" diameter
Efficiency @ 28°C, 1000 suns = 20% (w/silicon nitride coating)
Temperature coefficient = 0.3%/°C

The step-by-step calculation performed in determining the heat sink size is as follows:

Lens area = 0.0248 m^2

Incident energy on lens @ 1 kW/m^2 = 24.8 watt

Net cell power output for 15% η = 0.15*24.8 = 3.72 watts

Gross cell output with 2% wiring loss = 3.72/0.98 = 3.8 watt

Incident energy on cell, assuming no optical loss through the glass cover = 24.8*0.85 = 21.08 watt

Cell efficiency required for 3.8 watt output = 3.8/21.08 = 18.03%

The cell operating temperature (Tc) required for 18.03% η can be determined by:

$$\text{Cell } \eta = \text{Cell } \eta_{28^oC} * (1\text{-temp. coeff. } * (Tc-28))$$

$$0.1803 = 0.20 * (1 - 0.003 * (Tc-28))$$

$$Tc = \underline{\underline{60.83^oC}}$$

The thermal energy generated under the above conditions can be obtained by subtracting from the incident solar flux, the cell electrical output (3.8 watt) and the energy reflecting off the cell. The reflective losses consist of the loss from the encapsulation glass cover ($\sim$ 4%) and the loss due to infrared radiation (20% of solar spectrum) reflecting off ($\sim$ 70%) the nickel metallization layer. Thus, the total thermal energy generated is;

$$21.08 - 3.8 - (31.08 * 0.04) - (21.08 * 0.96 * 0.02 * 0.7)$$

$$= \underline{\underline{13.6 \text{ watt}}}$$

The thermal resistance from the cell to the heat sink is approximately 0.401°C/watt (0.271°C/watt from cell to copper heat spreader, 0.13°C/watt for copper to heat sink contact surface resistance). Thus, at standard test conditions:

$$\Delta T \text{ from cell to heat sink} = 13.6 \times 0.401 = 5.5^oC$$

$$\Delta T \text{ from } 20^oC \text{ ambient to heat sink} = 60.83 - 5.5 - 20.0 = 35.33^oC$$

So, the maximum heat sink thermal resistance allowed is 35.33/13.6 = 2.60°C/watt.

There are numerous off-the-shelf aluminum heat sink designs which have approximately the same weight for the required thermal resistance property. However, in order to facilitate the heat sink to cell mount to module housing integration, certain heat sink geometries are required: it must be flat on one side; the fin spacing at the center of the heat sink must be wide enough to accommodate the cell mount copper stud feed-through and the mounting surface must be narrow enough to prevent interference with the mounting of cell assembly to housing baseplate. As a

result, a Wakefield 3560-2 extruded heat sink, as shown in Figure 41, was selected for the prototype module application.

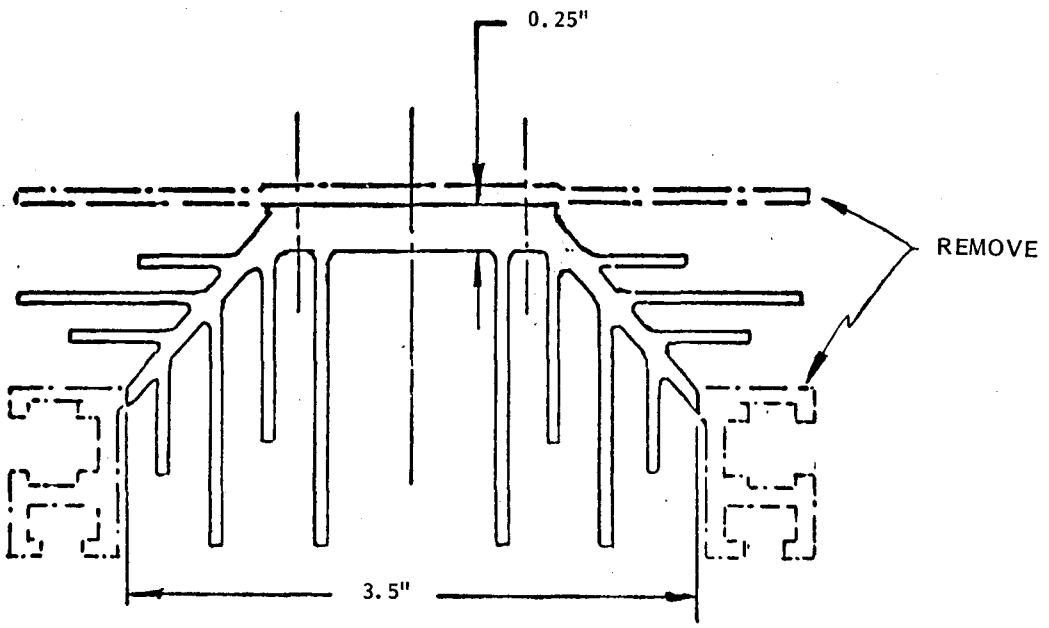

WAKEFIELD 3560-2, 2" LENGTH
STOCKED WEIGHT ~0.9 LB. THERMAL RESISTANCE, NATURAL CONVECTION = 1.25°C/WATT
MODIFIED PROTOTYPE WEIGHT ~0.3 LB.

Figure 41. Prototype Module Heat Sink Configuration

The thermal resistance for a 2" long 3560-2 heat sink in natural convection is 1.50°C/watt. The finished heat sink for the module after slight modification will weigh about 0.3 pound.

A verification effort was conducted in order to try and determine how well our thermal analysis model fits the experimentally measured data for currently available heat sinks. Excellent agreement was found between the computer predictions and manufacturer's data. A more detailed discussion of this analysis is found in Appendix A.

Protective Cone Analysis

During solar acquisition, the domed Fresnel lens collector undergoes a defined period of time during which the protective shield or cone is exposed to the off-axis focus of solar radiation. An analysis was made of the mask temperature during the off-axis transient to determine whether thermally insulating washers were necessary to protect the textolite receiver socket. If the cone is constructed of chrome or nickel plated steel, the analysis estimates only a very moderate temperature rise in the mask. In a worst case scenario, in which the collector remains fixed off-axis at maximum insolation, the mask would still survive, reaching an equilibrium temperature of about 400°F. A plot of cone temperature versus off-axis angle and dwell time is provided in Figure 42. A more detailed description of this analysis is provided in Appendix B.

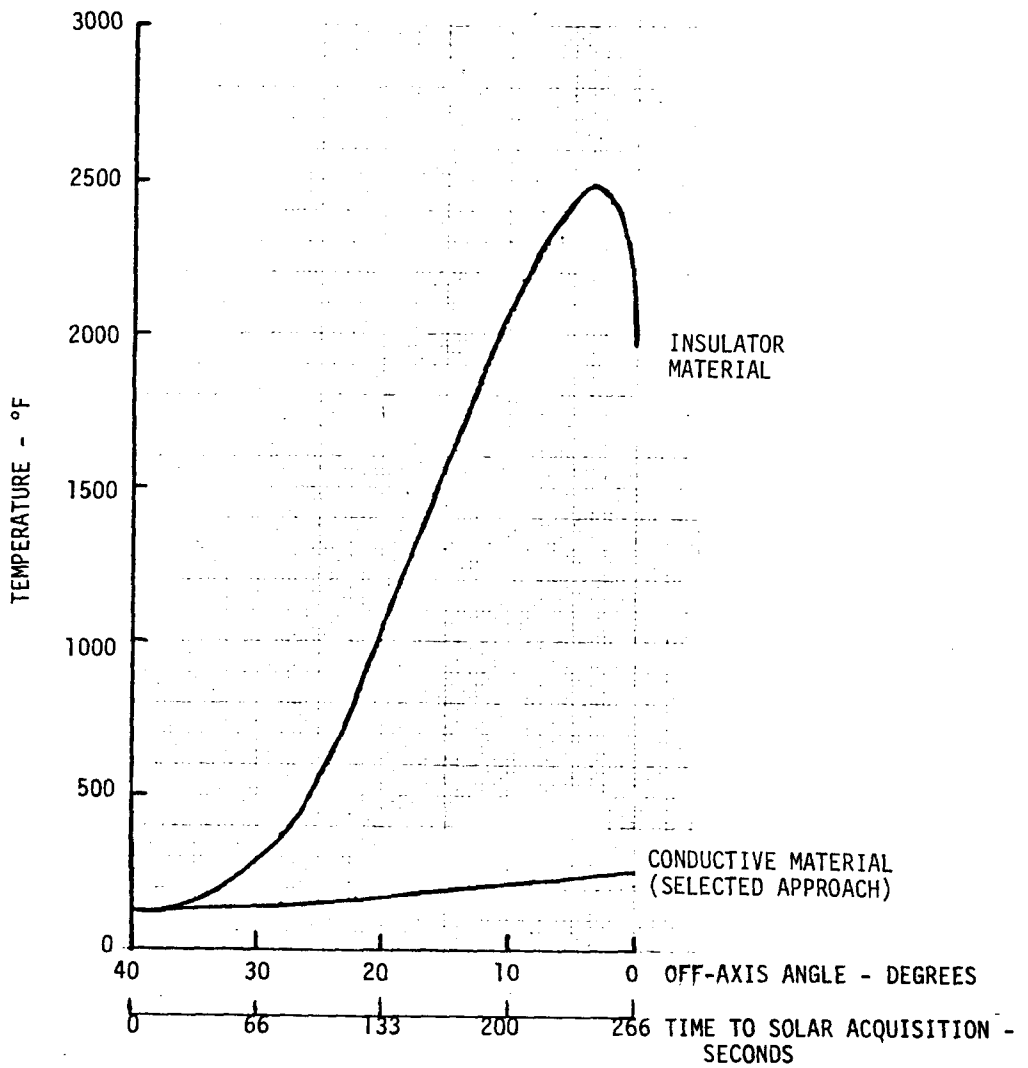

Figure 42. Protection Cone Temperature Rise During Solar Acquisition

Module Thermal Analysis

The temperature distribution within the PV module is of interest, for several reasons. The temperature attained by the module impacts on the choice of materials for the module; it also affects the focus of the Fresnel lens, due to absolute and differential thermal expansion of module parts. In order to determine the temperature distribution, an analysis was performed.

The analysis considered a module constructed of plastic material. Briefly, the thermal model consisted of 4 nodes, plus one for the ambient surrounds. The PV cell temperature was considered fixed, i.e., heat transfer from cell to heat sink to ambient was not examined here. Steady-state solutions for various conditions were obtained via a small finite - difference program, executed on the HP9810A calculator, the results of which are shown in Figure 43.

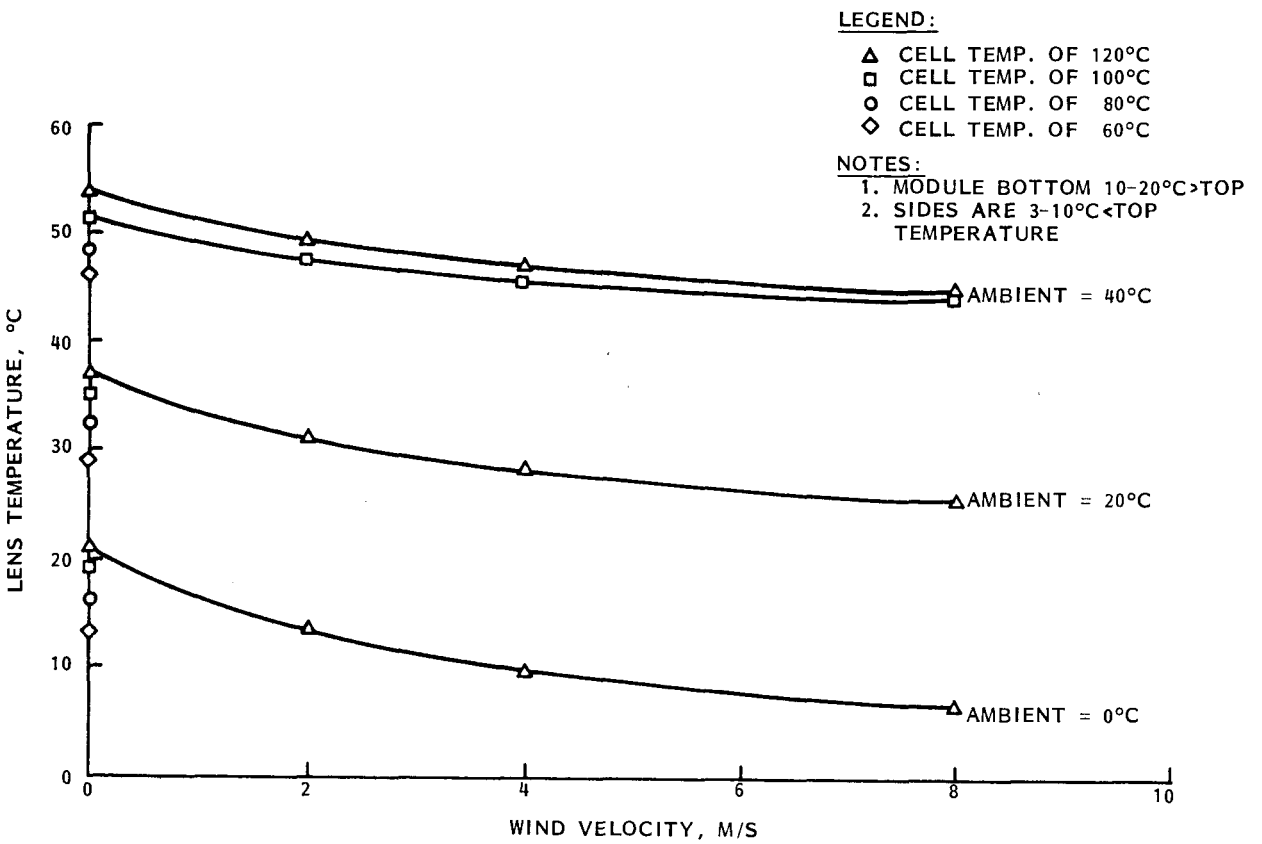

Figure 43. Module Temperature Analysis

SECTION 4

PROTOTYPE HARDWARE TESTING

SECTION 4

PROTOTYPE HARDWARE TESTING

4.1 TEST SUMMARY

Each lens, cell and cell mount was tested prior to module integration. The lenses were tested by OSG, GE and finally by Sandia. The cells were tested by Microwave Associates' prior to shipment to GE. GE then measured fill factor before and after cell mount fabrication. Mount thermal resistance and stand-off voltage was also measured.

Module performance testing consisted of obtaining I-V characteristics for individual lens-cell mount combinations under outdoor sunlight conditions. During the outdoor tests the prototype housing was used.

The balance of this section describes in more detail the lens, cell mount and module test efforts.

4.2 DOMED FRESNEL LENS TESTING

The main performance areas analyzed in the lab were:

1. Spot size (lens geometric concentration)
2. Intensity profile (peak to average concentration ratio)
3. Lens efficiency

The lab tests were not intended to simulate actual module conditions and their results cannot be used as an absolute indication of outdoor sunlight performance. However, the lab results were very useful in confirming the shape of the focused flux profile, optimum "focal" distance and lens concentration ratio. In addition, the lab tests indicated that the lens transmission appears to meet the specified transmission goal of 83%.

4.2.1 GE LENS TEST SET-UP

The tests were conducted in a room approximately 10' x 20' in size, using the test set-up shown in Figure 44 and described as follows:

1. Light Source - tungsten source ac (voltage regulated) made by Carl Zeiss.
2. Ground glass diffuser.
3. Aperture approximately 0.26" diameter, simulate sun's angular substance (approximately $1/2^{o}$ angle).
4. Baffle, black felt (approximately 2" square aperture).
5. Collimator - Fresnel lens 30" FL, approximately 20" x 30" size.
6. Holder for test lens.
7. 3 axis positioner in plane of cell (used for mounting Redicon detector or Weston cell).

The tungsten light source used was not corrected for air mass 1.5 solar spectrum. Thus, data taken is not expected to correlate precisely with data taken using the sun and silicon cell.

4.2.2 OSG LENS TEST SET-UP

The equipment used at OSG is shown in Figure 44. All data taken at OSG was for monochromatic light (6328 Å).

4.2.3 LENS SPOT PROFILE AND SIZE

The first data that was taken was to measure the size and profile of the concentrated light spot. A Redicon detector having 1024 sensors, each approximately 25 μm wide, was used. A series of photographs showing the intensity profile were taken, see Figure 45. These, through focus shots, show how the diameter and intensity distribution of the spot changes with cell to lens distance.

The best cell position seems to be approximately 0.100" further away from the lens than the original design value. It is believed that this 0.100" variation is due to the - 0.020" in lens thickness caused by manufacturing problems. This information was used in mounting the lens

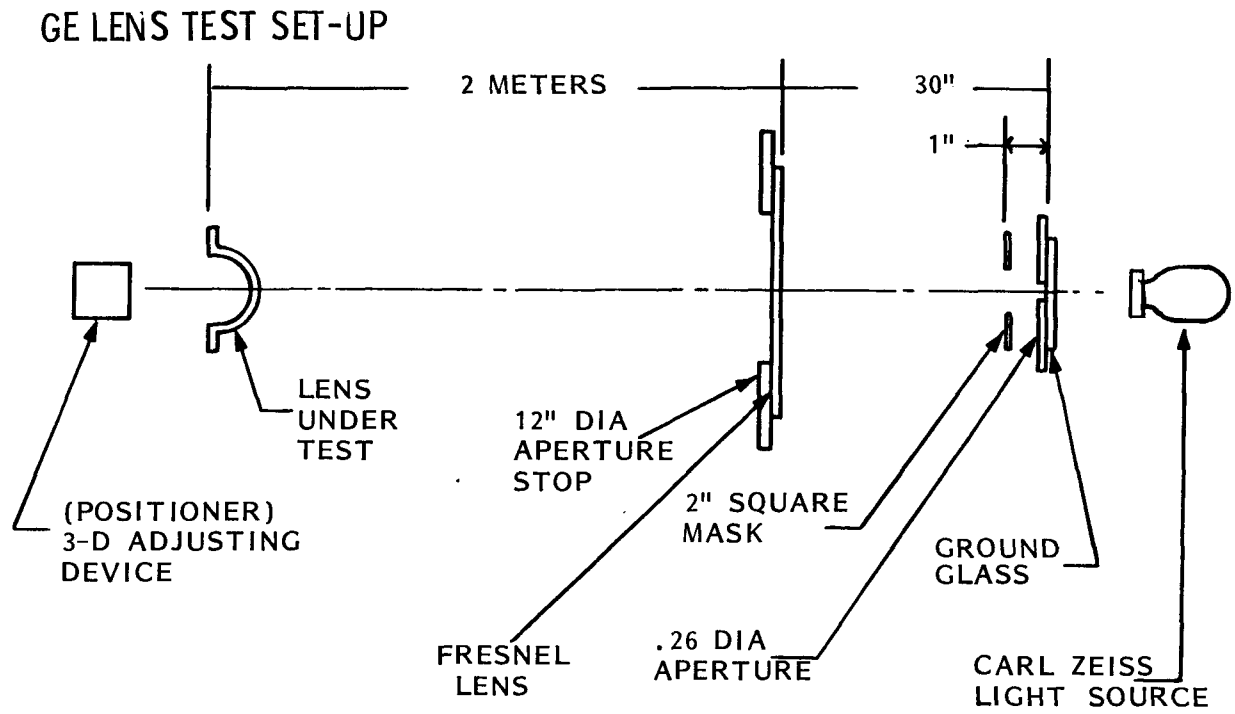

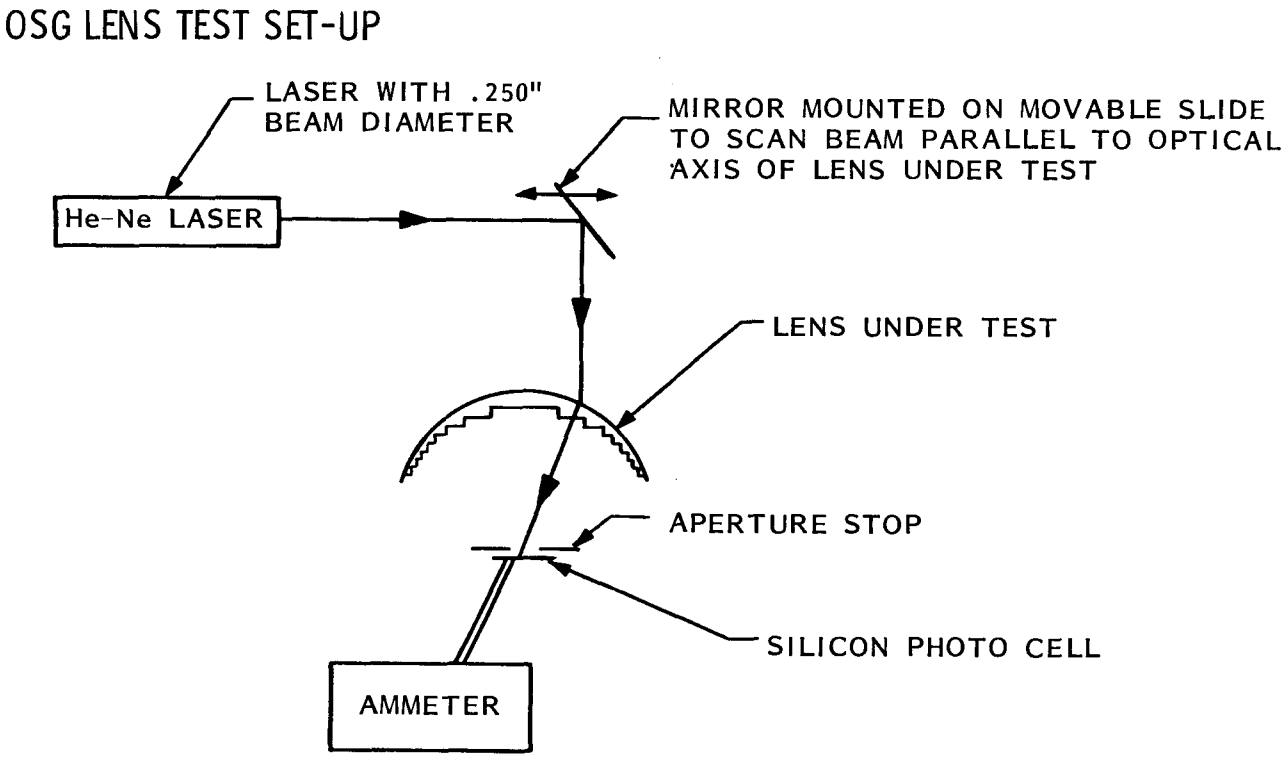

Figure 44. Lens Test Set-up

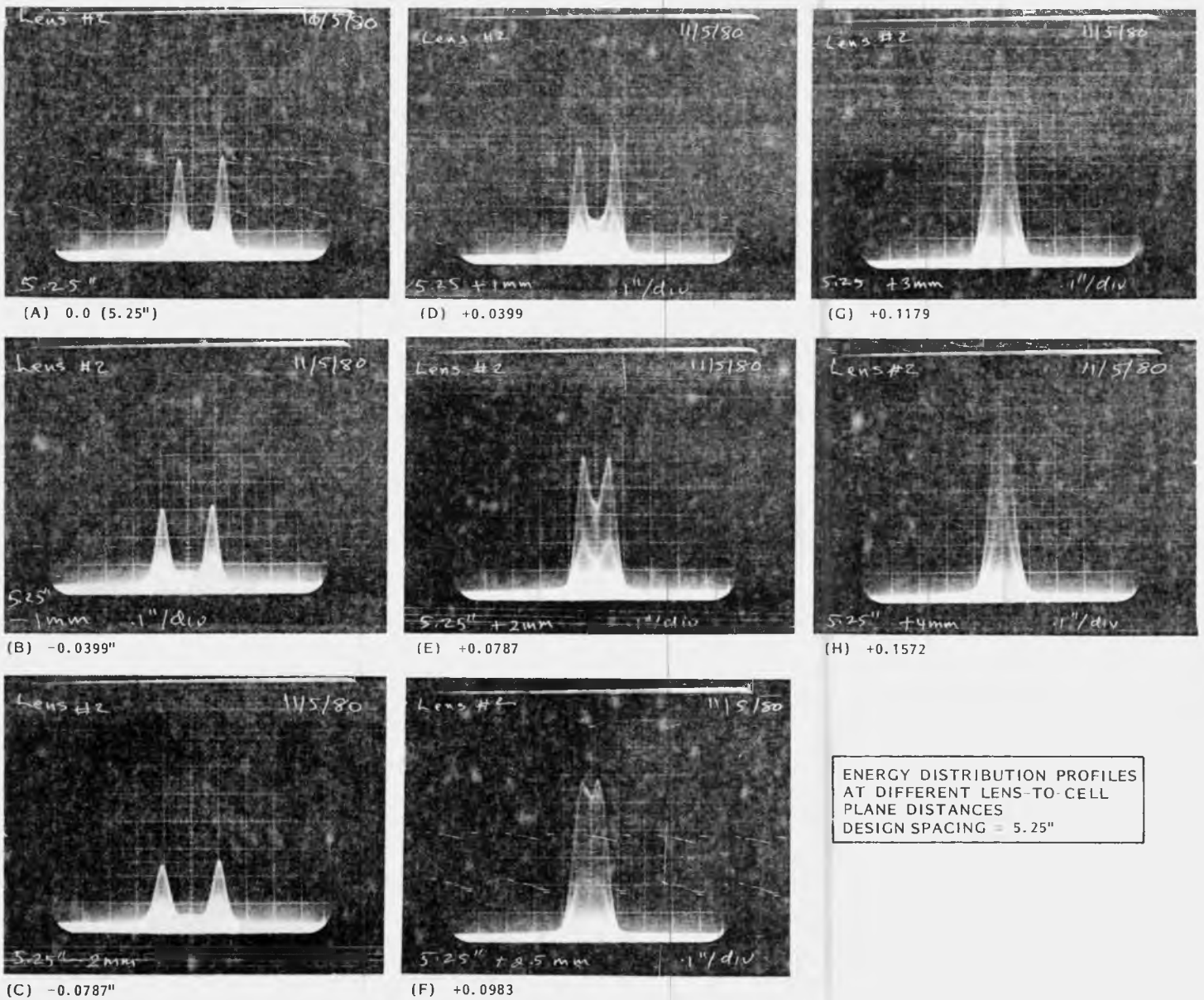

Figure 45. **Flux Profiles for Prototype Lens No. 2**

into the prototype module. Using the Redicon the spot size is seen to be approximately 0.200" with a peak to average intensity better than 3/1.

4.2.4 LENS EFFICIENCY

The next test that was performed was to measure the efficiency of the lens. Some measurements were taken at OSG before the lens was sent to GE. The results of the OSG test is shown in Figure 46.

For the efficiency tests at GE the Weston cell was positioned in the "best" cell plane (5.25" + 2.5 mm or approximately 5.35"). The meter was nulled and then a reading was taken. The cell was stopped down to 0.200" using an aperture stop. The current measurement was taken and the lens was removed. A tube, approximately 6" long and 3/4" diameter, was placed in front of the cell to try to minimize "stray" light hitting the cell. Even with the use of this baffle, the angular acceptance of light into the cell could have influenced the readings taken, causing the calculated lens efficiency to be lower than it really might be. In any case, a current reading was again taken. The ratio of the current with a lens to the current without a lens was defined as the actual concentration or efficiency of the lens. As recorded in Table 8, data was taken several times to determine the repeatability of the procedure. Also, data was taken with a 1.0" aperture. The comparison of the data @ 0.200" aperture versus 1.00" aperture shows that approximately 6% of the light being transmitted by the lens is scattered out of the usable spot size due to manufacturing problems.

A summary of the OSG and GE lens efficiency data is shown in Table 8.

Table 8. Summary of OSG and GE Lens Efficiency Data

OSG		GE - 0.020" DIAMETER CELL	
CELL DIAMETER	LENS EFFICIENCY	FOCAL DISTANCE	LENS EFFICIENCY
1.0"	87.6%	5.17"	84.5%
0.25"	84.1%	5.25"	80.8%
0.1875"	83.9%	5.35"	84.5%

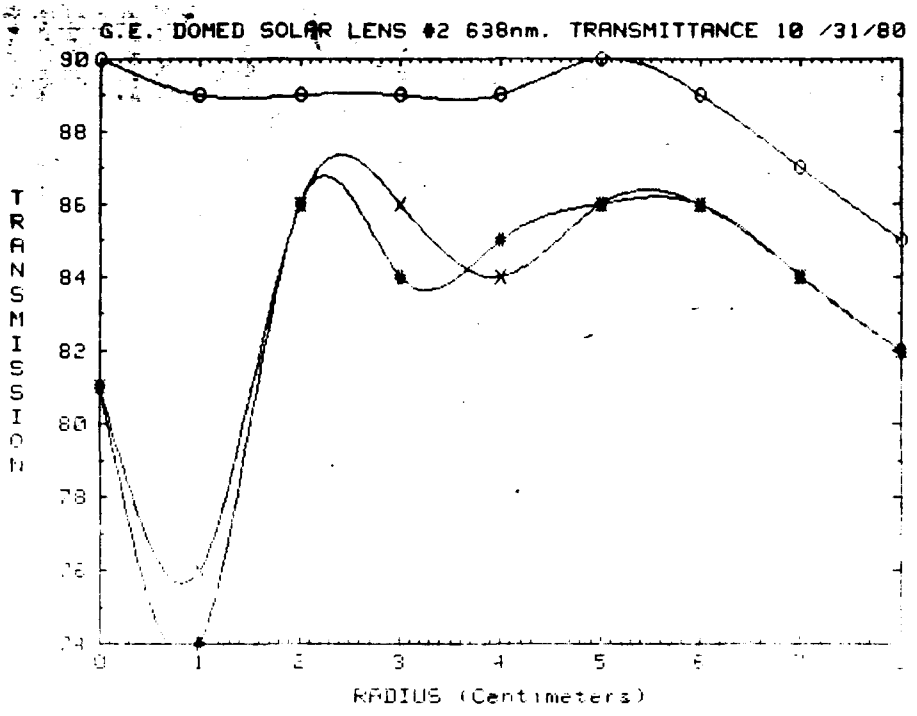

CURVE # 1 CELL DIAMETER 1"

X	Y
0	90
1	89
2	89
3	89
4	89
5	90
6	89
7	87
8	85

Area weighted average = 87.6%

CELL DIAMETER .250"

X	Y
0	81
1	76
2	86
3	86
4	84
5	86
6	86
7	84
8	82

Area weighted average = 84.1%

CURVE # 3 CELL DIAMETER .1875"

X	Y
0	81
1	74
2	86
3	84
4	85
5	86
6	86
7	84
8	82

Area weighted average = 83.9%

Figure 46. OSG Lens Efficiency Test Results

4.2.5 SANDIA LENS TESTING

Sandia conducted lens efficiency evaluations using their lens analyzer. The evaluations consisted of transmission efficiency and focused flux profile mapping. Results of these evaluations are shown in Figure 47. Efficiency as a function of tracking error was also measured. Figure 48 shows the measured performance for one of the prototype lenses.

The lens demonstrated a transmission efficiency of 84% with a peak-to-average intensity ratio of 2.29:1 (1600 x 609x). In addition, an efficiency drop off of only 8% was observed for a 0.5^{o} off-track error.

4.3 CELL MOUNT TESTING

The 1-sun fill factor, thermal resistance and stand-off voltage for five cell mount units were measured, see Table 9.

Table 9. Cell Mount Test Results

MOUNT NUMBER	1-SUN FILL FACTOR	MEASURED THERMAL RESISTANCE - ^{o}C/WATT	HI. POT. TEST - KV
MA-1	0.693	0.281	3.3
MA-2	0.670	0.229	3.1
MA-3	0.635	0.280	3.2
MA-4	0.735	0.198	3.5
MA-5	0.723	0.239	3.4

Cell mount assembly thermal resistance was measured using equipment schematically arranged as shown in Figure 49. This method makes use of the temperature dependent change in the dark forward voltage of the solar cell. With a small constant current (I_m) passed through the dark solar cell, the forward diode voltage is measured and its value recorded for different temperatures of the solar cell to determine V_F versus temperature at the measuring current I_m. Once this calibration is completed, a high current heating pulse is passed through the cell and the cell temperature determined as it cools after the heating pulse is removed. Measurements of V_F are made during the cooldown interval. These values are extrapolated back to find the temperature of the cell when the known heating pulse was terminated.

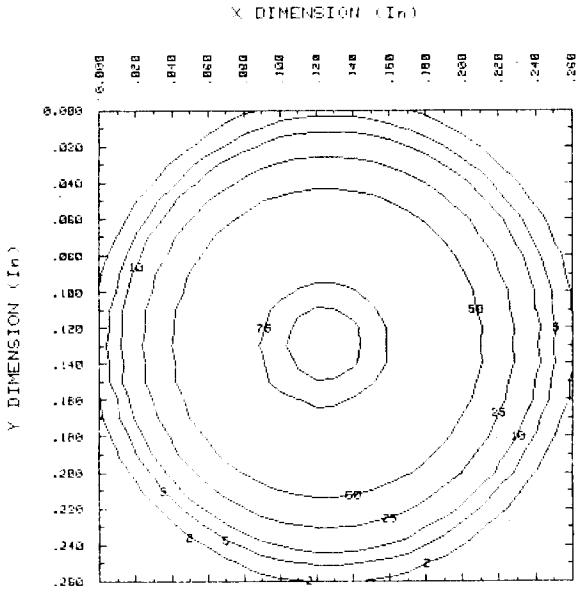

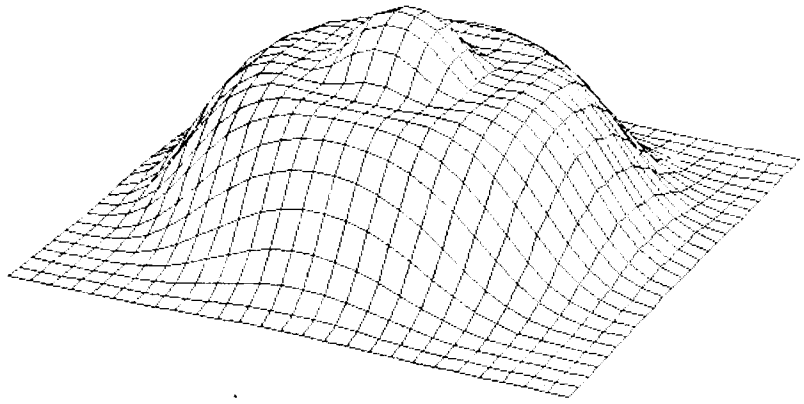

File GEOM2 recorded on 2/04/81 at 10:45 used 1 filter(s).
W# = CLEAR AND BREEZY
C# = GE 7" DIA DOMED LENS, BOT. OF LENS TO CELL=7.125
Ratio = 1.17776762535 Fltfac = 3256.52748409 F11
Pts = 27 Lns = 27

This circular lens has a diameter of 7 In.

File GEOM2 recorded on 2/04/81 at 10:45 used 1 filter(s).
W# = CLEAR AND BREEZY
C# = GE 7" DIA DOMED LENS, BOT. OF LENS TO CELL=7.125
Ratio = 1.17776762535 Fltfac = 3256.52748409 F1

This circular lens has a diameter of 7 In.

F.L = 5.245" thru .2" thk filter

Figure 47. Sandia Lens Test Results

- 724 X AVERAGE GEOMETRIC CONCENTRATION, 7" DIAMETER
- SANDIA OUTDOOR TEST DATA - 2/5/81

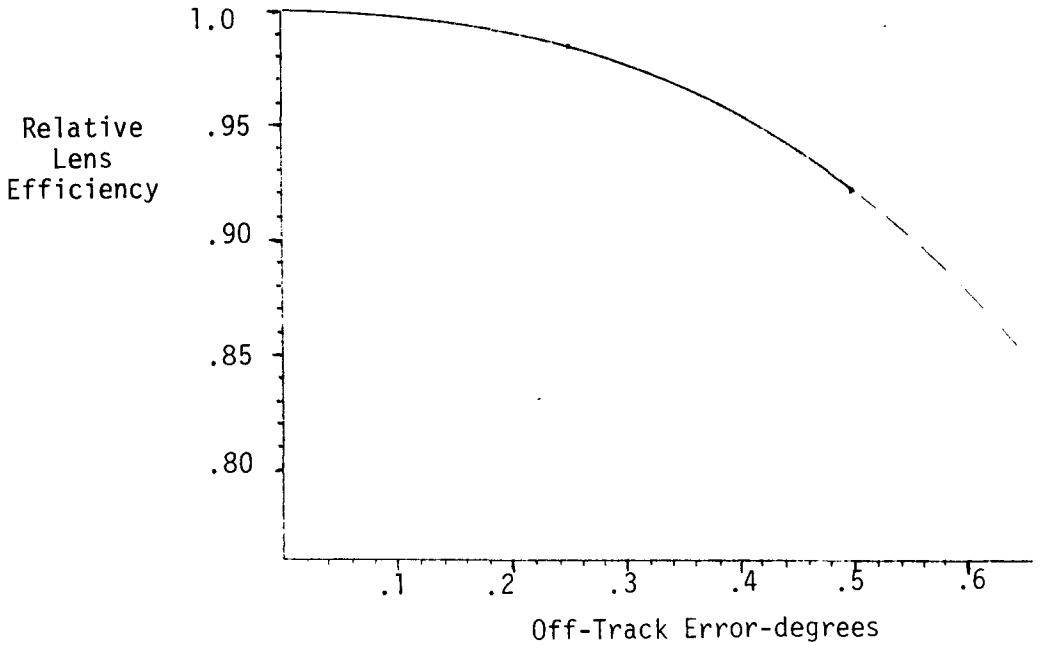

Figure 48. Efficiency Drop-off Due to Tracking Error for Domed Fresnel Lens

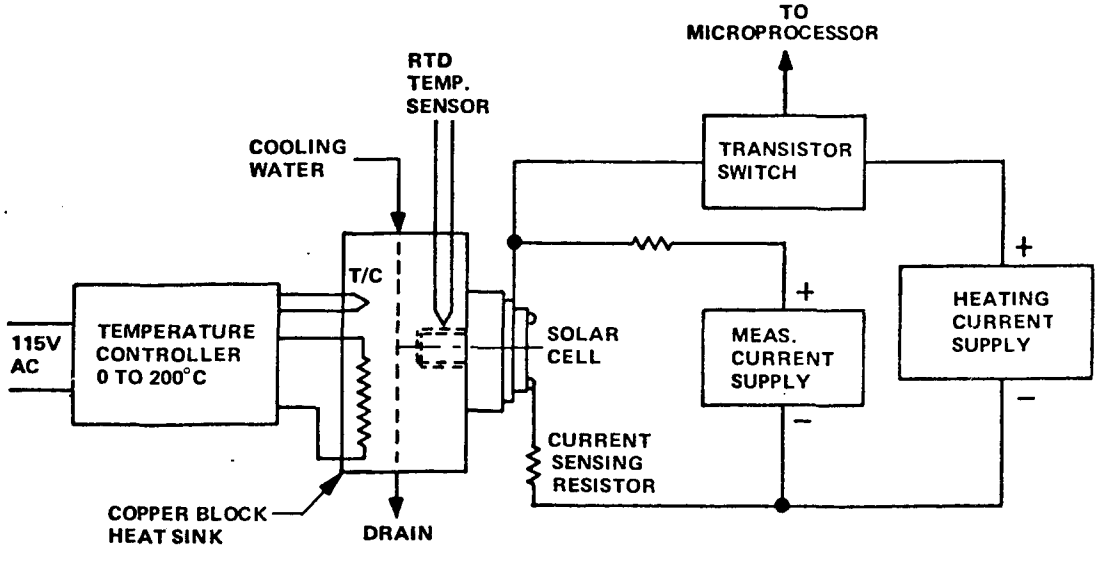

Figure 49. Schematic of Thermal Resistance Measurement Set-up

The thermal resistance can then be calculated from this information. All measurements are made by a digital voltmeter which is controlled by a small computer which makes five determinations of thermal resistance for each run. The average of these five readings is used as the measured value.

The thermal resistance measurements reported herein are referenced to a point which is 0.125 inch removed from the mounting surface of the copper heat spreader. It is estimated that these measurements include $0.05^{o}C$/watt for extra thermal resistance associated with the mounting block thickness and grease joint resistance.

4.4 MODULE TESTING

The test specimen was the prototype module housing shown in Figure 5 which was capable of mounting five (5) domed Fresnel lens/cell receiver combinations and thermal heat sinks. For this test program only one domed Fresnel lens/cell receiver combination and heat sink was mounted in the module housing.

The test facility used was a Mann Russell two-axis tracker which is hydraulically actuated and can be manually or automatically controlled. Site meterological and direct normal insolation data was available from an adjacent solar test facility.

The ancillary test equipment used to perform the module testing included the following:

1. Esterline Angus PD 2064 Data Logger.
2. Type K thermocouple wire to measure ambient, part and fin temperatures. See Figure 2 for thermocouple locations.
3. Interface mounting structure between the prototype module and the tracker platform.
4. Digital Voltmeter (two required).
5. X-Y Plotter.
6. Instrument Shunt (100 mV @ 20.0 amps)
7. Power Supply with a minimum capacity of 10V dc and 10 amps maximum PARD (ripple) 5 mV.

The test prototype module housing with one domed Fresnel lens/cell receiver combination and heat sink was mounted to the two-axis tracker platform as shown in Figure 50. Alignment of the module was obtained by moving the platform until peak current was observed (Accuracy $\approx$ 0.20^{o}). Thermocouples shown in Figure 51 were positioned and connected to the Easterline Angus Data Logger. The electrical test circuit was connected as shown in Figure 51.

Individual performance test runs were conducted at different direct normal insolation values between the range of 700 and 800 W/m^2 as sun availability permitted. During the time required to sweep the I-V characteristic of the circuit, the direct normal insolation was not to vary by more than $\pm$ 1%.

Figure 50. Prototype Module Mounted on Tracker Platform

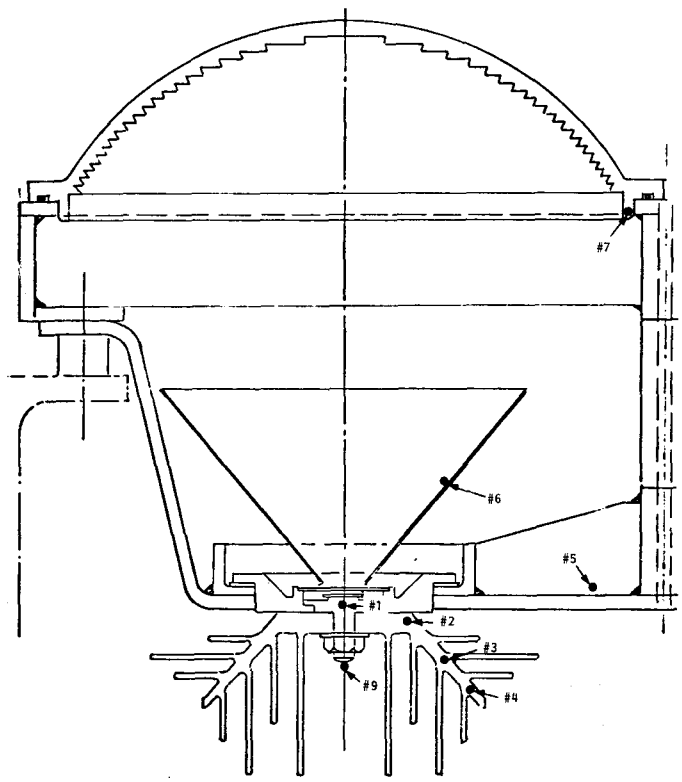

Figure 51. Thermocouple Locations for Prototype Test Module

For each performance run, the following data was recorded on the data sheet.

1. Ambient temperature
2. Thermocouple readings #1 - 9
3. Wind speed
4. Direct Normal Insolation (DNI) - pyrheliometer reading
5. Maximum power
6. Efficiency
7. Fill factor

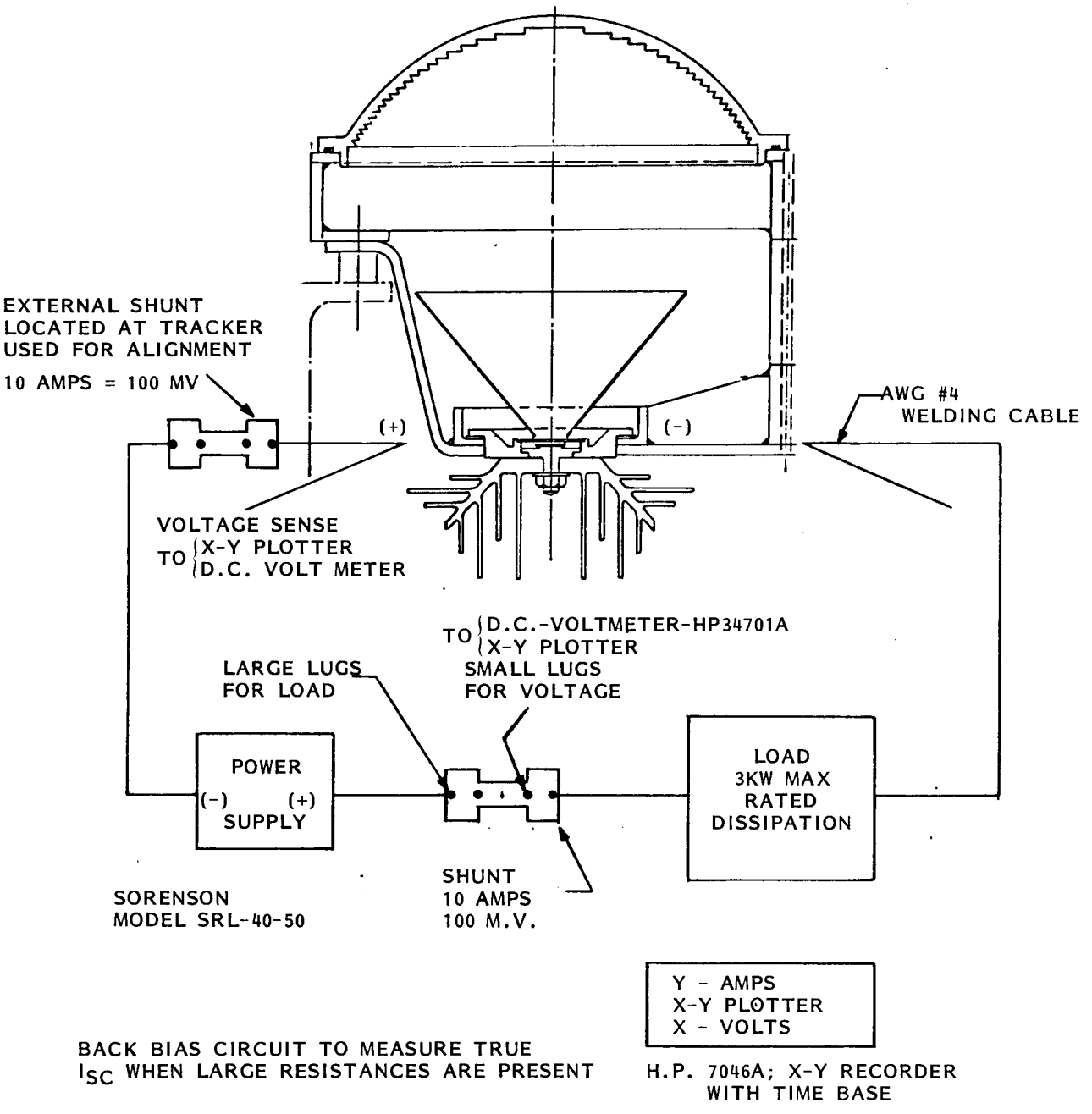

Figure 52. High Concentration Dome Fresnel Electrical Test Circuit

The electrical efficiency was calculated for each performance run in accordance with the following expression:

$$\eta_E = \frac{P_{max}}{A_a I_{dn}}$$

where

η_E = the module electrical efficiency

P_{max} = the measured receiver circur maximum power output (watts)

A_a = the aperture area of the prototype dome Fresnel lens (0.0248 m^2)

I_{dn} = the measure direct normal insolation (watts/m^2)

The specific test runs were as follows:

Date	Lens #	Cell Mount	Heat Sink
3/6/81	#2	#4 - 1/81 Cell Lot	2" width (0.3 lb)
3/13/81	#2 & #3	#4 - 1/81 Cell Lot	2" width (0.3 lb)

Data for these runs is summarized in Table 10. The I-V characteristics corresponding to two different tests are shown in Figure 53.

4.4.1 DISCUSSION OF TEST RESULTS

The existing two-axis tracker test platform could not maintain an accurate steady state track of the sun. As a result steady-state module efficiency data was not obtained. This helps explain why the protective cone's temperature was hotter than the cell (Thermocouples #6 and #1, respectively). Most of the time the lens-cell unit was not precisely aligned to the sun. Consequently, the lens was focusing onto the protective cone. Final alignment was accomplished by manually commanding the tracker platform to move until peak current was observed. An instantaneous I-V curve was then obtained. Precise alignment during this period was maintained for about one minute.

Table 10. Prototype Domed Fresnel Module Test Data

DATE	RUN NO.	AMBIENT AIR TEMP. °F	THERMOCOUPLE NO./TEMPERATURE (°F)								WIND SPEED M/SEC	DIRECT INSOLATION kW/M²	MAX. POWER -WATTS	EFF. %	FILL FACTOR
			1	2	3	4	5	6	7	9					
3-6-81	1	38.3	50.0	39.9	38.8	39.2	50.2	134.8	65.8	35.4	11.6	0.719	1.872	10.5	0.657
3-6-81	2	39.1	54.7	48.0	45.5	46.2	54.2	137.5	71.7	38.2	6.5	0.697	1.838	10.6	0.632
3-6-81	3	38.9	55.6	49.3	46.8	47.6	55.2	126.9	72.6	38.6	7.8	0.702	1.812	10.4	0.628
3-6-81	4	38.8	56.5	53.0	49.7	50.6	55.7	107.4	70.9	39.4	6.2	0.669	1.767	10.7	0.646
3-6-81	5	38.9	54.9	56.0	53.0	53.7	54.4	97.6	68.8	40.3	5.8	0.677	1.770	10.7	0.646
3-13-81	1	55.9	58.7	64.4	61.7	62π4	58.2	96.4	75.6	45.9	0.9	0.810	1.99	9.9	0.636
↑ LENS #2	2	56.2	65.4	61.3	59.2	58.9	65.9	116.2	85.4	47.2	4.0	0.750	1.86	10.0	0.628
↓	3	55.7	63.7	54.8	53.0	53.5	64.7	131.0	81.6	47.1	5.4	0.750	1.88	10.1	0.630
3-13-81	4	56.1	62.8	55.5	53.6	54.0	63.6	154.1	81.0	47.6	4.4	0.768	1.85	9.7	0.622
3-13-81	5	56.6	62.3	56.6	55.3	56.0	62.0	140.1	--	48.9	4.3	0.769	1.88	9.8	0.648
LENS #3	6	57.6	64.0	64.9	62.5	63.2	62.8	118.3	--	51.3	0.8	0.786	1.90	9.7	0.632
3-13-81	7	57.5	66.3	65.7	63.6	63.3	64.5	116.2	--	50.9	4.2	0.764	1.84	9.7	0.629

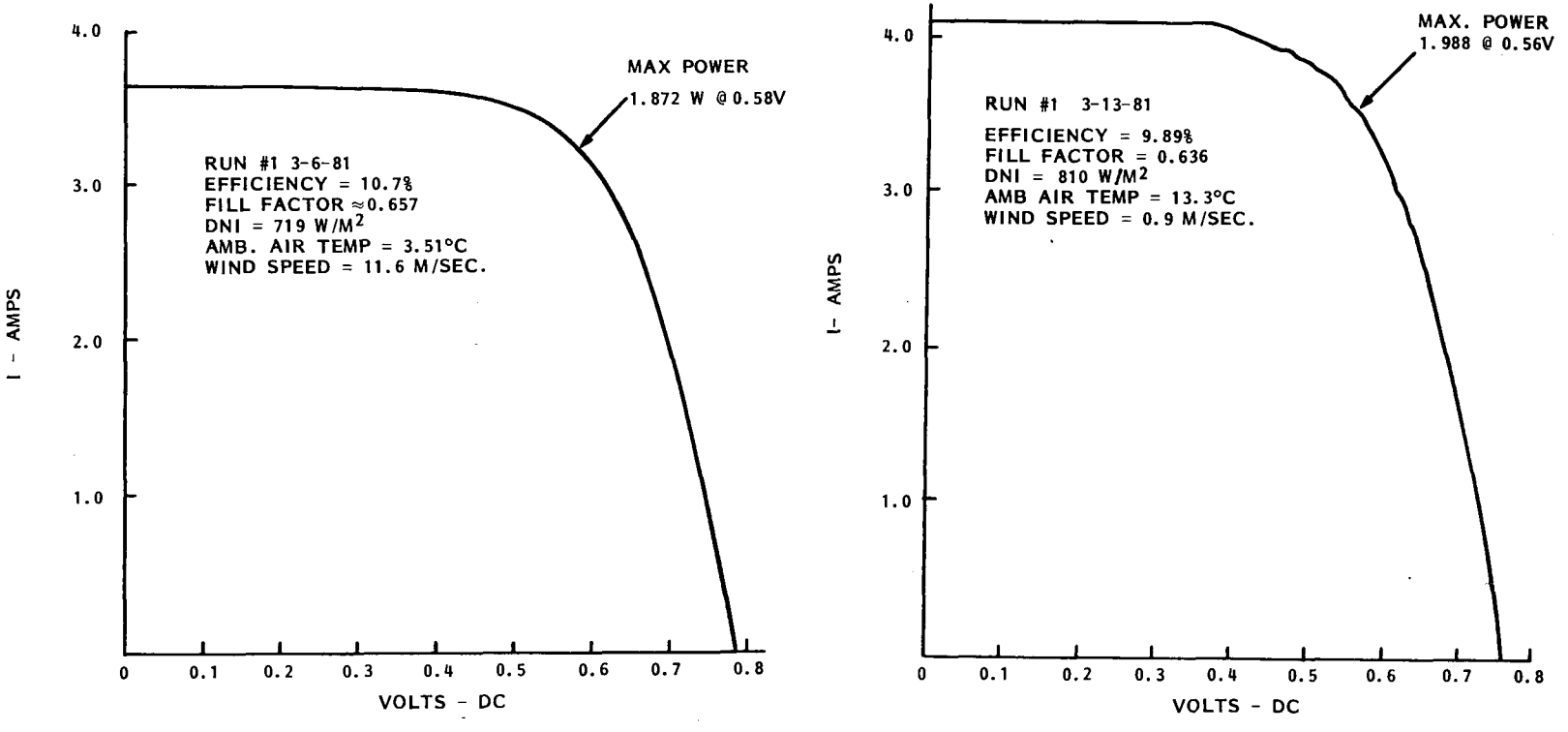

Figure 53. Representative I-V Characteristics

The module efficiency is below the goal of 15%. Component level testing of the lens confirmed its efficiency at 84%. Independent concentrated sunlight testing of the solar cell was not made. To further troubleshoot the lens-to-cell distance of 5.35" was checked several times. X-Y positioning of the lens was visually observed and it appeared to be correct (focused spot was located on the active cell area). Our conclusion is that the cell mount may not be demonstrating > 18% efficiency under concentrated sun light. This conclusion has been confirmed by a series of lens-cell tests conducted by Sandia. A summary of these tests is provided in Table 11.

Table 11. Sandia Lens-Cell Test Data

- All Test at 27-28°C Cell Temperature

Date	DNI w/m^2	Net Cell Concentration	V_{oc} Volts	I_{sc} Amps	FF	Power-Watts	Cell Eff.	Net Eff.
3/31/81	970	775	Not Available				15.5	12.4%
6/17/81 ①	959	528	.766	5.43	.761	3.16	17.5	13.3
6/17/81 ①	938	479	.765	5.01	.767	2.94	17.9	12.6

① Lens-to-Cell Distance 7.063"

SECTION 5

CONCLUSIONS AND RECOMMENDATIONS

SECTION 5

CONCLUSIONS AND RECOMMENDATIONS

5.1 CONCLUSIONS

The following represents the major accomplishments and conclusions arrived at during the course of the program.

Accomplishments

Performance

	Stated Goals	Proposed Design	Demonstrated
Concentration	400 - 200X	1000X	900X
Net Module Efficiency	15%	15 %	~ 13%
Tracking Accuracy For a < 5% Output Drop	$\geq \pm 0.1^{o}$	$\pm 0.18^{o}$	$\pm 0.40^{o}$

Performance Analysis

	Lens Efficiency	Cell Efficiency	Mount Thermal Resistance	Module Efficiency
Predicted	89 %	20 % @ 1000X	0.27^{o}C/W	17.8 % @ 28^{o}C
Assumed	84 %	18.5 %	0.25^{o}C/W	15 %
Measured	84 %	Three Different Cells: ~12%@ ~600X; ~15.5%@~775X; ~17.5%@~500X	0.25^{o}C/W	10-13%

Optimum Module Design

Selection of the optimum concentration ratio for the module to a large degree is dependent on the assumed cell characteristics. If, in fact, cell efficiency increases with increasing concentration one obviously would tend to select that concentration ratio that optimizes module output. Given the current state of high concentration cells it appears that their peak efficiency capability may not yet justify very high concentrations, i.e., 900X - 1500X. Especially in light of the impressive performance demonstrated by more conventional silicon devices at 50 - 100X (e.g., 18 - 19%).

The one key advantage to higher concentration is the increased power output per cell, hence, cell mount area. The following values are felt representative of today's technology:

68X	400 - 900X
Conventional Top Grid Concentrator Silicon Cells	Advanced Grooved Silicon and GaAl As Cells
0.9 - 1 w/cm^2*	4 - 7 w/cm^2*

* cm^2 of total cell chip area

Producibility and cost of the associated concentrator optics and cells also must be considered in selecting the optimum module concentration ratio. In addition, the corresponding tracking and manufacturing tolerance requirements must be analyzed and traded off against the benefits of going to the higher concentration.

Lens Design

The curved groove domed Fresnel lens met all of its performance goals. The measured transmission efficiency of 84% at an average target spot concentration of 902X is impressive. Equally impressive is the lens's tolerance to off track conditions. As measured, transmission efficiency only dropped by 8% at a 0.5^o off-track condition.

The high volume producibility of this lens is the critical issue that still remains. Thermo-Electron, in a parallel program, is investigating this issue in depth via the development of a tool to injection mold a domed Fresnel lens.

The speed of the developed lens may be too fast at F# 0.5. The resulting flux profile sensitivity to slight variations in focal distance presented slight problems in subsequent lens testing and module integration.

Concentrator Cell

Microwave Associates' EMVJ technology is still in development. The original program cell performance goal was 20% at 1000X. This goal has not yet been demonstrated.

Cell Mount

From a thermal resistance standpoint high concentration mount design met its program performance goals. The cell mounts demonstrated better than 0.25°C/watt thermal resistance values with voltage stand-offs in excess of 3 kV dc. This mount technology appears to be established and available to support continued high concentration module development. The issue of using an encapsulated cell was not studied. In order to ensure 20 year life encapsulated cell mount units may be needed.

Module Design

A potentially cost effective module design approach has been developed. The question of a metal versus plastic housing is still open. The benefits of using a secondary optical element were not thoroughly addressed. A program objective was to see how well we could do without one, thinking that you could always add one if needed.

The aluminum heat sink-cell mount combination adequately cooled the cell under concentrated sunlight. Passive cooling appears to be a viable cooling option for high concentration photovoltaic applications.

Test Results

The lens testing techniques utilized have surprisingly good agreement. The OSG, GE and Sandia lens efficiency values were all within 0.3% of each other.

OSG	GE	Sandia
84.1 %	83.7 %	84.0 %

Module level testing of the high concentration module is more involved than testing of lower concentration hardware, i.e., the GE 120X flat Fresnel module. It's more difficult to see the spot and confirm optimum focus when using the high concentration, small solar cell module hardware.

5.2 RECOMMENDATIONS

Optics

- Process development of high concentration optics should be pursued.
- The need for high concentration, i.e., > 500X optics requires further investigation and study.
- Further trade-offs are needed in the area of using secondary concentrator optical elements.

Solar Cell

- High concentration (> 200X) silicon cell technology should be continued.

Module

- Additional development is needed to confirm the best module design approach. A number of unanswered questions remain:
  - Do we need encapsulated cells?
  - Do we need a homogeneous housing lens material combination for expansion coefficient matching reasons?
  - Can you make a plastic housing that provides and maintains the necessary dimensional tolerances?

SECTION 6

REFERENCES

SECTION 6

REFERENCES

1. "High Performance GaAs Photovoltaic Cells for Concentrator Applications," SAND78-7018, Sandia Laboratories, Contract Report by Varian Associates, December 1977.

2. "GaAs Concentrator Solar Cells," SAND78-7036, Sandia Laboratories, Contract Report by Hughes Research Laboratories, July 1978.

3. "Photovoltaic Concentrator Technology Development Project - Third Project Integration Meeting," SAND79-0557, Sandia Laboratories, page 27, April 1979.

4. "Interim Report on Interdigitated Back Contact Solar Cells," SAND78-7041, Sandia Laboratories, Contract Report by Purdue University, February 1979.

5. "Performance and Manufacture of Large Scale Fresnel Lenses for Solar Energy Collection." Study for Ball State University, Munci, Indiana. Produced by Optical Sciences Group, Inc., March 14, 1975.

6. "Optimum Curvature of Cylindrical Fresnel Solar Concentrators." Paper prepared for Ball State University, Muncie, Indiana, by Optical Sciences Group, Inc., September 5, 1975.

7. Sater, B. L., Brandhorst, H. W., et al; "The Multiple Junction Edge Illuminated Solar Cell," IEEE 10th Photovoltaic Specialist Conference, No. 11-13, 1973, Palo Alto, California.

8. T. W. Ekstedt, J. E. Mahan, R. I. Frank, and R. Kaplow, "Open Circuit Voltage of Vertical Junction Photovoltaic Devices at High Intensity," Appl. Phys. Lett., 33, p. 422 (1978).

9. R. I. Frank and R. Kaplow, "Performance of a New High Intensity Silicon Solar Cell," Appl. Phys. Lett., 34, p. 65 (1979).

APPENDIX A

HEAT SINK THERMAL ANALYSIS MODEL VERIFICATION

GENERAL ELECTRIC
SPACE DIVISION
PHILADELPHIA

PROGRAM INFORMATION REQUEST / RELEASE

PIR NO.	*CLASS. LTR.	OPERATION	PROGRAM	SEQUENCE NO.	REV. LTR.
	U	7340	3N7	002	

*USE "C" FOR CLASSIFIED AND "U" FOR UNCLASSIFIED

FROM	TO
T. Chan	R. Hodge

DATE SENT	DATE INFO. REQUIRED	PROJECT AND REQ. NO.	REFERENCE DIR. NO.
4/28/80			

SUBJECT

Heat Sink Thermal Analysis Model Verification

INFORMATION REQUESTED/RELEASED

Introduction

It was recognized during the status review of the Domed Fresnel Module Development Program at Sandia on April 17, that the results of our heat sink optimization study deviated from Mike Edenburn's analysis. We have found that for a given lens size, the heat sink weight increases by 37% for a factor of 2 change in lens concentration ratio (500X to 1000X) while Mike's analysis indicates an increase of 11% from a concentration of 92X to 170X. Our optimized heat sink geometry also leans towards longer fins, shorter fin spacing and thinner fin substrate than that of Mike's design. For example, our predicted heat sink has a fin area ratio of 10, where fin area ratio is defined as (2*fin length+center to center spacing)/ center-to-center spacing, while Mike's design predicts a ratio fo 3.5. It is obvious that there is a discrepancy between Mike's analytical model and ours. Thus, a verification effort was conducted in trying to determine how well our thermal analysis model fits the experimentally measured data of a typical finned heat exchanger from a heat sink manufacturer. GE computer predictions were made for two heat sink configurations from Wakefield and the results (presented as heat sink to ambient thermal resistance as a function of wind speed) show excellent agreement with the manufacturer's data in both cases.

Analysis

Two heat sink configurations from EG&G Wakefield Engineering, series 510 (Figure 1) and series 517 (Figure 2) were selected from their Semiconductor Heat Sinks Catalog #1 as the basis for comparison. The heat sink thermal characteristics as shown in Figures 1 and 2 were experimentally measured in their laboratory. Thermal resistance (^{o}C/Watt) from heat sink to 20^{o}C ambient were measured as a function of volumetric flow passing through the heat sink. The linear air velocity (wind speed) can be obtained by dividing the volumetric flow by the void areas between the fins. All experimentally measured data were taken with the fins in the vertical upward orientation.

PAGE NO. ____ OF ____

√ RETENTION REQUIREMENTS

COPIES FOR	MASTERS FOR
☐ 1 MO.	☐ 3 MOS.
☐ 3 MOS.	☐ 6 MOS.
☐ 6 MOS.	☐ 12 MOS.
☐ MOS.	☐ MOS.
☐	☐ DO NOT DESTROY

The analytical heat sink thermal model was developed by Al Koenig and is part of a photovoltaic system simulation code currently being used for performance analysis of Fresnel and parabolic trough type photovoltaic array. In the case of Fresnel module, the heat sink model takes into account not only the heat transfer from the fin side of the heat sink but also losses within the module enclosure. The steady state heat sink temperature is calculated in the model through an iterative procedure until an energy balance is obtained at the surfaces of the solar cell, heat sink and the enclosure cover (i.e., Fresnel lens).

The performance of a 12" domed Fresnel module having design concentration ratio of 500x and a Microwave EMVJ solar cell of 1.763 cm square were simulated with a 3.5" Series 510 and a 3" Series 517 heat sinks in 20°C ambient and 1 kW/m^2 insolation under various wind conditions. The results of the simulation are presented in Table 1. The thermal resistance in °C/Watt from heat sink to ambient can be calculated from Table 1 as:

$$R\ ^{o}C/Watt = \frac{(\text{Heat Sink Temp.} - \text{Ambient Temp})}{(\text{Incident energy on cell} - \text{cell energy output}) * \text{cell area}}$$

where the energy terms are given in per m^2 of cell area. The two columns on the right of Table 1 show the relative magnitude of heat losses from the fins to ambient and from the heat sink substrate to the enclosure cover. The losses within the module enclosure can be as much as 23% of the total energy dissipated in still air (zero wind speed) to as low as 4% at high wind speed. The losses within the module include radiation heat transfer to the cover and free convection to the enclosure air.

The thermal resistance comparison between the analytical model and the measured data as reported in Figures 1 and 2 for a single source load is shown in Figure 3. For both heat sink configurations, the analytical results show excellent agreement with the measured data. Under natural convection, the analytical model indicates a 80.7°C temperature rise for 110 watt heat dissipation with a 3" Series 517 heat sink while the measured date indicates a 78°C temperature rise as shown in Figure 2. It should be noted that the orientation of heat sink plays an important part to its heat transfer characteristics especially under natural convection. According to Wakefield, the heat sink thermal resistance will increase by 5 to 10 percent if the fins are oriented in other than the vertical upward position. For the natural convection calculation indicated earlier, it was assumed that the fins are pointing downward at an angle of 20° from horizontal (corresponding to a January 1 array tracking position in Albuquerque at 9:00 AM).

As the results of this verification study indicated, our heat sink thermal model fits very well with the data reported by the heat sink manufacturer. This is a very important finding as this computer code is being used extensively in-house as the analytical tool in various photovoltaic programs.

FIGURE 1.

Series 510 (* F)

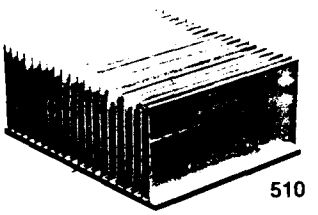

Series 510. The Series 510 High Fin Density extrusion is designed for optimal thermal characteristics in natural convection environments. The Series 510 also provides maximum surface area and performance with relatively low weight. Its broad flat base is ideally suited for back panel mounting and cooling of multiple power generating components. A 3" (76.2 mm) length will dissipate over 100 watts with only a 50°C mounting surface temperature rise.

Standard lengths are 3" (76.2 mm), 6" (152.4 mm), 9" (228.6 mm), and 12" (304.8 mm). Other lengths available on request.

How to Order: Note that the Series 510 is the only available from the factory.

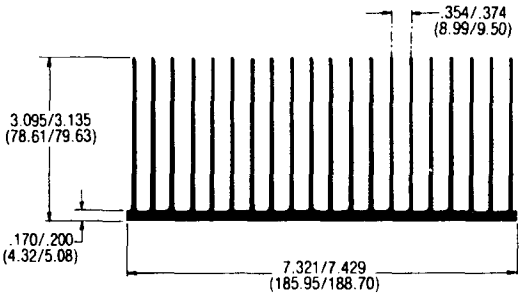

510

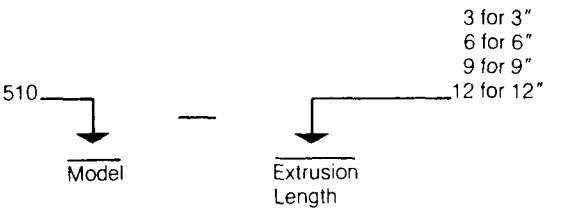

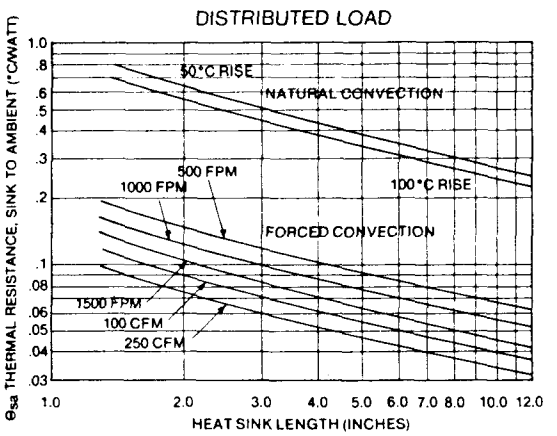

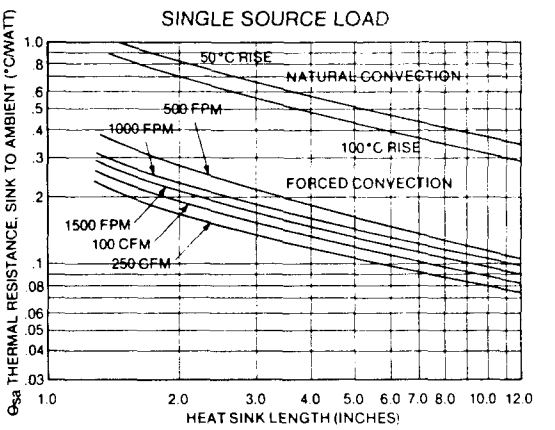

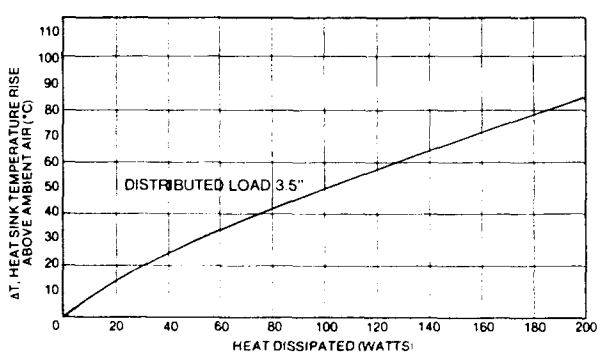

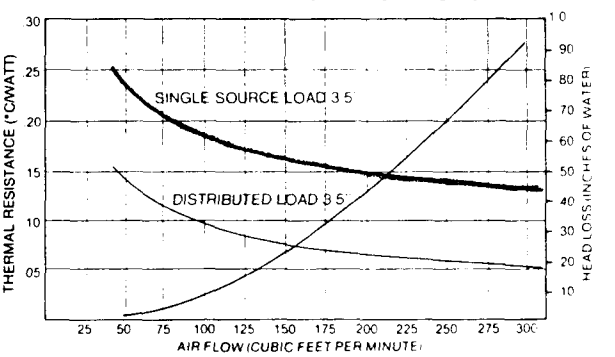

FIGURE 2

Series 517 and 518 (*F)

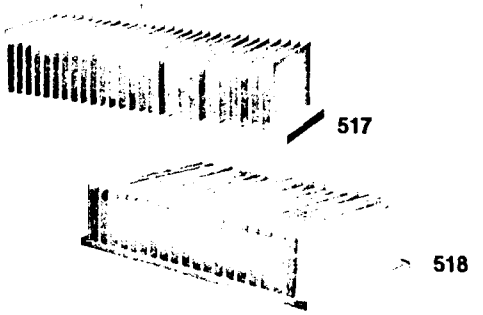

Series 517 and 518. The Series 517 and 518 High Fin Density extrusions are designed to supplement the popular EG&G Wakefield extrusion #1703. Series 517 and 518 have a large mounting surface (9.875 inches, 250.8 mm) for accommodating multiple components. The Series 517 and 518 are designed for optimum performance and maximum fin efficiency in natural convection. Fin spacing of these extrusions is correspondingly varied to provide optimal performance irrespective of vertical or cut length. The carefully engineered designs will dissipate at least 25% more power than the 1703 extrusion and yet occupy the same mounting surface.

Standard lengths are 3" (76.2 mm), 6" (152.4 mm), 9" (228.6 mm), and 12" (304.8 mm). Other lengths available on request.

How to Order: Note the Series 517 and 518 are only available from the factory.

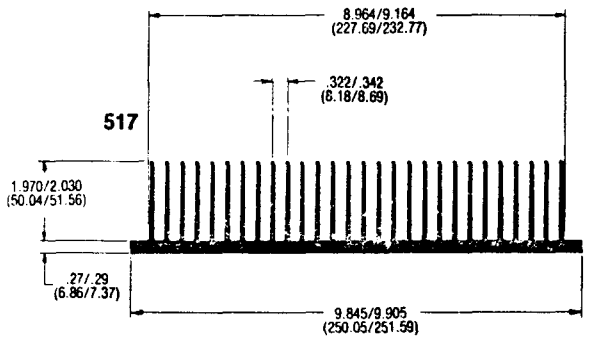

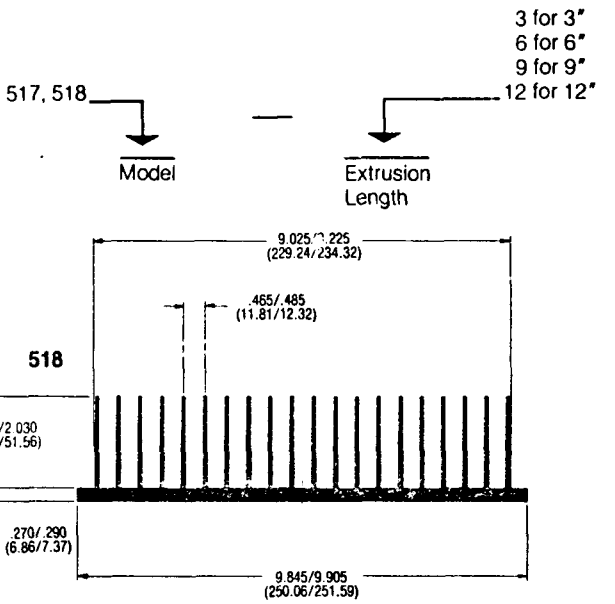

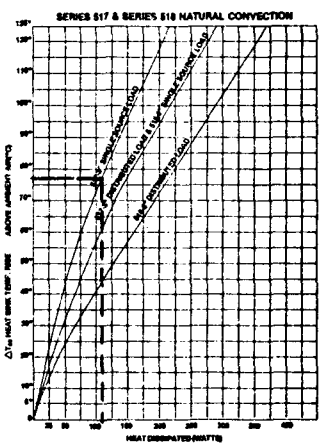

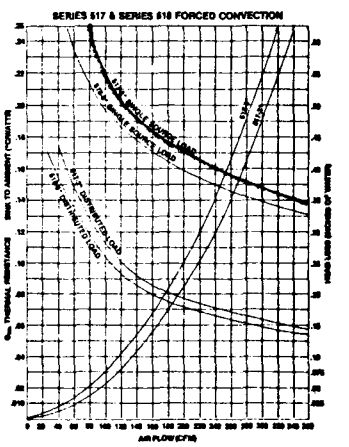

EG&G WAKEFIELD ENGINEERING 60 Audubon Rd., Wakefield, MA 01880 (617) 245-5900

Table 1. Analytical Model Results

INPUT DATA

SITE DATA
LATITUDE = 35.1 DEG
LONGITUDE = 106.6 DEG
TIME ZONE = 7.0

INCORRECT RXANG OF 0.
STANDARD FIXUP TAKEN. RXANG=90.

COLLECTOR ELEV. ANGLE = 0.

HEAT SINK WEIGHT = 0.267KG/SQ.CM.OF CELL

RIM ANGLE= 21.960

FOCAL IMAGE = PNT
CONCENTRATOR TYPE = RFR
TRACKING TYPE = TX
COOLING MODE = PAS
CONCENTRATION = 500.0
INTERCEPT FACTOR = 0.985
REQ'D CELL WIDTH = 0.018

M	D	HR	cell energy output (kwh/m²cell)	Cell Temp. (°C)	I_{DIRN} (KW/m²)	Incident energy on cell (Kwh/m²cell)	T_{AMB} (°C)	WIND (m/s)	Heat Sink Temp (°C)	Relative losses From Enclosure	Relative losses From Fins	
1	1	10	75.095	56.3	1.000	418.625	20.000	1.860	46.647	63.506	571.018	
1	1	11	76.005	52.3	1.000	418.625	20.000	2.790	42.741	58.231	607.567	
1	1	12	76.555	50.0	1.000	418.625	20.000	3.720	40.382	54.366	638.374	
1	1	13	76.955	48.3	1.000	418.625	20.000	4.650	38.765	50.491	662.676	Wakefield Series 510 3.5"
1	1	14	77.232	47.1	1.000	418.625	20.000	5.580	37.558	47.006	687.594	
1	2	10	77.448	46.2	1.000	418.625	20.000	6.510	36.617	42.087	710.500	
1	2	11	77.624	45.4	1.000	418.625	20.000	7.440	35.853	42.745	731.604	
1	2	12	77.770	44.8	1.000	418.625	20.000	8.370	35.218	42.373	751.428	
1	2	13	77.894	44.2	1.000	418.625	20.000	9.300	34.680	41.232	770.175	
1	2	14	78.001	43.8	1.000	418.625	20.000	10.230	34.217	39.380	788.009	
1	2	15	78.094	43.3	1.000	418.625	20.000	11.160	33.813	36.723	805.058	
1	1	9	62.532	110.7	1.000	418.625	20.000	0.	100.745	179.042	594.039	
1	1	10	75.200	55.8	1.000	418.625	20.000	3.870	46.228	64.965	767.609	Wakefield Series 517 3"
1	1	11	75.698	53.6	1.000	418.625	20.000	4.840	44.042	63.649	796.387	
1	1	12	76.074	52.0	1.000	418.625	20.000	5.800	42.434	61.319	820.999	
1	1	13	76.608	49.7	1.000	418.625	20.000	7.740	40.128	55.817	865.511	
1	1	14	77.250	46.9	1.000	418.625	20.000	11.610	37.360	47.742	939.053	
1	2	10	77.560	45.6	1.000	418.625	20.000	14.510	36.048	41.169	984.754	

Figure 3. Thermal Resistance (Heat Sink to Ambient) vs. Wind Speed

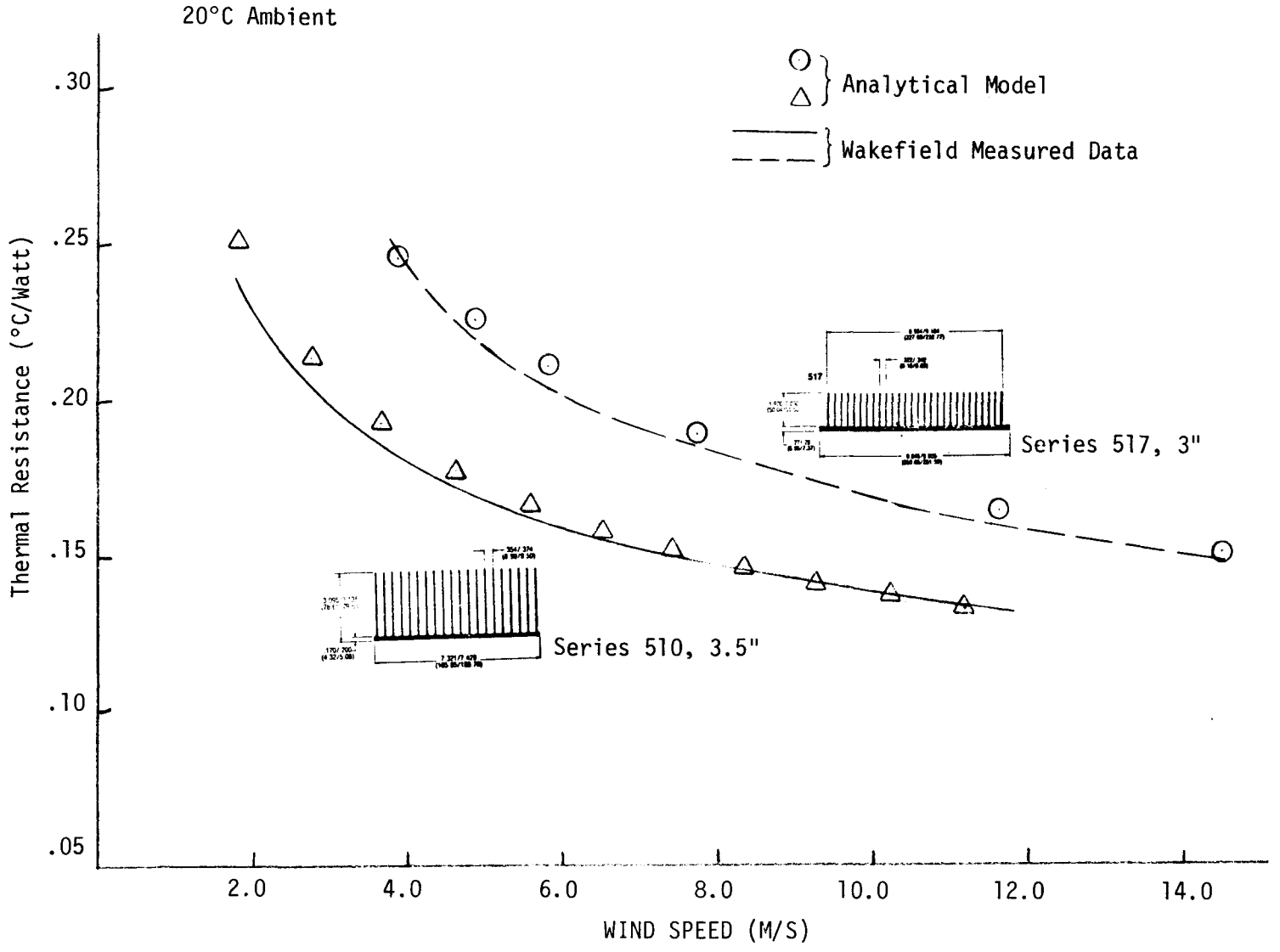

APPENDIX B

SURVIVABILITY OF PROTECTIVE SHIELD DURING SOLAR ACQUISITION

GENERAL ELECTRIC
SPACE DIVISION
PHILADELPHIA

PROGRAM INFORMATION REQUEST / RELEASE

	*CLASS. LTR.	OPERATION	PROGRAM	SEQUENCE NO.	REV. LTR.
PIR NO.	U	7340	3N7	006	

*USE "C" FOR CLASSIFIED AND "U" FOR UNCLASSIFIED

FROM	TO
E. Komito EK	R. Lambert

DATE SENT	DATE INFO. REQUIRED	PROJECT AND REQ. NO.	REFERENCE DIR. NO.
8/29/80			

SUBJECT

Survivability of Protective Shield During Solar Acquisition

INFORMATION REQUESTED/RELEASED

1.0 Summary

During solar acquisition, the domed Fresnel lens collector undergoes a defined period of time during which the protective shield or mask is exposed to the off-axis focus of solar radiation. An analysis was made of the mask temperature during the off-axis transient to determine whether thermally insulating washers were necessary to protect the textolite base. If the mask is constructed of chrome or nickel plated steel, the analysis estimates only a very moderate temperature rise in the mask. In a worst case scenario in which the collector remains fixed off-axis at maximum insolation, the mask would still survive, reaching an equilibrium temperature of about 400°F.

2.0 Background and Assumptions

The question of mask survivability was raised in Reference 1. This request to analyze the thermal environment inducted during solar acquisition included graphs of spot size, off-axis angle, and amount of insolation energy as functions of time. These graphs can be seen in Figures 1 and 2. Figure 3 contains a sketch of the mask and Figure 4 shows the mask in situ. As designed, the mask will be chrome or nickel-plated steel, 1/64 in. (0.4 mm) thick.

In order to analyze the mask temperature, several thermal properties of the material were required. Table 1 summarizes those properties used in the calculation. The shield emittance is taken to be that for chrome.[2] For nickel plate, available data [3] indicates that the emittance is such that slightly lower surface temperatures would result. This analysis has attempted to estimate the temperature rise in the protection shield in a wholly conservative manner. Since the conservative analysis shows that the as-designed mask is a viable concept, the actual performance can be expected to be even better. Using the data for chrome is consistent with this philosophy. Likewise, this analysis treats all incident radiation as being normal to the mask surface and considers the additional cooling by free convection a second order effect.

J. Chan
W. Chiu
J. Graf
J. Hatman
R. Hodge

PAGE NO. 1 OF 8

✓ RETENTION REQUIREMENTS	COPIES FOR	MASTERS FOR
	☐ 1 MO.	☐ 3 MOS.
	☐ 3 MOS.	☐ 6 MOS.
	☐ 6 MOS.	☐ 12 MOS.
	☐ MOS.	☐ MOS.
	☐	☐ DO NOT DESTROY

3.0 Analysis

3.1 Solar Acquisition

The incident radiation is given in Figure 1 as the fraction of full aperture. In this case, full aperture is the maximum solar insolation of 1 kw/m^2 irradiating a 7" diameter lens with a transmissivity of 0.9. The energy transmitted at full aperture is thus 0.022 kw (1.271 BTU/min.). By integrating the aperture curve as a function of time using the trapezoidel role, the total energy incident on the mask can be determined to be 1.22×10^{-3} kw-hr (4.171 BTU).

The temperature-time curve for the mask is derived from an energy balance taking into account the following:

1) Energy absorbed by the mask is given by

$$E_{absorbed} = \varepsilon_s E_{incident},$$

where ε_s is the material emittance at solar wavelengths.

2) Energy re-radiated by the mask is given by

$E_{rerad} = \sigma (\varepsilon(T) T^4 - \varepsilon_\infty T_\infty^4) A_s \Delta t$, where σ is the Stefan-Boltzmann constant, 5.6688×10^{-8} W/M^2K^4, A_s is the appropriate surface area, and Δt is the time interval.

3) The mask temperature is then found from:

$T(t)=T(t-\Delta t) + \left(\frac{E_{absorbed} - E_{rerad}}{MC}\right)$, where M is the appropriate mask mass and C is the material specific heat.

Since T, the mask temperature, is used in both of the last two equations, an iterative procedure is used for the solution.

The surface area and mass used in the above equations depend on the mask material. For materials with low conductivity, the incident energy would be conducted throughout the mask slowly, resulting in high temperature rises at the irradiated spot. For insulators, the reradiating surface area and energy-absorbing mass are those for the spot given in Figure 2. For materials with high conductivity, no more than a 5% error is introduced by assuming a uniform temperature on the entire mask.[2] For conductors, the surface area and mass are those for the entire mask. As designed, the high conductivity of the metal mask insures that it will act as a conductor in this case.

The mask temperature during solar acquisition, calculated from the above equations, can be seen in Figure 5. This figure demonstrates that if the mask were constructed out of an insulating material, a severe hot spot would develop (insulator curve). However, the current design calls for a chrome or nickel plated steel, so only a moderate temperature rise can be expected during the time it takes to reach focus (conductor curve).

3.2 Worst Case Scenario

In the event that the collector would remain fixed in an off-axis position and expose the mask to maximum insolation for an indefinite period of time, the as-designed mask would still be viable. Using a similar analysis as above, but with a constant energy influx at full aperture, it is determined that the metallic mask will rise in temperature until the point is reached at which the incident energy is exactly balanced by the reradiated energy. The temperature reached by the mask in this case is 397°F.

4.0 Conclusions

An energy balance conducted on the protective shield indicates that a chrome or nickel plated mask will undergo only a moderate temperature rise during solar acquisition. It is not anticipated that an insulating washer between the attachment screws and the textolite base will be required. Even in a worst case scenario, the mask temperature reaches only 397°F. To gain perspective on this temperature rise, it is noted that nickel-plated steels have been experimentally raised to 750°F with no ill effects in evidence.[5] The choice of nickel plate over chrome plate may be justified on the basis of the fact that the linear expansion coefficients for both nickel and steel are very similar, so spalling problems may be avoided. The final recommendation, of course, should be made by a materials engineer.

5.0 References

1. R. Lambert, "Action Item #9",June 17, 1980.

2. F. Kreith, Principles of Heat Transfer, 2nd ed., Intl Textbook Co., Scranton, 1968, Table 5-1, p. 215.

3. W.M. Rohsenow & J.P. Hartnett, Handbook of Heat Transfer, McGraw-Hill, NY, 1973, Table 4, p. 3-22.

4. R.E. Bolz & G.L. Tuve, Handbook of Tables for Applied Eng. Science, CRC, Cleveland, 1970, Table 1-53, p. 97.

5. V. Petrillo, Private communication, GE/AEPD, Aug, 1980.

Table 1

Assumed Thermal Properties of the Protective Shield

k, Thermal conductivity, BTU/hr-ft-°F		26
C, Specific heat, BTU/lbm°F		0.12
ρ, Density, lbm/cu. ft.		491
ε, Emissivity	@ 100°F	.08
	@ 500°F	.17
	@ 1000°F	.26
	@ 2500°F	.40
	Solar	.49
T_∞, Ambient temperature		131°F (55°C)

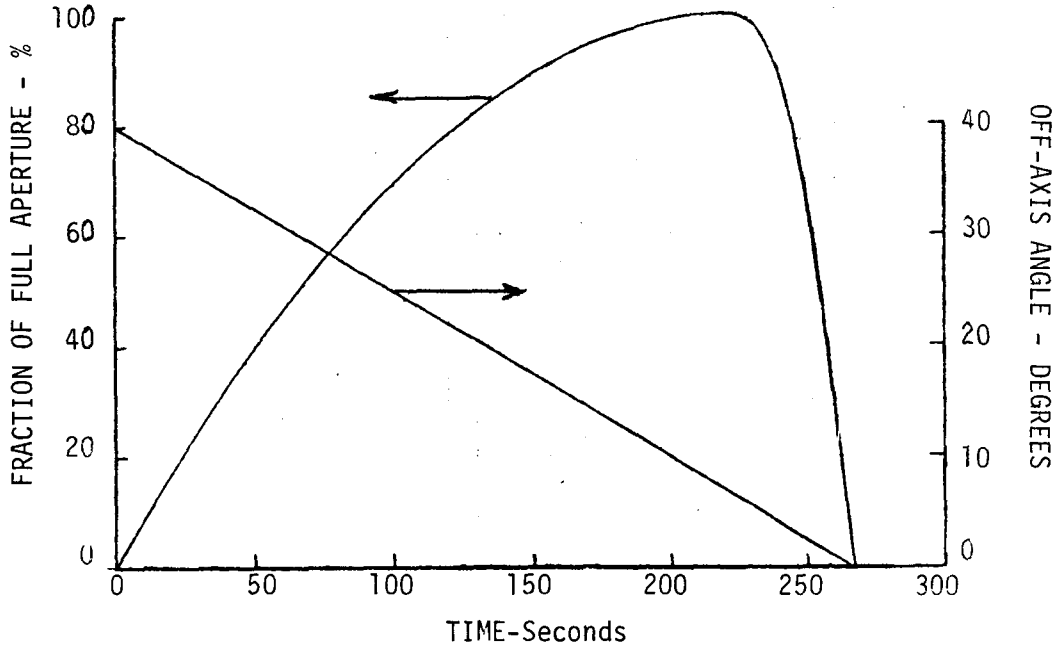

Figure 1. Energy on Mask and Off-axis Angle versus Time to Solar Acquisition

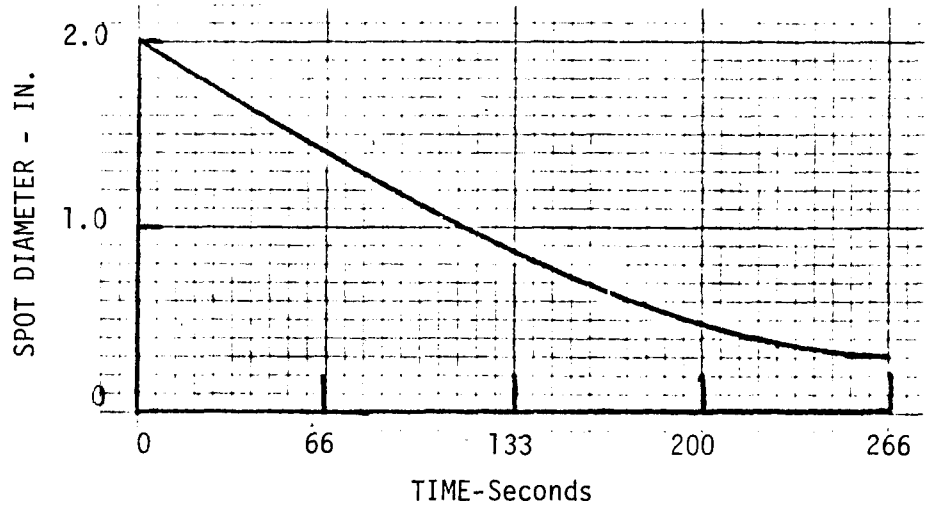

Figure 2. Spot Size on Mask versus Time to Solar Acquisition

Figure 3.

PROTECTION SHIELD

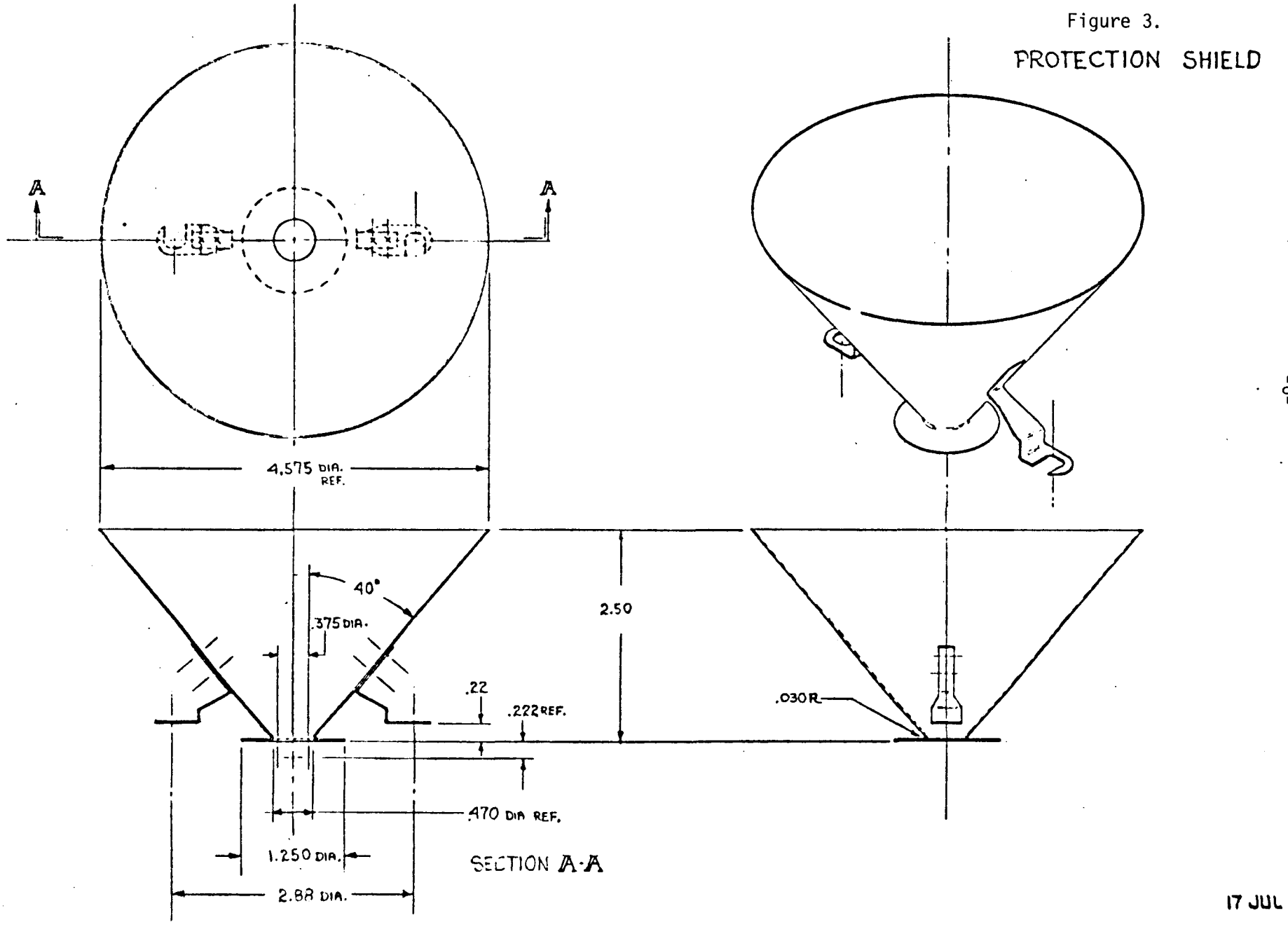

Figure 4. Diagram of Mask in Situ

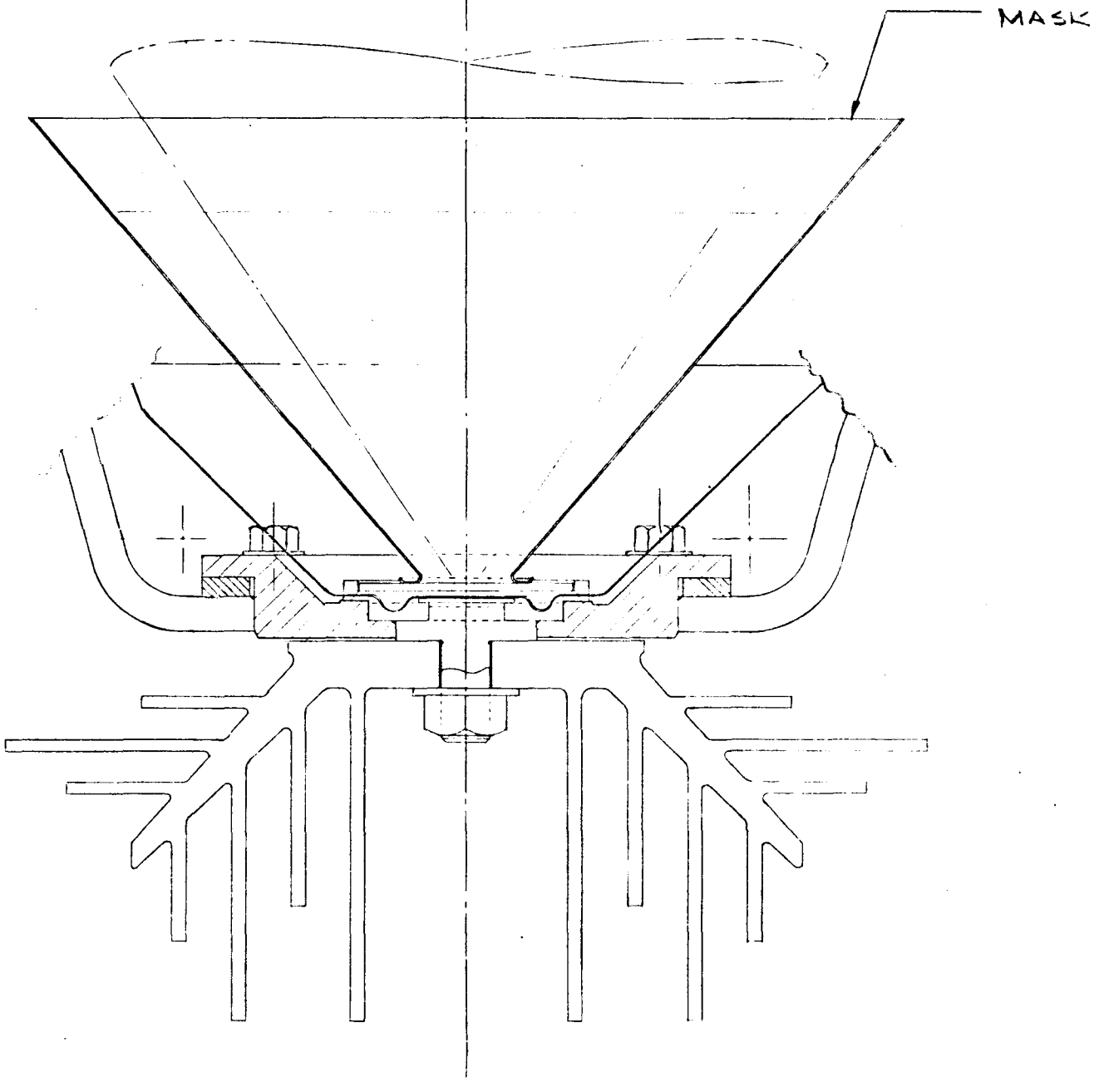

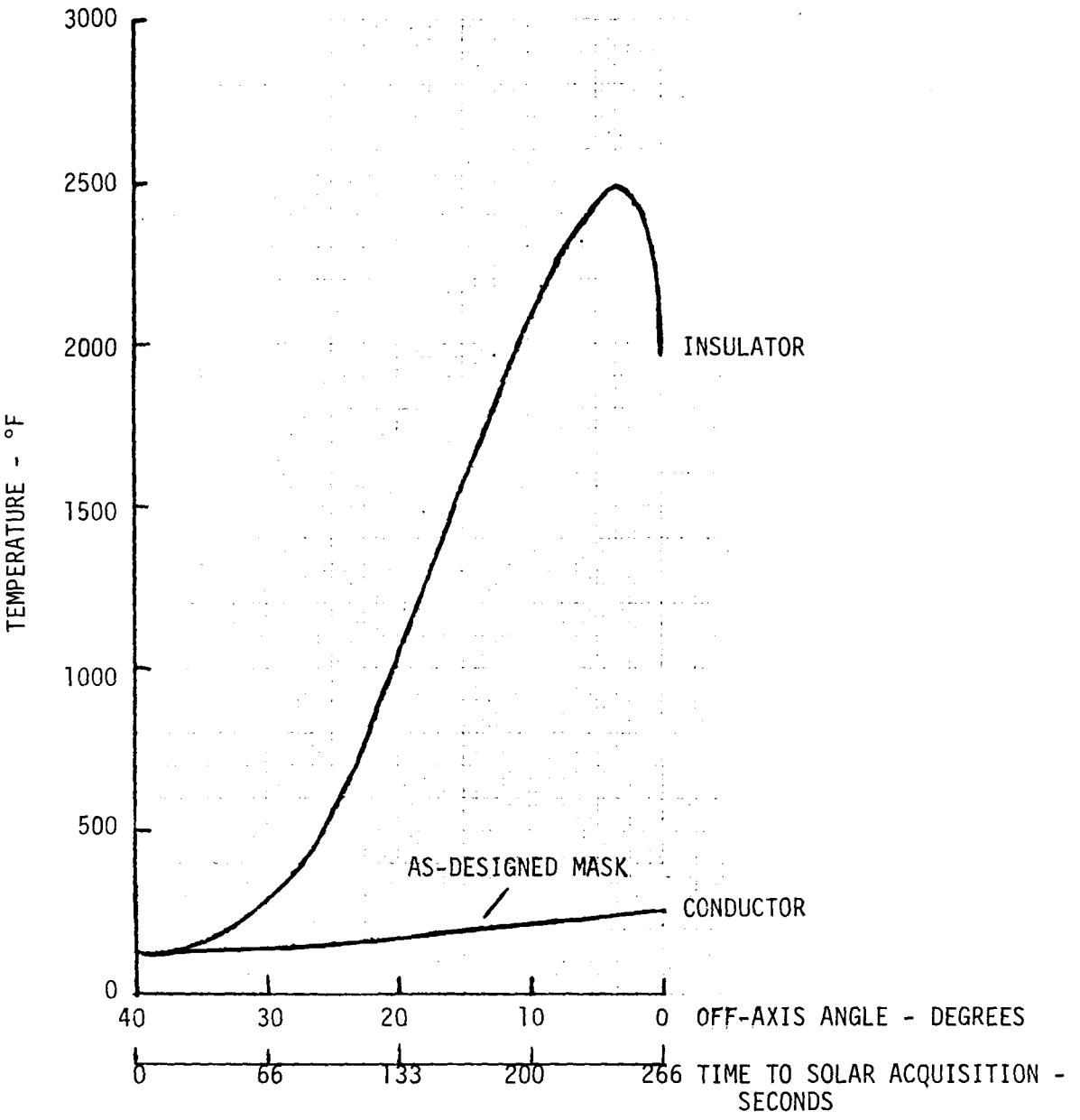

Figure 5. Temperature Rise during Solar Acquisition. The Mask Material should Definitely be a Conductor.

DISTRIBUTION LIST:

Acurex Corporation (3)
Attn: George Sutton
Bob Spencer
John Kull
485 Clyde Avenue
Mountain View, CA 94042

Aerospace Corporation
Attn: Ed Simburger
2350 El Segundo Blvd.
El Segundo, CA 90266

Alliance Tool Corp.
Fresnel Optics Division
Attn: Helmut Walter
1300 Mt. Read Blvd.
Rochester, NY 14606

Applied Solar Energy Corp. (3)
Attn: Steve Olah
Frank Ho
Ken Ling
15251 E. Don Julian Road
City of Industry, CA 91746

ARCO Power Systems
Attn: Floyd Blake
Suite 307
7061 S. University Blvd.
Littleton, CO 80122

Arizona State University (2)
Attn: Charles Backus
Robert Sanderson
College of Engineering
Tempe, AZ 85281

Ray Bahm & Associates
Attn: Ray Bahm
2513 Kimberly Court NW
Albuquerque, NM 87130

Battelle
Attn: Don Carmichael
505 King Avenue
Columbus, OH 43201

The BDM Corporation (3)
Attn: Tim Lambarski
Wayne Kauffman
Bill Schwinkendorf
1801 Randolph Road SE
Albuquerque, NM 87111

Boeing Engineering & Const. Co.
Attn: Roger Gillette
P. O. Box 3707
Seattle, WA 98124

Burns & Roe, Inc. (2)
Attn: G. A. Fontana
800 Kinderkamack Road
Oradell, NJ 07649

Chevron Research (2)
Attn: John Cape
R. Creek
576 Standard Avenue
Richmond, CA 94802

Cyro Industries
697 Route 46
Clifton, NJ 07015

U. S. Dept. of Energy (2)
ALO
Attn: James Morley
Ethan Walker
P. O. Box 5400
Albuquerque, NM 87115

U. S. Dept. of Energy (7)
Div. of PV Energy Technologies
Attn: M. B. Prince (5)
L. A. Barrett
A. Scollaro
1000 Independence Ave. SW
Washington, DC 20585

E-Systems (2)
Attn: Mark O'Neill
A. J. McDanal
P. O. Box 226118
Dallas, TX 75266

General Electric Co.
Attn: Ron Hodge
P. O. Box 527
King of Prussia, PA 19406

International Rectifier
Attn: Harold Weinstein
235 Kansas Street
El Segundo, CA 91214

Intersol Power Corporation
Attn: John Sanders
7400 W. Radcliff Avenue
Littleton, CO 80123

Jet Propulsion Lab (3)
Attn: K. Shimada
R. Ferber
Solar Data Center
4800 Oak Grove Drive
Pasadena, CA 91109

Martin Marietta (4)
Attn: S. Broadbent
R. Hein
D. Hughes
J. Baumann
P. O. Box 179
Denver, CO 80201

Microwave Associates
Attn: Jonathon Chapple-Sokol
South Avenue MS-116
Burlington, MA 01803

3M
Attn: Sanford Cobb
Industrial Optics
235 2D15
3M Center
St. Paul, MN 55144

Motorola
Attn: Keith
Kingston
GED
8201 E. McDowell
Scottsdale, AZ 85252

NASA, HQ
Attn: John Loria
Code RET-1
Washington, DC 20546

New Shelter Home Magazine
9317 Shoshone
Albuquerque, NM 87111

Oak Ridge National Lab
Attn: Steve Kaplan
P. O. Box X
Oak Ridge, TN 37830

Oklahoma University
571 South University Blvd.
Norman, OK

Photowatt (2)
Attn: William Taylor
Mike Keeling
2414 W. 14th Street
Tempe, AZ 85281

Power Hybrids
Attn: Jeff Meyer
1742 Crenshaw Blvd.
Torrance, CA 90501

PRC
Attn: E. Stirewalt
5201 Leesburg Pike
Suite 400
Falls Church, VA 22070

Purdue University (2)
Attn: Richard Schwartz
Mark Lundstrom
Electrical Engineering Dept.
West Lafayette, IN 47907

Quantum Specialties
Attn: James E. Molle
163 Verde Circle
Rohnert Park, CA 94928

Research Triangle Institute
Attn: Mayrant Simons
Box 12194
Research Triangle Park, NC 27709

SERI (3)
Attn: Gene Blakeslee
Lee Cole
John Benner
1617 Cole Blvd.
Golden, CO 80401

SERI, Library (2)
1536 Cole Blvd., Bldg. #4
Golden, CO 80401

Southern Cal Edison
Attn: Spencer Carlisle
2244 Walnut Grove Ave.
Rosemead, CA 91770

Spectrolab
Attn: Brian Elm
12500 Gladstone Avenue
Sylmar, CA 91342

Spire (3)
Attn: S. Tobin
M. Nowlan
R. Little
Patriots Park
Bedford, MA 01730

Star Light Energy
Attn: J. Furber
1717 18th Street NW
Washington, DC 20009

Strategies Unlimited
201 San Antonio Circle
Suite 205
Mountain View, CA 94040

Solar Works
Attn: Paul Wilkins
Route 2, Box 274
Santa Fe, NM 87501

Thermo Electron
Attn: Ron Scharlack
45 First Avenue
Waltham, MA 02154

UNM/NMERI
Attn: G. Leigh
Campus Box 25
Albuquerque, NM 87131

Varian & Associates (2)
Attn: Peter Borden
N. Kaminar
611 Hansen Way K-219
Palo Alto, CA 94303

Wright Patterson AFB
Attn: Jack Geis
AFWAL/POOC
Wright Patterson AFB, OH

Wyle Labs (2)
Attn: Dave Christenson
George Meares
7800 Governors Drive West
Huntsville, AL 35807

DO NOT MICROFILM

2142 B. Rose
2146 M. Garner
2146 B. Hanson
2146 B. Nasby
2146 J. Rodriguez
2146 H. Weaver
4700 E. Beckner
4720 D. Schueler
4721 H. Gerwin
4721 W. Schimmel
4723 E. Burgess
4724 D. Arvizu
4724 L. Beavis
4724 E. Boes
4724 C. Chiang
4724 M. Edenburn
4724 D. King
4724 A. Maish
4724 M. Rios
4724 C. Stillwell
5133 R. Chaffin
5133 J. Wiczer
5811 R. Assink
5822 J. Sweet
Attn: M. Moss
R. Pettit
5823 M. Chamberlain
5845 R. Eagan
3141 L. J. Erickson (5)
3151 W. L. Garner (3)
3154-3 C. H. Dalin (25)
For DOE/TIC (Unlimited Release)
8214 M. A. Pound